

Formation kinetics of europium(III) complexes of DOTA and its bis(phosphonate) bearing analogs



Soňa Procházková^a, Jakub Hraníček^b, Vojtěch Kubíček^{a,†}, Petr Hermann^a

^aDepartment of Inorganic Chemistry, Faculty of Science, Charles University, Hlavova 2030, 128 40 Prague 2, Czech Republic

^bDepartment of Analytical Chemistry, Faculty of Science, Charles University, Hlavova 2030, 128 40 Prague 2, Czech Republic

article info

Article history:

Received 1 February 2016

Accepted 19 March 2016

Available online 25 March 2016

Keywords:

Dota-like ligands

Complexation mechanism

Kinetics

Lanthanide(III) complexes

Bisphosphonate

abstract

Complexation of Eu(III) ions with H₄dota and its bis(phosphonate)-bearing analogs, H₈do3aP^{BP} with phosphinate spacer and H₇dotam^{BP} with carboxamide spacer, was studied by UV–Vis spectrophotometry and luminescence life-time measurements. The results show formation of two types of *out-of-cage* intermediates. The [EuL]^{oc} intermediate is formed under metal ion excess, whereas [EuL₂]^{oc} intermediate is formed under ligand excess. At room temperature, their conversion to *in-cage* complex is comparable but the [EuL₂]^{oc} transformation into the *in-cage* complex is significantly faster at elevated temperatures. Both bis(phosphonate)-bearing ligands show slower complexation rate than H₄dota. Comparison of reactivity of H₈do3aP^{BP} and H₇dotam^{BP} show important role of the spacer connecting the bis(phosphonate) group with the macrocycle. Presence of phosphinate in H₈do3aP^{BP} leads to significantly faster (3–4 orders of magnitude) complexation than in case of the amide spacer in H₇dotam^{BP}. Both bis(phosphonate)-bearing ligands show nonlinear dependence of the complexation rate on concentration of hydroxide anions due to changes in protonation state of the bis(phosphonate) moiety.

© 2016 Elsevier Ltd. All rights reserved.

1. Introduction

In modern medicine, lanthanides and related metals (Sc, Y, In) are widely used as radiopharmaceuticals – tracers for Positron Emission Tomography (PET; ⁴⁴Sc, ⁸⁶Y, ¹¹⁰In) and Single-Photon Emission Computed Tomography (SPECT; ¹¹¹In) or agents for radiotherapy (⁹⁰Y, ¹⁵³Sm, ¹⁶⁶Ho, ¹⁷⁷Lu) [1–4]. Other Ln(III) complexes are used as Magnetic Resonance Imaging (MRI) contrasts agents (Gd(III) complexes increasing relaxation rate of water protons in tissues) [5] or optical imaging probes (Eu(III), Tb(III) and Yb(III) complexes as fluorescence probes) [6,7].

For *in vivo* applications, the lanthanide(III) ion must be bound in a complex endowed with a high thermodynamic stability and a high kinetic inertness to avoid toxic effects or non-specific deposition of the unbound metal ion [5]. Two types of ligands dominate for complexation of Ln(III) ions – open-chain H₅dtpa and macrocyclic H₄dota analogues (Scheme 1). The macrocyclic ligands form more stable complexes than open-chain ones and, even more importantly, complexes of macrocyclic ligands are endowed with significant kinetic inertness. On the other hand, macrocyclic

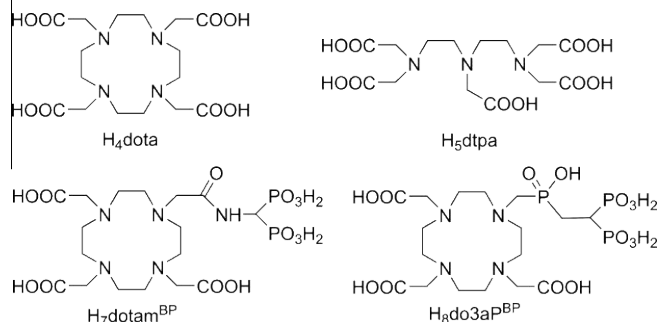
ligands suffer from slow complex formation. This is of high importance mainly in the field of radiopharmaceuticals.

Formation of Ln(III)-dota complexes has been previously studied by spectrophotometry, potentiometry, luminescence spectroscopy, NMR spectroscopy and EXAFS [8–13]. Some intermediates have also been characterized by molecular modeling [14]. Less attention has been paid to kinetic behavior of other analogs bearing amide [15–16], alcohol [17,18] or phosphorus acid pendant arms [19–22]. The generally accepted mechanism of Ln(III) complexation by dota-like ligands is a two-step process. The first step is immediate formation of an *out-of-cage* intermediate with metal ion bound by pendant donor groups and with doubly protonated macrocycle. Later, in the rate-determining step, the intermediate is transformed into the *in-cage* complex with the metal ion bound through four nitrogen atoms of macrocycle and four donor atoms of the pendants (commonly N₄O₄ coordination).

Recently, we have studied two dota-analogs bearing a bis(phosphonate) group attached to phosphinate or amide pendant arm, H₈do3aP^{BP} and H₇dotam^{BP}, respectively (Scheme 1) [23–26]. The bis(phosphonate) group is a strongly complexing moiety. So, it could be expected that it would participate on coordination of metal ion in the *out-of-cage* intermediates. H₈do3aP^{BP} shows significantly faster complexation of lanthanide(III) ions than H₇dotam^{BP} [26]. The ligands have been intensively studied as complexing agents for ¹⁷⁷Lu for treatment of bone metastases

[†] Corresponding author. Tel.: +420 22195 1436; fax: +420 22195 1253.

E-mail address: kubicek@natur.cuni.cz (V. Kubíček).



Scheme 1. Ligands discussed.

[25,27,28] and ^{177}Lu -H₇dotam^{BP} has been successfully used in patients [29]. To evaluate the role of the spacer between both complexing units – bis(phosphonate) and macrocycle – we present here detailed complexation study of the ligands with Eu(III) ions. In practice, complexation of radioisotopes is mostly performed at elevated temperatures and with a huge ligand excess. Thus, we focused our attention on temperature dependence of the complexation rate and a ligand excess was utilized in the experiments. Further, to obtain directly comparable data with the parent ligand, we re-examined formation of Eu(III)-dota complex. Despite formation of Ln(III)-dota complexes has been well described [8–22], the present study brings new information about nature and behavior of the intermediate *out-of-cage* species. Europium(III) ion was selected as its complex formation can be studied by both absorption and luminescence spectroscopy.

2. Material and methods

The ligands were prepared according to previously described procedures: H₄dota [30], H₈do3aP^{BP} [23] and H₇dotam^{BP} [24]. A stock solution of Eu(III) ($c_{\text{Eu}} \approx 0.1$ M) was prepared by dissolving EuCl₃ · xH₂O in distilled water. The concentration was determined by titration with Na₂H₂edta using xylenol orange as an indicator. Stock solutions of H₄dota, H₈do3aP^{BP} and H₇dotam^{BP} ($c_{\text{L}} \approx 0.1$ M, pH = 4) were prepared by dissolving the ligands in deionized water with addition of aq. NaOH to reach desired pH.

2.1. Spectrophotometric measurements

The measurements were carried out on spectrophotometer Specord 50 Plus (Analytik Jena AG) at the temperature range 30–70 ± 0.1 °C maintained by Peltier block and in the pH range 4.5–7.5. Constant pH was maintained by the following lanthanide(III) non-coordinating buffers ($c = 0.4$ M): 1,4-dimethylpiperazine (pH < 5), acetic acid (pH 5–5.5), MES (pH 5.5–6.5) and HEPES (pH 6.5–7.5). Formation kinetic of the complexes was followed under second and pseudo-first order conditions ($c_{\text{Eu}} = 2.5 \cdot 10^{-3} - 2.5 \cdot 10^{-2}$ M, $c_{\text{L}} = 2.5 \cdot 10^{-3} - 5.0 \cdot 10^{-2}$ M) at pH = 3.5 for H₄dota and H₈do3aP^{BP} and at pH = 4.0 for H₇dotam^{BP}, respectively, in the wavelength range 250–320 nm. The kinetics was studied in 1-cm sample cells. The experiments were initiated by the final addition of the Eu(III) stock solution into the cell. After mixing of all reagents, the first data were measured after 15 s (reaction dead time). Examples of the spectra progress are shown in Figs. S1 and S2.

2.2. Luminescence measurements

The luminescence lifetime measurements were carried out on Luminescence Spectrometer AMINCO Bowman Series 2 (Thermo

Spectronic) at room temperature using flash lamp (excitation wavelength 395 nm, emission wavelength 615 nm). Experimental setup was the same as for spectrophotometric measurements.

3. Results

3.1. Formation of Eu(III)-dota

The formation of Eu(III) complexes was studied by UV-Vis spectroscopy in the wavelength range 250–320 nm at the temperature range 30–70 °C. For H₄dota, the experiments were performed at pH = 3.5 under metal ion excess as well as under ligand excess. As it is shown in Fig. 1, both types of experiments provide a shape that is typical for the final *in-cage* complex formation via an intermediate *out-of-cage* complex (indicated in formulas with superscript oc) that is transformed into the *in-cage* complex (indicated in formulas with superscript ic) in the rate-determining step. This is in full accordance to previously published results [8–22].

In the presence of a large metal ion excess or large ligand excess, the complex formation proceeds under pseudo-first-order conditions and its rate can be expressed as in Eq. (1).

$$\frac{d_{1/2}[\text{EuL}]^{\text{ic}}}{dt} \approx \frac{1}{4} k_{\text{obs}} \cdot \frac{[\text{Eu}]_{\text{tot}}}{[\text{L}]_{\text{tot}}} \quad \text{or} \quad \frac{d_{1/2}[\text{EuL}]^{\text{ic}}}{dt} \approx \frac{1}{4} k_{\text{obs}} \cdot \frac{[\text{Eu}]_{\text{tot}}}{[\text{L}]_{\text{tot}}} \quad (1)$$

where [L]_{tot} and [Eu]_{tot} are the total concentrations of ligand and metal ion, respectively, and k_{obs} is a pseudo-first-order constant. At comparable concentrations of metal ion and ligand, the process must be treated as bimolecular reaction described using bimolecular reaction constant k_{2f} as in Eq. (2).

$$\frac{d_{1/2}[\text{EuL}]^{\text{ic}}}{dt} \approx \frac{1}{4} k_{2f} \cdot \frac{[\text{L}]_{\text{tot}} \cdot [\text{Eu}]_{\text{tot}}}{[\text{L}]_{\text{tot}} + [\text{Eu}]_{\text{tot}}} \quad (2)$$

Then, k_{obs} is expressed as in Eq. (3)

$$k_{\text{obs}} \approx \frac{1}{4} k_{2f} \cdot \frac{[\text{Eu}]_{\text{tot}}}{[\text{L}]_{\text{tot}}} \quad \text{or} \quad k_{\text{obs}} \approx \frac{1}{4} k_{2f} \cdot \frac{[\text{L}]_{\text{tot}}}{[\text{Eu}]_{\text{tot}}} \quad (3)$$

Taking into account formation of [EuL]^{oc} intermediate with 1:1 metal-to-ligand stoichiometry only, the dependence of k_{obs} on the metal ion or ligand concentrations can be expressed as in Eq. (4) [10].

$$k_{\text{obs}} \approx \frac{1}{4} \frac{k_1 - K_1^* \cdot \frac{[\text{Eu}^{3\text{P}}]_{\text{tot}}}{[\text{L}]_{\text{tot}}}}{1 + \beta \frac{[\text{Eu}^{3\text{P}}]_{\text{tot}}}{[\text{L}]_{\text{tot}}}} \quad \text{or} \quad k_{\text{obs}} \approx \frac{1}{4} \frac{k_1 - K_1^* \cdot \frac{[\text{L}]_{\text{tot}}}{[\text{Eu}^{3\text{P}}]_{\text{tot}}}}{1 + \beta \frac{[\text{L}]_{\text{tot}}}{[\text{Eu}^{3\text{P}}]_{\text{tot}}}} \quad (4)$$

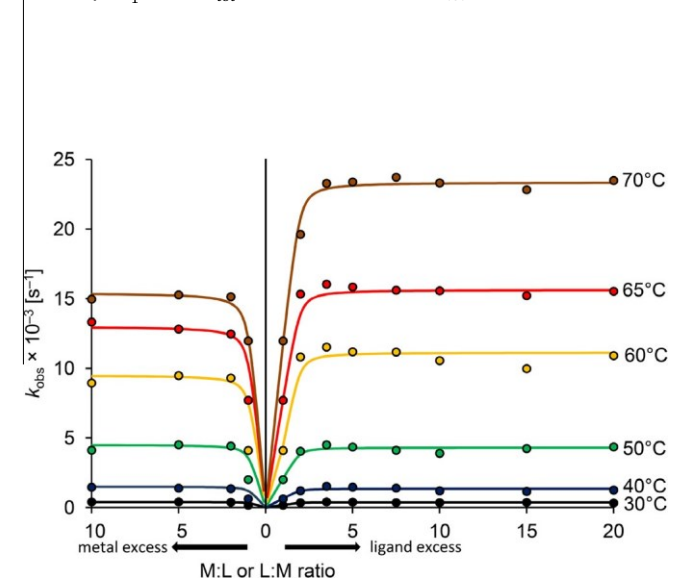


Fig. 1. Complex formation in Eu(III)-dota system performed under ligand excess (right, $c_{\text{Eu}} = 2.5 \cdot 10^{-3}$ M) or metal ion excess (left, $c_{\text{L}} = 2.5 \cdot 10^{-3}$ M) at pH = 3.5. The curves are for guiding eyes only.

where k_1 is a rate constant corresponding to the rate of the *out-of-cage* \rightarrow *in-cage* complex transformation and K_1^* is the conditional stability constant of the $[\text{EuL}]^{\text{oc}}$ intermediate.

Surprisingly, the significant increase of complexation rate was observed, especially at higher temperatures, in the ligand excess compared to the metal ion excess. It implies different complexation mechanism comprising other stable intermediates. This could be rationalized by formation of $[\text{EuL}]^{\text{oc}}$ and $[\text{EuL}_2]^{\text{oc}}$ intermediates under metal ion and ligand excess, respectively. This hypothesis is supported by luminescence life-time measurements (see below). In that case, equilibrium between both *out-of-cage* species must be included (Scheme 2) and k_{obs} is expressed as in Eqs. (5) and (6) for the metal excess and the ligand excess, respectively:

$$k_{\text{obs}} \approx \frac{k_1 - K_1^* \cdot \frac{[\text{Eu}^{3\text{P}}]_{\text{tot}}}{[\text{L}]_{\text{tot}}}}{1 + K_1^* \cdot \frac{[\text{Eu}^{3\text{P}}]_{\text{tot}}}{[\text{L}]_{\text{tot}}}} \quad (5)$$

$$\text{or } k_{\text{obs}} \approx \frac{k_1 - K_1^* \cdot \frac{[\text{L}]_{\text{tot}}}{[\text{Eu}^{3\text{P}}]_{\text{tot}}} + k_2 - K_2^* \cdot \frac{[\text{L}]_{\text{tot}}^2}{[\text{Eu}^{3\text{P}}]_{\text{tot}}}}{1 + K_1^* \cdot \frac{[\text{L}]_{\text{tot}}}{[\text{Eu}^{3\text{P}}]_{\text{tot}}} + K_2^* \cdot \frac{[\text{L}]_{\text{tot}}^2}{[\text{Eu}^{3\text{P}}]_{\text{tot}}}} \quad (6)$$

Each of the curves reaches almost immediately a plateau. It indicates that thermodynamic stability constants of the *out-of-cage* intermediates (K_1^* , K_2^*) are excessively high and cannot be obtained from the fitting. For such high K_1^* and K_2^* values (i.e. $1 \ll K_1^* \cdot \frac{[\text{Eu}^{3\text{P}}]_{\text{tot}}}{[\text{L}]_{\text{tot}}}$ or $1 \ll \delta K_1^* \cdot \frac{[\text{L}]_{\text{tot}}}{[\text{Eu}^{3\text{P}}]_{\text{tot}}} + K_2^* \cdot \frac{[\text{L}]_{\text{tot}}^2}{[\text{Eu}^{3\text{P}}]_{\text{tot}}}$), the equation describing experiments performed under the metal ion excess could be simplified as Eq. (7).

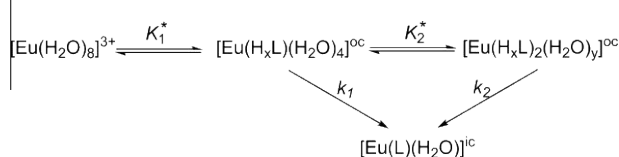
$$k_{\text{obs}} \approx k_1 \quad (7)$$

For the ligand excess, the above mentioned simplification could be also utilized. Moreover, shape of the curves indicates a dominant role of the $[\text{ML}_2]^{\text{oc}}$ complex and, thus, the rate equation could be further simplified as Eq. (8).

$$k_{\text{obs}} \approx k_2 \quad (8)$$

Thus, rate constants k_1 and k_2 were fitted as an average of the plateau values. The results are listed in the Table S1. At low temperatures, rate constants obtained under the ligand excess are comparable to those obtained for the metal ion excess. However, they are progressively more different at higher temperatures where complexation under the ligand excess is significantly faster than complexation under the metal ion excess. Evaluation of activation parameters (Table 1, Fig. S3) shows that activation energy is higher for transformation of the $[\text{EuL}_2]^{\text{oc}}$ intermediate than that for conversion of the $[\text{EuL}]^{\text{oc}}$ intermediate.

To get a better insight into the nature of the *out-of-cage* species, the system was studied using luminescence life-time measurements. The Eu(III) ion is the most appropriate luminescence probe in view of its non-degenerate emissive state $^5\text{D}_0$. Quenching of the Eu(III) luminescence by high-energy O–H vibrations allows assessment of a number of inner-sphere water molecules, q , from life-time measurements. The data were treated according to literature [31]. As it has been previously reported for the Eu(III)-dota system, the *out-of-cage* complex bearing ~ 4 water molecules is formed immediately after mixing [9]. The intermediate is slowly transformed to the *in-cage* complex with one coordinated water molecule. However using ligand excess, a hydration number of



Scheme 2. Mechanism of complexation in the Eu(III)-dota system.

Table 1

Activation parameters for formation rate constants of the studied Eu(III)-L systems (pH = 3.5 for H_4dota and $\text{H}_8\text{do3aP}^{\text{BP}}$; pH = 4.0 for $\text{H}_7\text{dotam}^{\text{BP}}$).

Ligand	Rate constant	E_A [kJ mol ⁻¹] ^a	DH^\ddagger [kJ mol ⁻¹] ^b	DS^\ddagger [J K ⁻¹ mol ⁻¹] ^b
H_4dota	k_1	79.0 ± 0.2	76.4 ± 0.2	-180.5 ± 0.4
	k_2	89.4 ± 0.1	86.7 ± 0.1	-176.7 ± 0.2
$\text{H}_8\text{do3aP}^{\text{BP}}$	k_2	90.2 ± 0.2	85.7 ± 0.1	-176.3 ± 0.3
$\text{H}_7\text{dotam}^{\text{BP}}$	k_2	116.9 ± 0.3	114.2 ± 0.2	-168.4 ± 0.2

^a $\ln k = \ln A - E_A/RT$.

^b $\ln(k/T) = -(DH^\ddagger/RT) + (DS^\ddagger/R) + \ln(k_0/h)$.

the *out-of-cage* complex is decreased (Fig. S4). Thus, the hydration number of the *out-of-cage* complex was studied as function of ligand excess (Fig. 2). The results are in good agreement with the mechanism proposed above. The $[\text{EuL}]^{\text{oc}}$ complex bearing 4 water molecules is formed in the equimolar mixture, and $[\text{EuL}_2]^{\text{oc}}$ complex is formed with hydration number <3 at ligand excess. So, effective hydration number can be expressed as in Eq. (9).

$$q \approx \delta q_{\text{Eu}} \cdot \frac{[\text{Eu}(\text{H}_2\text{O})_8] + [\text{EuL}]^{\text{oc}} + [\text{EuL}_2]^{\text{oc}}}{[\text{Eu}]_{\text{tot}}} \quad (9)$$

where q_{Eu} is hydration number of free aquaion and q_{ML} and q_{ML_2} are hydration numbers of $[\text{EuL}]^{\text{oc}}$ and $[\text{EuL}_2]^{\text{oc}}$ species, respectively. Taking into account thermodynamic equilibrium of Eu(III) species and adopting $q_{\text{Eu}} = 8$ and $q_{\text{ML}} = 4$ values [9], treatment of the data

according Eq. (9) yielded $q_{\text{ML}_2} = 2.8 \pm 0.1$. The values of stability constants of each *out-of-cage* complex are high (estimated from the fitting as $\log K_1^* > 6$ and $\log K_2^* \sim 3$) and the $[\text{EuL}_2]^{\text{oc}}$ complex is fully formed at fivefold ligand excess. To confirm presence of these two reaction intermediates, UV–Vis spectra of Ce(III)-dota system were measured immediately after mixing (Fig. S5A). Fitting the data (Fig. S5B) yielded values of stability constants of the *out-of-cage* complexes ($\log K_1^* \sim 6$ and $\log K_2^* \sim 2-3$) which are slightly lower than those found for the Eu(III)-dota system. It is in a good agreement with common trends of complex stabilities in the lanthanide series.

3.2. Formation of Eu(III)-do3aP^{BP} and Eu(III)-dotam^{BP} complexes

For bis(phosphonate) bearing ligands, the attention was paid mainly to experiments utilizing ligand excess as it is more relevant to lanthanide radioisotope complexation. Further, bis(phosphonates) with metal ion excess forms polynuclear species and

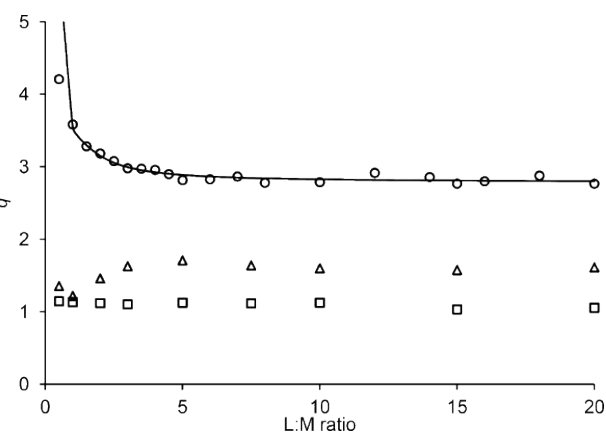


Fig. 2. Eu(III) hydration number in the *out-of-cage* complexes (measured immediately after mixing) determined for various ligand:metal initial ratios (25 °C, $c_{\text{Eu}} = 2.5 \cdot 10^{-3}$ M); H_4dota (circles, pH = 3.5), $\text{H}_8\text{do3aP}^{\text{BP}}$ (triangles, pH = 3.5), $\text{H}_7\text{dotam}^{\text{BP}}$ (squares, pH = 4.0). The line corresponds to the best fit of Eu(III)-dota system obtained according to Eq. (9).

coordination oligomers [32] and, thus, detailed understanding and evaluation of experiments performed with the metal ion excess would be extremely difficult. Complexation of H_8do3aP^{BP} was measured at $pH = 3.5$ and it shows similar behavior as that of H_4dota (Fig. 3A). Thus, data were processed as described above. As for H_4dota , high stability of the *out-of-cage* intermediate results in almost constant values of k_{obs} for various ligand excesses. A representative experiment performed under metal ion excess showed slower complexation if compared with the data for ligand excess at the same temperature. The results are summarized in Table S2 and the calculated activation parameters are listed in Table 1.

Complexation of $Eu(III)$ ions with H_7dotam^{BP} is significantly slower than that with other two ligands. To reach reasonable reaction rates, the experiments had to be performed at $pH = 4.0$. The experiments performed under the metal ion excess at $70^\circ C$ (Fig. 3B) showed a low complexation rate and the shape of the curve corresponds to a high stability the $[EuL]^{oc}$ intermediate. Under the ligand excess, complexation is accelerated. The curves show saturation shape indicating a weak coordination of the second ligand molecule in the $[EuL_2]^{oc}$ intermediate (Fig. 3B) and value of the second consecutive conditional stability constant could be estimated $K_2 = 2-3 \times 10^2$. The results are summarized in Table S3 and the calculated activation parameters are listed in Table 1.

Both bis(phosphonate)-bearing complexes show different hydration number characteristics than the H_4dota complex. Immediately after mixing of H_8do3aP^{BP} or H_7dotam^{BP} with $Eu(III)$ ions, there are less than two water molecules in $Eu(III)$ first coordination sphere and the initial hydration number remains almost constant

during the time of transformation into the *in-cage* complex (Figs. S6 and S7). Similarly, dependence of the *out-of-cage* complex hydration number on ligand excess is almost unchanged ($q = 1-2$) along the whole studied range (Fig. 2). The increase of q value for $Eu(III)$ - H_8do3aP^{BP} system might be ascribed to water molecules interacting with bis(phosphonate) groups through hydrogen bonds (the second-sphere hydration) as they can also contribute to the luminescence quenching [33,34]. For both ligands, formation of the final *in-cage* complex was independently confirmed by 1H and ^{31}P NMR and the spectra are in the full accordance with those reported previously [23,24].

3.3. pH dependence of the formation rate

To get more information about pH influence on complexation process, formation rate of all complexes, $Eu(III)$ - $dota$, $Eu(III)$ - $do3aP^{BP}$ and $Eu(III)$ - $dotam^{BP}$, was studied under ten-fold ligand excess at various pH. This ligand excess was chosen to reach the complete complexation of $Eu(III)$ ion in the $[EuL_1]^{oc}$ or $[EuL_2]^{oc}$ intermediates. Such conditions allow to follow only rate of conversion of the intermediates into the final *in-cage* complex. Results are depicted in Figs. 4 and S4. All complexes show higher formation rate with increasing pH. The generally accepted mechanism [8–22] suggests that the rate-determining step is deprotonation of a ring nitrogen atom of the *out-of-cage* complex coupled with transfer of $Eu(III)$ ion into the macrocyclic cavity (Scheme S1). In

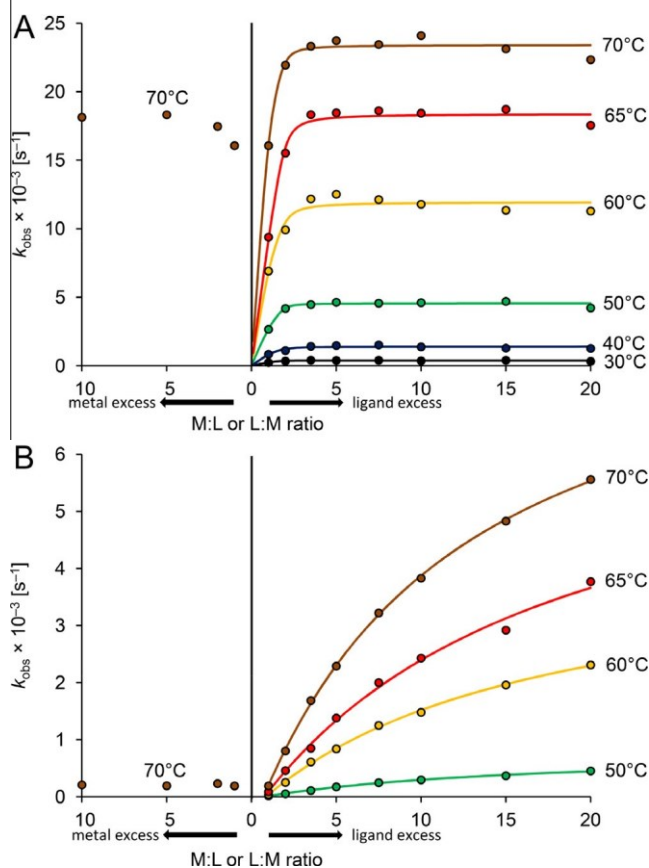


Fig. 3. Complex formation in $Eu(III)$ - $do3aP^{BP}$ (A; $pH = 3.5$; the curves are for guiding eyes only) and $Eu(III)$ - $dotam^{BP}$ (B; $pH = 4$; the curves represent best fits according to Eq. (5)) systems performed under ligand excess (right, $c_{Eu} = 2.5 \cdot 10^{-3} M$) or metal excess (left, $c_L = 2.5 \cdot 10^{-3} M$).

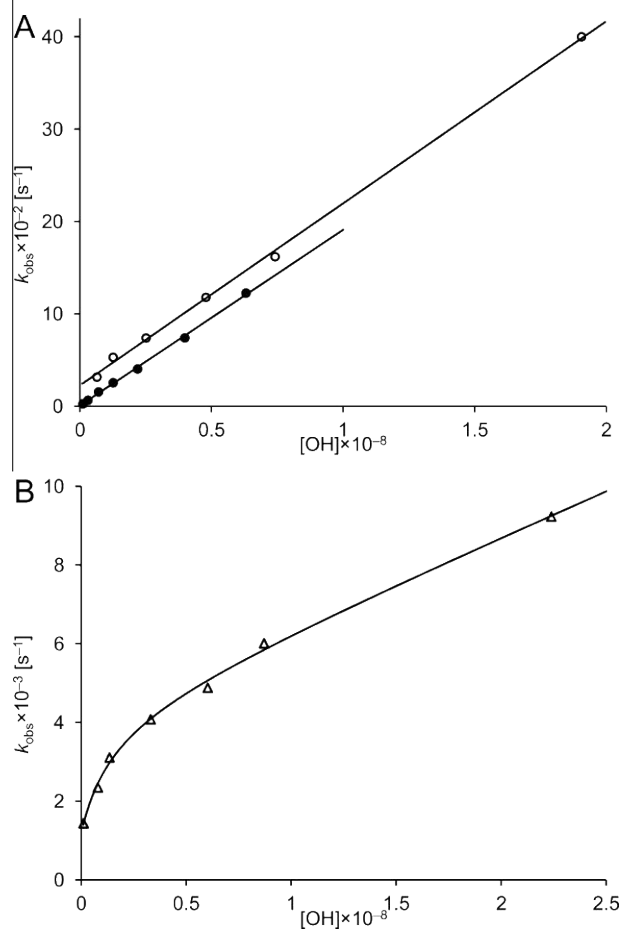


Fig. 4. pH dependence of the formation rate constants of $Eu(III)$ - $dota$ (A, $25^\circ C$, full symbols $c_{Eu} = 2.5 \cdot 10^{-3} M$, $c_L = 2.5 \cdot 10^{-2} M$, open symbols $c_{Eu} = 2.5 \cdot 10^{-2} M$, $c_L = 2.5 \cdot 10^{-3} M$) and $Eu(III)$ - $do3aP^{BP}$ complexes ($25^\circ C$, $c_{Eu} = 2.5 \cdot 10^{-3} M$, $c_L = 2.5 \cdot 10^{-2} M$). The solid lines correspond to the best fits obtained according to Eqs. (10) (A) or (12) (B).

such case, the rate constant k_{obs} should show linear dependence on concentration of hydroxide ions $[\text{OH}^-]$ and could be expressed as in Eq. (10).

$$k_{\text{obs}} = \frac{1}{4} \delta^{0\text{H}} k_0 + \delta^{1\text{H}} k_1 [\text{OH}^-] \quad (10)$$

where ${}^{0\text{H}}k_0$ and ${}^{0\text{H}}k_1$ are rate constants characterizing the OH-independent and OH-dependent transformation of the diprotonated *out-of-cage* intermediate into the *in-cage* complex [10]. This model could be successfully used for description of the Eu(III)-dota system (Fig. 4A) as it shows linear increase of k_{obs} with $[\text{OH}^-]$ under both ligand or metal ion excesses. At room temperature, formation rate under metal ion excess is slightly faster than that under ligand excess over the entire studied pH range. However, values of ${}^{0\text{H}}k_1$ are almost the same for both processes. The difference is caused by a difference in ${}^{0\text{H}}k_0$ values as it is negligible under the ligand excess whereas it becomes significant under the metal ion excess. In the course of the reaction, proton is transferred from the reaction intermediate to hydroxide anion. Alternatively, the role of the proton scavenger could be played by other Bronsted base (e.g. buffer) and it results in a nonzero ${}^{0\text{H}}k_0$ value [13].

Both bis(phosphonate) ligands show a different shape of the pH dependence plot than H_4dota . This could be rationalized by the fact that bis(phosphonates) generally form stable protonated complexes. Here, fully rigorous determination of the protonation states of such *out-of-cage* intermediates is not possible. However, it can be supposed that only one (de)protonation event of such complexes can happen in the studied pH range (5–7.5) [26,35,36]. Thus, the system treatment can be simplified with assumption that the *out-of-cage* species are likely present in two different protonated states differing by just one proton, “X” and “HX”. Then, overall rate constant could be expressed as a sum of contributions from both such species.

$$k_{\text{obs}} = \frac{[\text{X}]_{\text{tot}}}{4} \delta^{0\text{H}} k_{\text{X}0} + \delta^{1\text{H}} k_{\text{X}1} [\text{OH}^-] + \frac{[\text{HX}]_{\text{tot}}}{4} \delta^{0\text{H}} k_{\text{HX}0} + \delta^{1\text{H}} k_{\text{HX}1} [\text{OH}^-] \quad (11)$$

where $[\text{X}]_{\text{tot}}$ is overall concentration of all forms of the *out-of-cage* species and ${}^{0\text{H}}k_{\text{X}0}$, ${}^{0\text{H}}k_{\text{X}1}$, ${}^{0\text{H}}k_{\text{HX}1}$ and ${}^{0\text{H}}k_{\text{HX}2}$ are rate constants for the *out-of-cage* \rightarrow *in-cage* conversion of species with the “X” and “HX” bis(phosphonate) protonation state, and di- or monoprotonated ring amines, respectively. Using the mass balance and the protonation equilibrium equations for the *out-of-cage* species, Eq. (11) could be rewritten as

$$k_{\text{obs}} = \frac{1}{4} \frac{\delta^{0\text{H}} k_{\text{X}0} + \delta^{1\text{H}} k_{\text{X}1} \frac{K_{\text{a}}}{[\text{H}^+]}}{1 + \frac{[\text{H}^+]}{K_{\text{a}}}} + \frac{1}{4} \frac{\delta^{0\text{H}} k_{\text{HX}0} + \delta^{1\text{H}} k_{\text{HX}1} \frac{K_{\text{a}}}{[\text{H}^+]}}{1 + \frac{[\text{H}^+]}{K_{\text{a}}}} \quad (12)$$

where K_{a} is dissociation constant describing the “X” and “HX” equilibrium of bis(phosphonate) group in the *out-of-cage* complex. Results obtained for the Eu(III)-do3aPBP system are shown in Fig. 4B. Values of the rate and dissociation constants are listed in Table 2. Treatment of the data showed that contribution described by constant ${}^{0\text{H}}k_{\text{X}0}$ is negligible and, so, it was omitted. Similar experiments were performed with the Eu(III)-dotamBP system and results

Table 2
Kinetic and thermodynamic parameters obtained in Eu(III)-dota and Eu(III)-do3aPBP systems.

H_4dota metal excess	${}^{0\text{H}}k_0$	$(2.3 \pm 0.3) \cdot 10^{-2} [\text{s}^{-1}]$
	${}^{0\text{H}}k_1$	$(1.97 \pm 0.03) \cdot 10^7 [\text{s}^{-1} \text{M}^{-1}]$
H_4dota ligand excess	${}^{0\text{H}}k_0$	$(7 \pm 9) \cdot 10^{-4} [\text{s}^{-1}]$
	${}^{0\text{H}}k_1$	$(1.90 \pm 0.03) \cdot 10^7 [\text{s}^{-1} \text{M}^{-1}]$
$\text{H}_8\text{do3aPBP}$ ligand excess	${}^{0\text{H}}k_{\text{X}1}$	$(2.3 \pm 0.2) \cdot 10^5 [\text{s}^{-1} \text{M}^{-1}]$
	${}^{0\text{H}}k_{\text{HX}0}$	$(1.1 \pm 0.2) \cdot 10^{-3} [\text{s}^{-1} \text{M}^{-1}]$
	${}^{0\text{H}}k_{\text{HX}1}$	$(3.1 \pm 1.1) \cdot 10^6 [\text{s}^{-1}]$
	K_{a}	$(6.7 \pm 3.1) \cdot 10^{-6} [\text{M}]$

showed the same trend as it was observed for the Eu(III)-do3aPBP (Fig. S8). Due to the low stability constant of the *out-of-cage* complex, the corresponding rate constants cannot be determined. However, fitting according to Eq. (12) gave value of dissociation constant $pK_{\text{a}} = 5.9$ ($K_{\text{a}} = (1.4 \pm 0.3) \times 10^{-6} \text{M}$).

From practical point of view, a direct comparison of the measured reaction rates is interesting. It shows significant differences between the ligands with order $\text{H}_4\text{dota} > \text{do3aPBP} > \text{H}_7\text{dotamBP}$ along the whole studied pH range (Fig. 5).

4. Discussion

It is generally accepted that complexation of lanthanide(III) ions by dota-like ligands is a two-step process. First, ligand immediately binds the metal ion by the pendant arms only forming the intermediate *out-of-cage* complex where the macrocyclic amine groups still remain protonated. Such intermediate re-arranges in the rate-determining base-catalyzed step in which protons from the cycle are removed and metal ion is transferred into the ligand cavity forming the final *in-cage* complex (Scheme S1). Thus, there are two important parameters influencing the overall complexation rate: (i) thermodynamic stability of the intermediate and (ii) rate of the *out-of-cage* \rightarrow *in-cage* complex transformation. In the case of Ln(III)-dota complexation, the structure of the *out-of-cage* intermediate is mostly described as $[\text{Ln}(\text{H}_2\text{dota})(\text{H}_2\text{O})_4]^{0\text{c}}$ (stoichiometry ML_1) where two ring nitrogen atoms are protonated and only the acetate groups are coordinated. It was detected by spectrophotometry [10,11], NMR [12] and luminescence spectroscopy [9] and similar coordination mode was reported for dota-like complexes also in the solid state [37,38]. A luminescence lifetime study revealed a number of water molecules coordinated to the Eu(III) ion in the intermediate is between four and five [9]. The detailed studies have been mostly performed using metal ion excess under pseudofirst-order reaction conditions and showed formation of the ML_1 intermediate [8–22]. However, the results presented here indicate that composition of intermediate is different when ligand excess is used. A number of coordinated water molecules in this intermediate drops down ($q = 2–3$). It could be explained by coordination of oxygen atoms of the second ligand molecule forming a $[\text{Ln}(\text{H}_2\text{dota})_2(\text{H}_2\text{O})_{2–3}]^{0\text{c}}$ intermediate (stoichiometry ML_2). The number of coordinated water molecules indicates that some carboxylate groups of the ligand molecules remain uncoordinated. It could be ascribed to repulsion of negatively charged carboxylates what does not allow for coordination of all eight groups. Similar

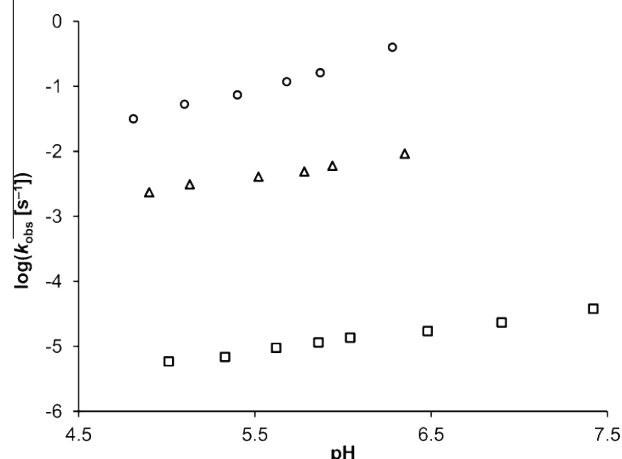


Fig. 5. pH dependence of the formation rate constants of Eu(III) complexes (25 °C, $c = 2.5 \cdot 10^{-3} \text{M}$, $c = 1.25 \cdot 10^{-2} \text{M}$); H_4dota (circles), $\text{H}_8\text{do3aPBP}$ (triangles), $\text{H}_7\text{dotamBP}$ (squares).

out-of-cage arrangement where a trivalent ion interacts with two ligand molecules has been recently reported for solid-state structure of dinuclear Sc(III)-dota complex [39]. The structure contains two different Sc(III) ions. One is coordinated in the *in-cage* mode (N_4O_4 coordination sphere) whereas the other metal ion is bound in the *out-of-cage* fashion between a molecule of free macrocyclic-diprotinated ligand and molecule of the *in-cage* complex ($O_4O^{\delta-}_4$ coordination sphere); acetate groups of the *in-cage* complex are bridging both metal ions. As the negative charge is partially reduced by presence of the *in-cage*-bound metal ion, the Sc(III) ion located *out-of-cage* is coordinated by all eight carboxylates.

Each *out-of-cage* complex (ML_1 and ML_2) shows different temperature dependence of the rate of the second reaction step – formation of the *in-cage* complex. At room temperature, the ML_1 complex is transformed slightly faster but the difference is not significant. It is in agreement with previous study performed at room temperature that reports the same reaction rate under ligand as well as under metal ion excesses [13]. The difference between two species is clearly pronounced at elevated temperatures where transformation of ML_2 complex is significantly faster. The difference is reflected in values of activation energy (79 versus 89 kJ mol⁻¹ for ML_1 and ML_2 , respectively; Table 2).

The studied bis(phosphonate)-bearing ligands, H_8do3aP^{BP} and H_7dotam^{BP} , show different behavior. Exact stoichiometry of the *out-of-cage* complexes cannot be estimated from their hydration number as it remains almost unchanged in the course of complexation as well as with increasing ligand excesses. The low hydration number of the *out-of-cage* complexes ($q = 1-2$) could be rationalized by strong complexation of the bis(phosphonate) group. Bis(phosphonates) are known to act as bridging ligands forming polynuclear species [35]. So, the coordination sphere of Ln(III) ion in these *out-of-cage* complexes is occupied not only by carboxylates but also by phosphonate groups originating from one or more ligand molecules. However, the results clearly show different nature of the *out-of-cage* complexes formed under ligand or metal ion excess, respectively. Exact composition of the complexes is difficult to determine due to the mentioned high coordination ability of bis(phosphonates) as well as due to their ability to form stable protonated complexes. Under the metal ion excess, even more than two metal ions might be bound to one bis(phosphonate) group. On the other hand under ligand excess, coordination of not more than two molecules per metal ion could be expected due to the high negative charge of the ligand carboxylates and bis(phosphonates). However, formation of polynuclear reaction intermediates cannot be excluded even under ligand excess due to a high bridging ability of the bis(phosphonate group) [32]. Anyway, the high coordination ability of bis(phosphonate) group should result in high stability of the ML_1 *out-of-cage* complex. So, the saturation character of the curves describing formation of the Eu(III)-dotam^{BP} complex (Fig. 3B) arises from a low value ($K_2 = 2-3 \times 10^2$) of the consecutive stability constant describing coordination of the second ligand molecule.

The lower overall reaction rates observed for both bis(phosphonate)-bearing ligands indicate that presence of additional strongly complexing unit on pendant arms is not favorable for future design of ligands if faster *in-cage* complexation is desired. On the other hand, the difference between H_8do3aP^{BP} and H_7dotam^{BP} reaction rates points to a high importance of the spacer connecting macrocycle and bis(phosphonate). Complexation of the ligand with amide spacer is more than one order of magnitude slower than that of the ligand with phosphinate spacer despite the experiments were performed at higher pH (3.5 versus 4.0 for H_8do3aP^{BP} and H_7dotam^{BP} , respectively). It is probably due to a low coordinating ability of the amide group in comparison with that of phosphinate. More likely, phosphinate better assists the transport of the metal ion into the macrocyclic cavity. Furthermore, the non-coordinated

oxygen atom of phosphinate might assist in transfer of proton(s) from the macrocycle to the bulk water.

In the second complexation step, metal ion is transferred into the macrocyclic cavity forming the *in-cage* complex. The formation rate of the process was found to be directly proportional to the OH⁻ concentration and it is in agreement with previously reported data [9–22]. In the mechanism, deprotonation of ring nitrogen atoms in the *out-of-cage* complex is crucial process in the rate-determining step. For H_4dota , experiments performed under metal ion excess as well as under ligand excess provided similar linear dependence of k_{obs} on OH⁻ concentration. For both experiments, values of the rate constant $^{OH}k_1$ are identical (1.97×10^7 s⁻¹ M⁻¹ versus 1.91×10^7 s⁻¹ M⁻¹ for metal excess and ligand excesses, respectively) and they are in a good agreement with those previously reported (1.1×10^7 s⁻¹ M⁻¹ or 7.2×10^6 s⁻¹ M⁻¹) [9,10].

For H_8do3aP^{BP} and H_7dotam^{BP} , the dependence of k_{obs} on OH⁻ concentration is not linear due to different protonation state of the coordinated bis(phosphonate) group in the *out-of-cage* complex. The determined values of the dissociation constants ($pK_a = 5.2$ and 5.9 for H_8do3aP^{BP} and H_7dotam^{BP} , respectively) are in the expected range [35,36]. For H_8do3aP^{BP} , rate constants $^{OH}k_{HX1}$ (for protonated form of the bis(phosphonate) group) and $^{OH}k_{X1}$ (for deprotonated form of the bis(phosphonate) group) describing hydroxide-assisted transfer of the metal ion into the macrocyclic cavity were determined. The value is, on the first sight surprisingly, higher for the protonated form. However, deprotonated form of bis(phosphonate) is stronger complexing agent and, so, it decelerates the *out-of-cage* → *in-cage* transfer of metal ion more efficiently than its protonated form. It confirms the suggested mechanism and shows that presence of too strongly binding side arm slows down *in-cage* complex formation. Analogous effect has been observed for complexation of gallium(III) by a NOTA derivative bearing a bis(phosphonate) group if compared with that of NOTA [40].

5. Conclusion

It is the first work which has tried to thoroughly investigate and evaluate complexation under whole range of metal-to-ligand ratios. The data obtained under ligand excess are much harder to quantitatively interpret than those obtained under metal ion excess. Anyway, even only semi-quantitative treatment used here allows drawing some conclusions important for design of new chelator for radiopharmaceuticals.

Comparison of H_4dota with its monophosphinate and monoamide analogs bearing bis(phosphonate) group shows decelerating effect of the strongly chelating moiety on rate of the rearrangement of the *out-of-cage* intermediate to the *in-cage* complex. The rate is strongly dependent on the nature of the spacer connecting macrocycle with the bis(phosphonate) group. Better coordination ability of the phosphinate spacer results in significantly faster complexation compared to weakly coordinating amide moiety.

The work shows presence of different intermediates if complexation of Eu(III) ions by dota-like ligands is proceeding in the metal or ligand excess. Significantly different complexation rates were observed when working under these conditions. In radiomedical applications, complexation is mostly performed using a huge ligand excess (1000-fold or more). Thus, formation of intermediates with 1:2 metal-to-ligand ratio could be expected. Therefore, the characteristics obtained from the experiments performed under ligand excess are more relevant for potential application of the ligands in radiopharmacy.

To improve efficiency of metal radioisotope incorporation into chelators, coordinating side group(s) on pendant arms can highly accelerate the *in-cage* complex formation with macrocyclic ligands

[41–43]. However, data presented here show that the complexing ability of the side groups and nature of the coordinating spacer must be properly tuned to get the desired effect. Groups weakly binding the particular metal ion seem to be the most suitable for design of macrocyclic ligands with fast metal ion complexation.

Acknowledgements

Support from the Grant Agency of Charles University (No. 272314) and the Grant Agency of the Czech Republic (13-08336S) is acknowledged.

Appendix A. Supplementary data

Supplementary data associated with this article can be found, in the online version, at <http://dx.doi.org/10.1016/j.poly.2016.03.039>.

References

- [1] T.J. Wadas, E.H. Wong, G.R. Weisman, C.J. Anderson, *Chem. Rev.* 110 (2010) 2858.
- [2] R.E. Mewis, S.J. Archibald, *Coord. Chem. Rev.* 254 (2010) 1686.
- [3] C.S. Cutler, H.M. Hemmkens, N. Sisay, S. Huclier-Markai, S.S. Jurisson, *Chem. Rev.* 113 (2013) 858.
- [4] E.W. Price, C. Orvig, *Chem. Soc. Rev.* 43 (2014) 260.
- [5] A.E. Merbach, L. Helm, É. Tóth, *The Chemistry of Contrast Agents in Medical Magnetic Resonance Imaging*, John Wiley & Sons, Chichester, 2013.
- [6] S. Faulkner, S.J.A. Pope, B.P. Burton-Pye, *Appl. Spectrosc. Rev.* 40 (2005) 1.
- [7] X. Wang, H. Chang, J. Xie, B. Zhao, B. Liu, S. Xu, W. Pei, N. Ren, L. Huang, W. Huang, *Coord. Chem. Rev.* 273–274 (2014) 201.
- [8] J. Moreau, E. Guillon, J.-C. Pierrard, J. Rimbault, M. Port, M. Aplincourt, *Chem. Eur. J.* 10 (2004) 5218.
- [9] S.L. Wu, W.D. Horrocks, *Inorg. Chem.* 34 (1995) 3724.
- [10] É. Tóth, E. Brücher, I. Lázár, I. Tóth, *Inorg. Chem.* 33 (1994) 4070.
- [11] E. Brücher, G. Laurency, Z. Makra, *Inorg. Chim. Acta* 139 (1987) 141.
- [12] X. Wang, T. Jin, V. Comblin, A. Lopez-Mut, E. Merciny, J.F. Desreux, *Inorg. Chem.* 31 (1992) 1095.
- [13] L. Burai, I. Fábrián, R. Király, E. Szilágyi, E. Brücher, *J. Chem. Soc., Dalton Trans.* (1998) 243.
- [14] C.A. Chang, Y.-L. Liu, C.-Y. Chen, X.-M. Chou, *Inorg. Chem.* 40 (2001) 3448.
- [15] Z. Baranyai, I. Banyai, E. Brücher, R. Király, E. Terreno, *Eur. J. Inorg. Chem.* (2007) 3639.
- [16] Z. Baranyai, E. Brücher, T. Ivanyi, R. Király, I. Lázár, L. Zékány, *Helv. Chim. Acta* 88 (2005) 604.
- [17] K. Kumar, M.F. Tweedle, *Inorg. Chem.* 32 (1993) 4193.
- [18] E. Szilágyi, É. Tóth, Z. Kovács, J. Platzek, B. Radüchel, E. Brücher, *Inorg. Chim. Acta* 298 (2000) 226.
- [19] P. Táborský, I. Svobodová, P. Lubal, Z. Hnatejko, S. Lis, P. Hermann, *Polyhedron* 26 (2007) 4119.
- [20] P. Táborský, I. Svobodová, Z. Hnatejko, P. Lubal, S. Lis, M. Försterová, P. Hermann, I. Lukeš, J. Havel, *J. Fluorescence* 15 (2005) 507.
- [21] P. Táborský, P. Lubal, J. Havel, J. Kotek, J. Rudovský, P. Hermann, I. Lukeš, *Collect. Czech. Chem. Commun.* 70 (2005) 1909.
- [22] L. Burai, R. Király, I. Lázár, E. Brücher, *Eur. J. Inorg. Chem.* (2001) 813.
- [23] T. Vitha, V. Kubíček, P. Hermann, Z.I. Kolar, H.T. Wolterbeek, J.A. Peters, I. Lukeš, *Langmuir* 24 (2008) 1952.
- [24] V. Kubíček, J. Rudovský, J. Kotek, P. Hermann, L. Vander Elst, R.N. Muller, Z.I. Kolar, H.T. Wolterbeek, J.A. Peters, I. Lukeš, *J. Am. Chem. Soc.* 127 (2005) 16477.
- [25] T. Vitha, V. Kubíček, P. Hermann, L. Vander Elst, R.N. Muller, Z.I. Kolar, H.T. Wolterbeek, W.A.P. Breeman, I. Lukeš, J.A. Peters, *J. Med. Chem.* 51 (2008) 677.
- [26] T. Vitha, V. Kubíček, J. Kotek, P. Hermann, L. Vander Elst, R.N. Muller, I. Lukeš, J.A. Peters, *Dalton Trans.* (2009) 3204.
- [27] M. Meckel, A. Nauth, J. Timpe, K. Zheronosekov, A.D. Puranik, R. Baum, F. Roesch, *Cancer Biother. Radiopharm.* 30 (2015) 94.
- [28] R. Bergmann, M. Meckel, V. Kubíček, J. Pietzsch, J. Steinbach, P. Hermann, F. Rösch, *EJNMMI Res.* 6 (2016) 5.
- [29] R.P. Baum, H.R. Kulkarni, *Theranostics* 2 (2012) 437.
- [30] J.F. Desreux, *Inorg. Chem.* 19 (1980) 1319.
- [31] T. Kimura, Y. Kato, $q = 1.05 \times S_{H}^{-1} - 0.44$, where S_{H}^{-1} is luminescence decay rate measured in H₂O, *J. Alloys Compd.* 275 (1998) 806.
- [32] V. Kubíček, T. Vitha, J. Kotek, P. Hermann, L. Vander Elst, R.N. Muller, I. Lukeš, J.A. Peters, *Contrast Media Mol. Imaging* 5 (2010) 294.
- [33] S. Aime, M. Botta, E. Terreno, P.L. Anelli, F. Uggeri, *Magn. Reson. Med.* 30 (1993) 583.
- [34] Z. Kotková, G.A. Pereira, K. Djanashvili, J. Kotek, J. Rudovský, P. Hermann, L. Vander Elst, R.N. Muller, C.F.G.C. Geraldes, I. Lukeš, J.A. Peters, *Eur. J. Inorg. Chem.* (2009) 119.
- [35] E. Matczak-Jon, V. Videnova-Adrabska, *Coord. Chem. Rev.* 249 (2005) 2458.
- [36] V. Kubíček, J. Kotek, P. Hermann, I. Lukeš, *Eur. J. Inorg. Chem.* (2007) 333.
- [37] P.A. Stenson, A.L. Thompson, D. Parker, *Dalton Trans.* (2006) 3291.
- [38] J. Šimeček, P. Hermann, J. Havlíčková, E. Herdtweck, T.G. Kapp, N. Engelbogen, H. Kessler, H.-J. Wester, J. Notni, *Chem. Eur. J.* 19 (2013) 7748.
- [39] M. Pniok, V. Kubíček, J. Havlíčková, J. Kotek, A. Sabatie-Gogová, J. Plutnar, S. Huclier-Markai, P. Hermann, *Chem. Eur. J.* 20 (2014) 7944.
- [40] J. Holub, M. Meckel, V. Kubíček, F. Rösch, P. Hermann, *Contrast Media Mol. Imaging* 10 (2015) 122.
- [41] J. Notni, P. Hermann, J. Havlíčková, J. Kotek, V. Kubíček, J. Plutnar, N. Loktionova, P.J. Riss, F. Rösch, I. Lukeš, *Chem. Eur. J.* 16 (2010) 7174.
- [42] J. Šimeček, M. Schulz, J. Notni, J. Plutnar, V. Kubíček, J. Havlíčková, P. Hermann, *Inorg. Chem.* 51 (2012) 577.
- [43] T. David, V. Kubíček, O. Gutten, P. Lubal, J. Kotek, H.-J. Pietzsch, L. Rulíšek, P. Hermann, *Inorg. Chem.* 54 (2015) 11751.

Formation kinetics of europium(III) complexes of DOTA and its bis(phosphonate) bearing analogues

Soňa Procházková^a, Jakub Hraníček^b, Vojtěch Kubíček^{a,*} and Petr Hermann^a

^a Department of Inorganic Chemistry, Faculty of Science, Charles University, Hlavova 2030, 128 40 Prague 2, Czech Republic; tel.: +420 22195 1436; e-mail: kubicek@natur.cuni.cz

^b Department of Analytical Chemistry, Faculty of Science, Charles University, Hlavova 2030, 128 40 Prague 2, Czech Republic

Content

Figure S1. Progress of absorption spectra in the course of europium(III) complexation with H₄dota.

Figure S2. Progress of absorption spectra in the course of europium(III) complexation with H₈do3aP^{BP}.

Figure S3. The Arrhenius type of temperature dependence of formation rate constants employed for estimation of activation parameters.

Figure S4. Time dependence of Eu(III) hydration number in the course of complexation with H₄dota

Figure S5. UV-VIS spectra of Ce-dota *out-of-cage* complexes.

Figure S6. Time dependence of Eu(III) hydration number in the course of complexation with H₈do3aP^{BP}.

Figure S7. Time dependence of Eu(III) hydration number in the course of complexation with H₇dotam^{BP}.

Figure S8. pH dependence of the formation rate constants of Eu(III)-dotam^{BP}.

Scheme S1. Suggested mechanism of europium(III) complexation with H₄dota.

Table S1. Rate constants obtained for Eu(III)-dota formation.

Table S2. Rate constants obtained for Eu(III)-do3aP^{BP} formation.

Table S3. Rate constants obtained for Eu(III)-dotam^{BP} formation.

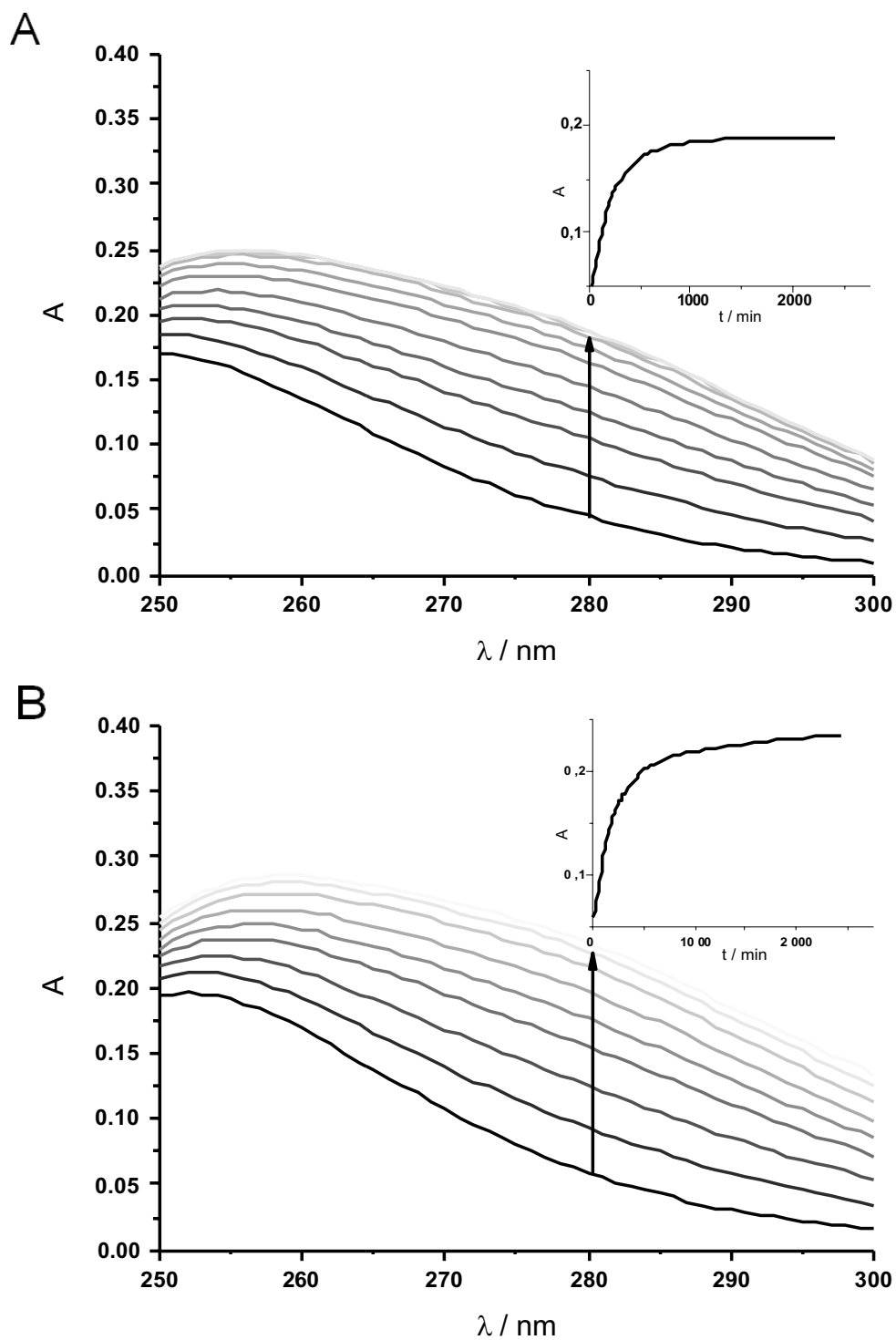


Figure S1. Progress of absorption spectra in the course of europium(III) complexation with H_4dota and time dependence of absorbance at $\lambda = 280 \text{ nm}$ (inset). A) $c_L = c_M = 2.5 \cdot 10^{-3} \text{ M}$; B) $c_L = 5 \cdot 10^{-3} \text{ M}$, $c_M = 2.5 \cdot 10^{-3} \text{ M}$.

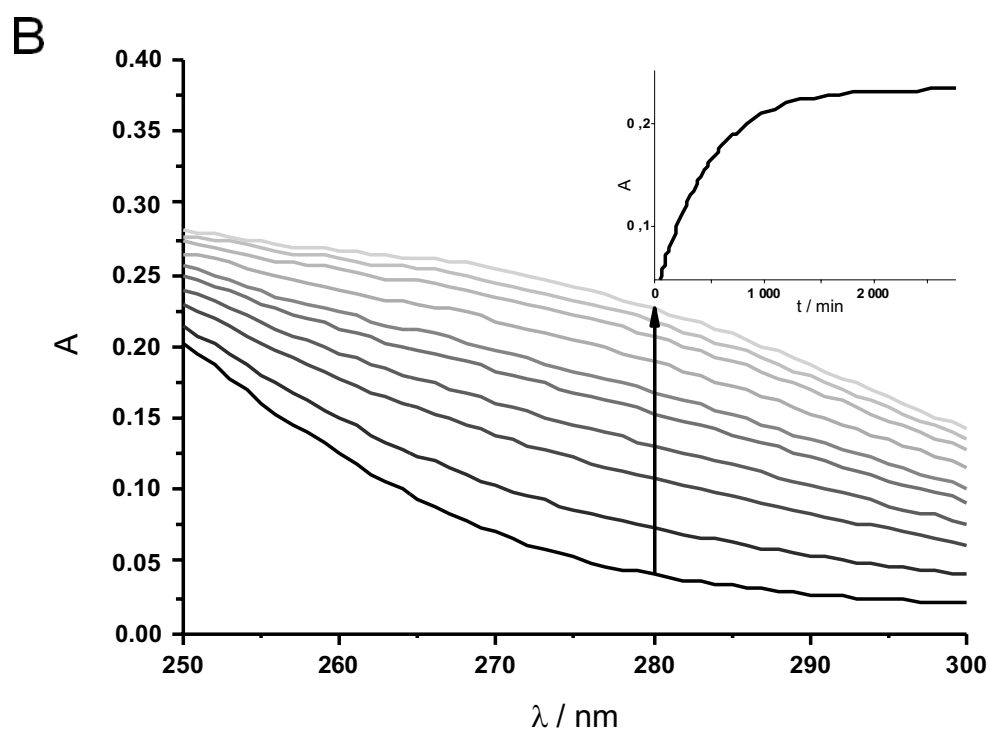
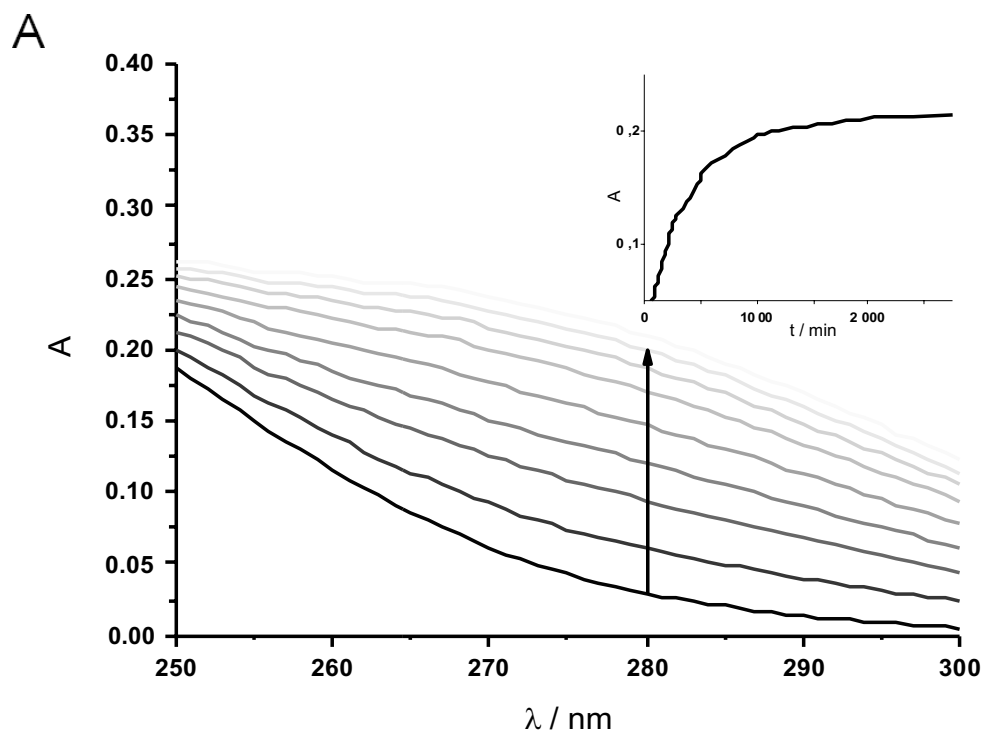


Figure S2. Progress of absorption spectra in the course of europium(III) complexation with H_8do3aP^{BP} and time dependence of absorbance at $\lambda = 280 \text{ nm}$ (inset). A) $c_L = c_M = 2.5 \cdot 10^{-3} \text{ M}$; B) $c_L = 5 \cdot 10^{-3} \text{ M}$, $c_M = 2.5 \cdot 10^{-3} \text{ M}$.

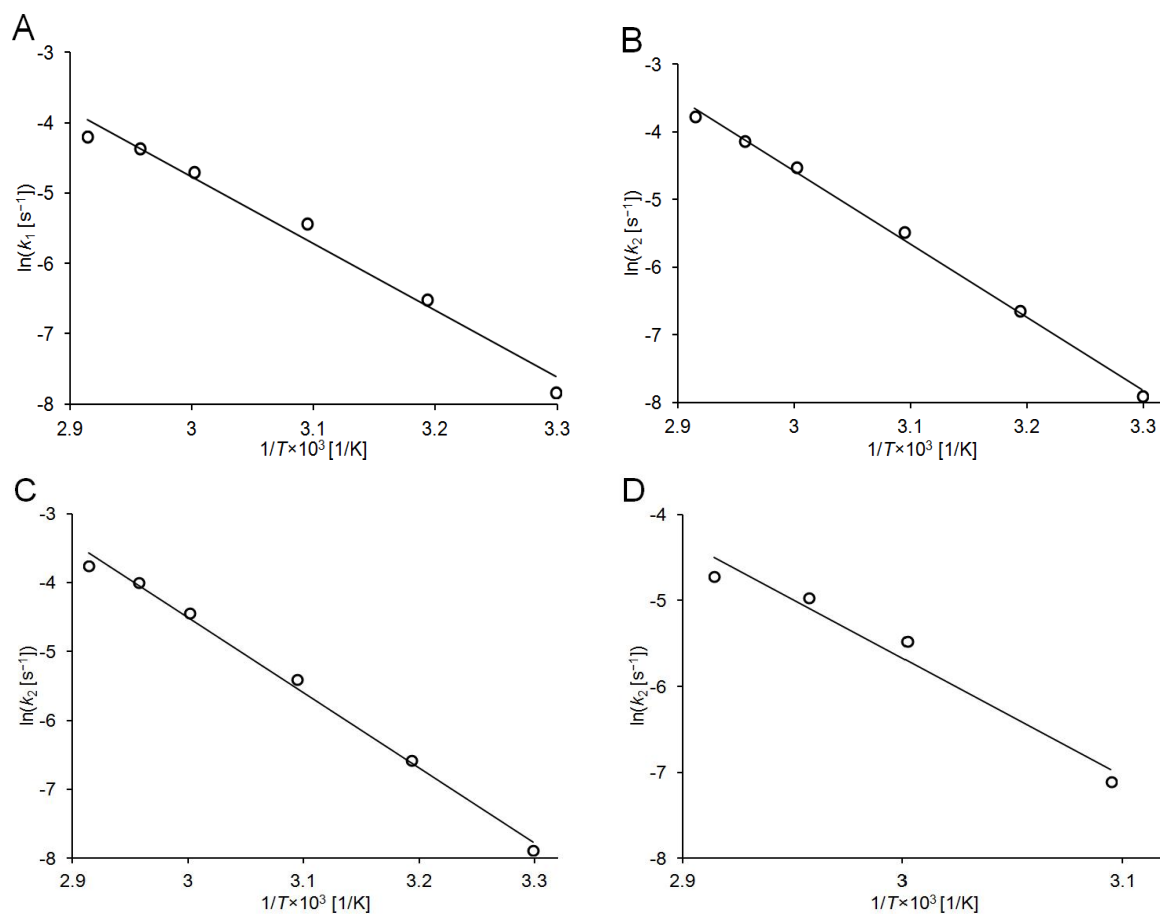


Figure S3. The Arrhenius type of temperature dependence of formation rate constants employed for estimation of activation parameters. A) Eu(III)-dota: metal excess; B) Eu(III)-dota: ligand excess; C) Eu(III)-do3aP^{BP}: ligand excess; D) Eu(III)-dotam^{BP}: ligand excess.

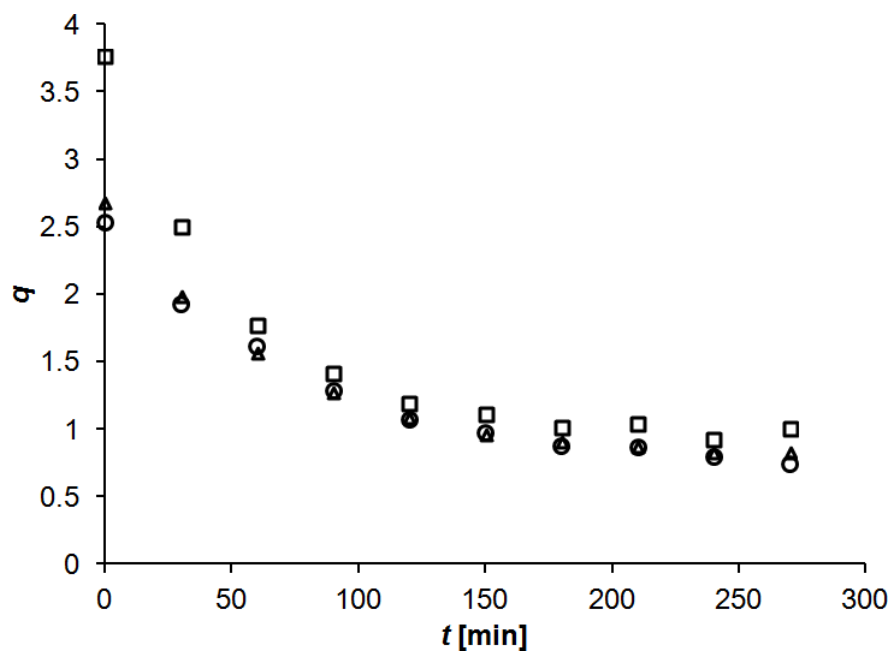


Figure S4. Time dependence of Eu(III) hydration number (q) in the course of complexation with H_4dota (at $pH = 3.5$); $c_{Eu} = 2.5 \cdot 10^{-3} M$, $c_L = 2.5 \cdot 10^{-3} M$ (squares), $c_L = 2.5 \cdot 10^{-2} M$ (circles), $c_L = 5 \cdot 10^{-2} M$ (triangles).

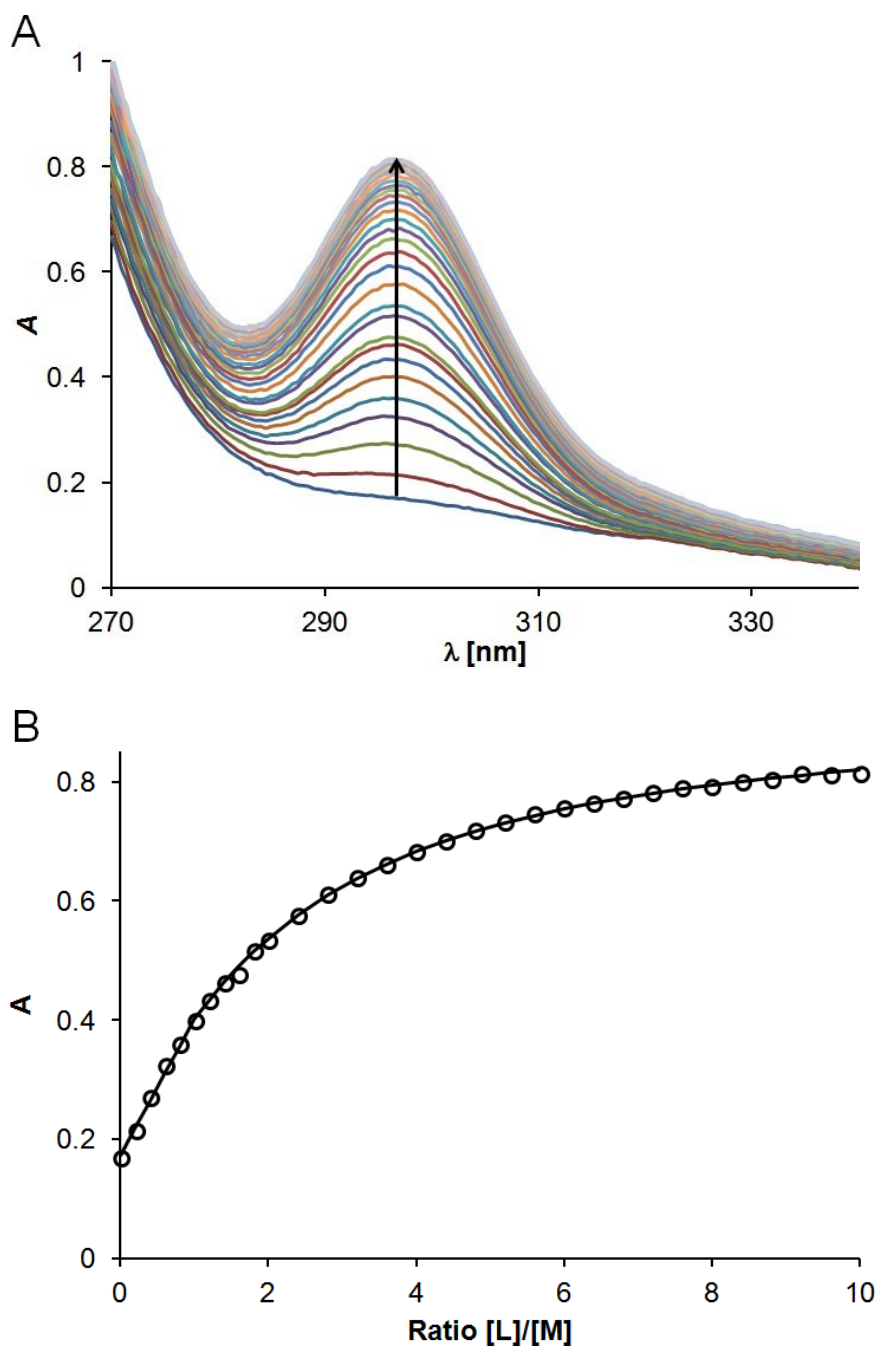


Figure S5. UV-VIS spectra of Ce(III)-dota out-of cage complexes (A) and dependence of absorbance at 297 nm on metal to ligand ratio (B). pH = 3, $c_M = 2.5 \cdot 10^{-3}$ M, $c_L = 0-25 \cdot 10^{-3}$ M, the line corresponds to the best fit.

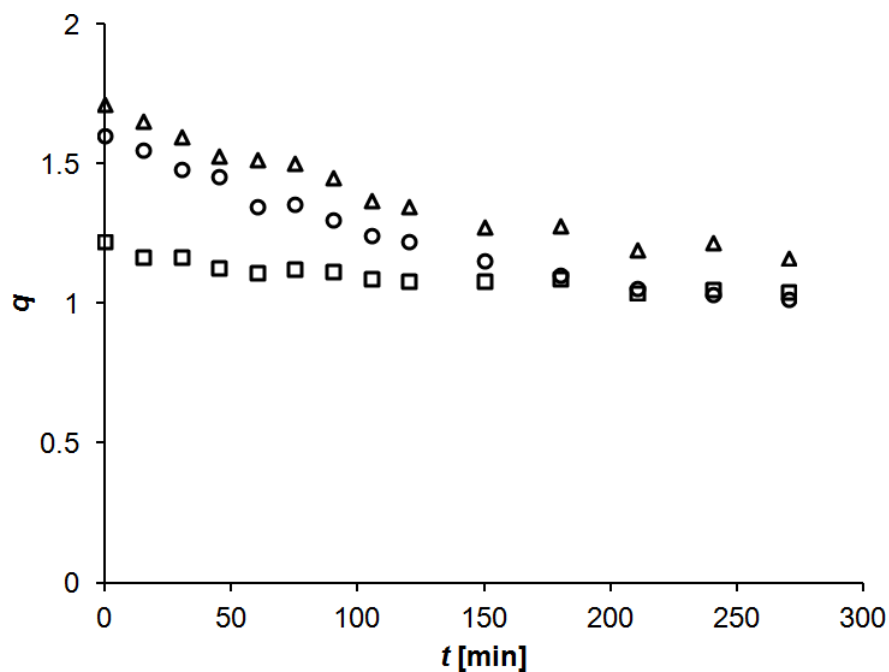


Figure S6. Time dependence of Eu(III) hydration number (q) in the course of complexation with $\text{H}_8\text{do3aP}^{\text{BP}}$ (at $\text{pH} = 3.5$); $c_{\text{Eu}} = 2.5 \cdot 10^{-3} \text{ M}$, $c_L = 2.5 \cdot 10^{-3} \text{ M}$ (squares), $c_L = 2.5 \cdot 10^{-2} \text{ M}$ (circles), $c_L = 5 \cdot 10^{-2} \text{ M}$ (triangles).

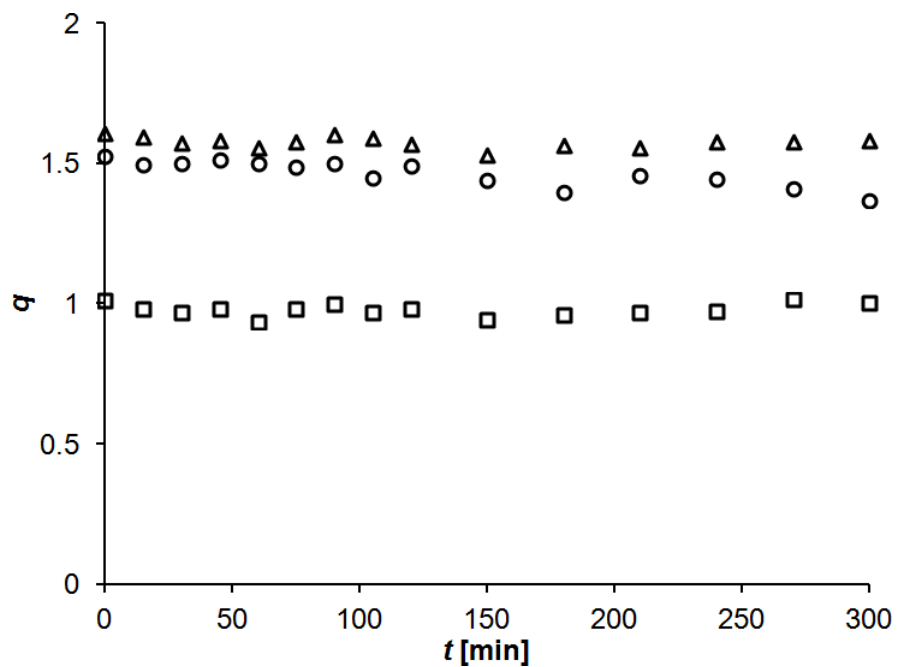


Figure S7. Time dependence of Eu(III) hydration number in the course of complexation with $\text{H}_7\text{dotam}^{\text{BP}}$ (at $\text{pH} = 4.0$); $c_{\text{Eu}} = 2.5 \cdot 10^{-3} \text{ M}$, $c_L = 2.5 \cdot 10^{-3} \text{ M}$ (squares), $c_L = 2.5 \cdot 10^{-2} \text{ M}$ (circles), $c_L = 5 \cdot 10^{-2} \text{ M}$ (triangles).

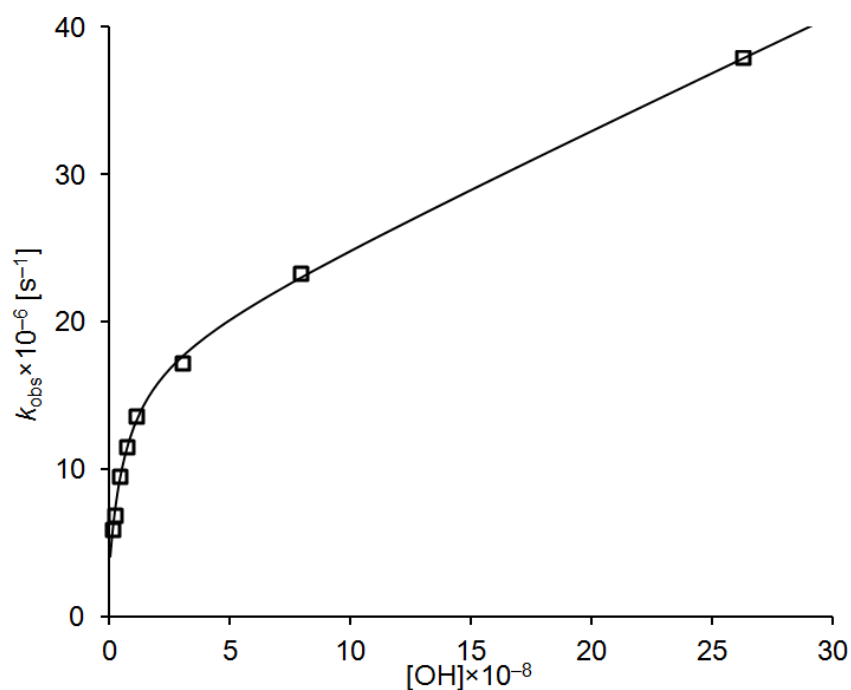
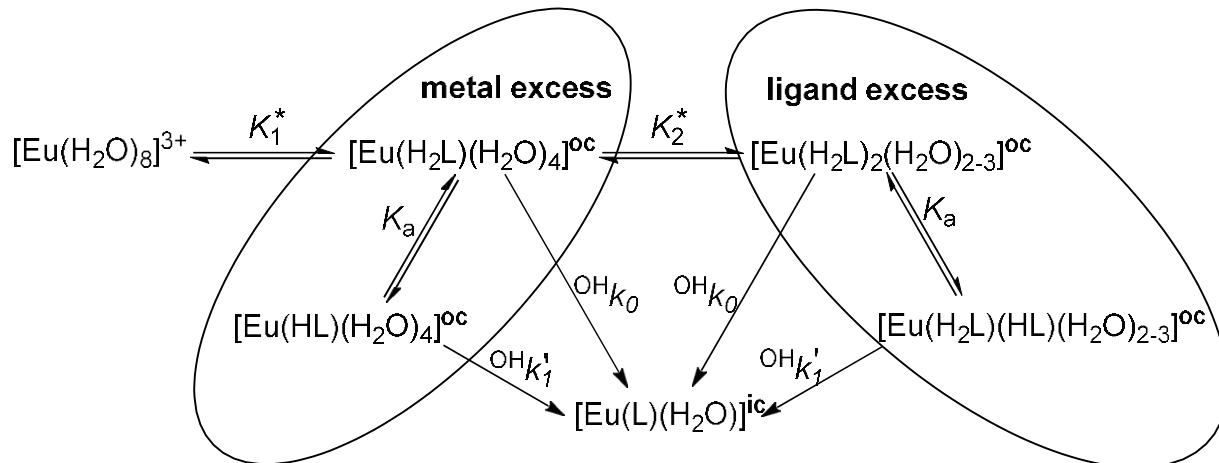


Figure S8. pH dependence of the formation rate constants of Eu(III)-dotam^{BP} complex (25 °C, $c_{\text{Eu}} = 2.5 \cdot 10^{-3}$ M, $c_{\text{L}} = 1.25 \cdot 10^{-2}$ M). The solid line corresponds to the best fits obtained according to Equation 12.



Scheme S1. Suggested mechanism of europium(III) complexation with H₄dota. For both reaction pathways ${}^{\text{OH}}k_1 = {}^{\text{OH}}k_1' \cdot K_a$. The two constants ${}^{\text{OH}}k_1'$ and K_a cannot be individually determined and only rate constant ${}^{\text{OH}}k_1$ is available from the measured data.

Table S1. Rate constants obtained for Eu(III)-dota formation (pH = 3.5).

<i>T</i> / K	303.15	313.15	323.15	333.15	338.15	343.15
<i>k</i> ₁ [s ⁻¹]	(4.0±0.1) ×10 ⁻⁴	(1.49±0.05) ×10 ⁻³	(4.4±0.2) ×10 ⁻³	(9.2±0.3) ×10 ⁻³	(1.29±0.04) ×10 ⁻²	(1.51±0.01) ×10 ⁻²
<i>k</i> ₂ [s ⁻¹]	(3.7±0.3) ×10 ⁻⁴	(1.3±0.2) ×10 ⁻³	(4.2±0.2) ×10 ⁻³	(1.09±0.05) ×10 ⁻²	(1.6±0.3) ×10 ⁻²	(2.30±0.03) ×10 ⁻²

Table S2. Rate constants obtained for Eu(III)-do3aP^{BP} formation (pH = 3.5).

<i>T</i> / K	303.15	313.15	323.15	333.15	338.15	343.15
<i>k</i> ₂ [s ⁻¹]	(3.8±0.3) ×10 ⁻⁴	(1.4±0.1) ×10 ⁻³	(4.5±0.2) ×10 ⁻³	(1.18±0.05) ×10 ⁻²	(1.84±0.05) ×10 ⁻²	(2.34±0.07) ×10 ⁻²


Table S3. Rate constants obtained for Eu(III)-dotam^{BP} formation (pH = 4.0).

<i>T</i> / K	323.15	333.15	338.15	343.15
<i>k</i> ₁ [s ⁻¹]	(1.3±0.7) ×10 ⁻⁵	(3±2) ×10 ⁻⁵	(9±9) ×10 ⁻⁵	(2.0±0.4) ×10 ⁻⁴
<i>k</i> ₂ [s ⁻¹]	(8.2±0.7) ×10 ⁻⁴	(4.2±0.2) ×10 ⁻³	(7.0±0.9) ×10 ⁻³	(9.0±0.2) ×10 ⁻³
<i>K</i> ₂ [*] [M ⁻¹]	25±4	25±2	23±6	33±1



Cite this: *Dalton Trans.*, 2017, 46, 10484

DOTA analogues with a phosphinate- iminodiacetate pendant arm: modification of the complex formation rate with a strongly chelating pendant†

Soňa Procházková, Vojtěch Kubíček,  * Zuzana Böhmová, Kateřina Holá, Jan Kotek
and Petr Hermann

The new ligand H_6do3aP^{ida} combines the macrocyclic DOTA-like cavity and the open-chain iminodiacetate group connected through a coordinating phosphinate spacer. Its acid–base and coordination properties in solution were studied by potentiometry. Thermodynamic coordination characteristics of both chelating units are similar to those reported for H_4dota and iminodiacetic acid themselves, respectively, so, macrocyclic and iminodiacetate units behave independently. The formation kinetics of the $Ce(III)$ – H_6do3aP^{ida} complex was studied by UV-Vis spectrophotometry. Various out-of-cage intermediates were identified with 1 : 1, 1 : 2 and 2 : 1 ligand-to-metal ratios. The presence of the strongly coordinating iminodiacetate group significantly slows down the metal ion transfer into the macrocyclic cavity and, so, the formation of the in-cage complex is two orders of magnitude slower than that reported for the $Ce(III)$ – H_4dota system. The kinetic inertness of the $[Ce(do3aP^{ida})]^{3-}$ complex towards acid-assisted dissociation is comparable to that of the $[Ce(dota)]^-$ complex. The coordination modes of the ligand are demonstrated in the solid-state structure of $[Cu_4(do3aP^{ida})(OH)(H_2O)_4]Cl \cdot 7.5H_2O$.

Received 17th May 2017,
Accepted 14th July 2017

DOI: 10.1039/c7dt01797a

rsc.li/dalton

Introduction

The macrocyclic ligand H_4dota (Chart 1) and its analogues are used as chelating agents for complexation of various metal ions. The most attention has been focused on lanthanide(III)

complexes as the denticity and size of the cavity in DOTA-like ligands are optimal for these ions. The complexes have found applications mainly in medical imaging techniques, such as Magnetic Resonance Imaging (MRI), Single-Photon Emission Computed Tomography (SPECT), Positron Emission Tomography (PET) or Optical Imaging (OI), and in radiotherapy.^{1–7}

The critical point in the applications of DOTA-like complexes in radiomedicine is their complex formation rate. Slow complexation that is typical of macrocyclic ligands becomes the limiting factor mainly while working with short living radioisotopes. The harsh conditions usually used for the lanthanide(III) complexation are often incompatible with biomolecules (*e.g.* oligopeptides or antibodies) which are used as vectors in the agents currently developed and studied for targeted imaging and therapy. Thus, the improvement of the complexation rate still attracts a lot of attention. The complexation rate is governed by various factors such as the basicity of the macrocycle amino groups, the number and the nature of the pendant arms, the symmetry of the complexes, *etc.* The complexation of DOTA-like ligands is commonly described as a two-step process.^{8–14} In the first step, the metal ion is swiftly coordinated by the pendant arm oxygen atoms forming an out-of-cage complex. In such an intermediate, the macrocycle amino groups are protonated and the rate-determining step of

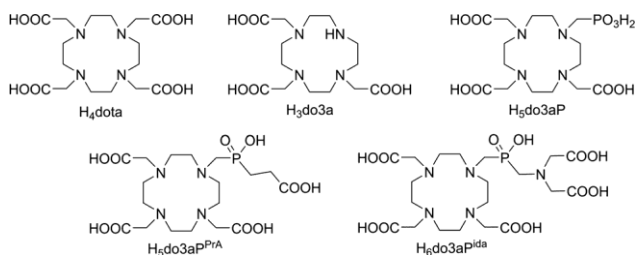


Chart 1 Ligands discussed in the text.

Department of Inorganic Chemistry, Faculty of Science, Charles University, Hlavova 2030, 128 40 Prague 2, Czech Republic. E-mail: kubicek@natur.cuni.cz; Fax: +420 221951253; Tel: +420 221951436

† Electronic supplementary information (ESI) available: NMR spectra, detailed description and results of potentiometry, distribution diagrams, tables and figures related to solid-state structures, and UV-Vis spectra of the complexes. CCDC 1482406 and 1482407. For ESI and crystallographic data in CIF or other electronic format see DOI: 10.1039/c7dt01797a

the complexation is the deprotonation of the ring nitrogen atoms and the transfer of the metal ion into the central ligand cavity which results in the formation of an in-cage complex with the metal ion coordinated by the four nitrogen and four oxygen atoms. Recently, we have shown that the presence of the phosphonate and/or phosphinate pendants increases the complexation rate in comparison with commonly used carboxylate arms.^{15–17} The group attached to the phosphinate moiety further modifies the complexation rate. The significantly enhanced rate was described for the phosphinates bearing another coordinating (donor) group(s).^{18–20} However, the role of another coordinating group in the pendant arm for the coordination properties of the ligands is not fully understood.

In this work, we report on the synthesis and characterization of a DOTA-like ligand bearing an iminodiacetate (IDA) group attached to the phosphinate pendant arm, H₆do3a^{P_{ida}} (Chart 1). The IDA group was chosen as we expected the formation of the out-of-cage complexes with well-defined stoichiometry and sufficient stability so that the results might be easily evaluated. In recent years, several DOTA-like ligands bearing an iminodiacetate group in the pendant arm have been reported as radionuclide carriers,^{21–25} calcium responsive agents^{26,27} or bone targeting²⁸ and micellar²⁹ luminescent probes. However, the effect of the IDA group on the coordination properties of the ligands has been studied only briefly. Here, we evaluate the formation rate, thermodynamic stability and kinetic inertness of metal complexes with the title ligand with respect to their potential applications in MRI and radiomedicine.

Experimental part

Materials and methods

Commercially available chemicals were used as received. *t*-Bu₃do3a·HBr (H₃do3a = 1,4,7,10-tetraazacyclododecane-1,4,7-triacetic acid) was synthesized according to the published procedure.³⁰ ¹H (400 or 300 MHz), ¹³C (100 or 75 MHz) and ³¹P (162 or 122 MHz) NMR spectra were acquired at 25 °C (unless stated otherwise) with Varian Unity Inova-400 and -300 spectrometers, respectively. For the ¹H and ¹³C NMR measurements in D₂O, the methyl signal of *t*-BuOH was used as an internal standard ($\delta = 1.2$ and 31.2 ppm for ¹H and ¹³C NMR, respectively). The ³¹P chemical shifts were measured with respect to 1% H₃PO₄ in D₂O as an external reference. ESI-MS spectra were recorded on a Bruker Esquire 3000 spectrometer equipped with an electrospray ion source and ion-trap detection system.

[N,N-Bis(carboxymethyl)aminomethyl]phosphinic acid

Iminodiacetic acid (5.02 g, 38 mmol) was suspended in water (50 ml). The mixture was heated at 40 °C and 50% aq. H₃PO₂ (24.82 g, 188 mmol) was added over 10 min. Then, paraformaldehyde (1.25 g, 42 mmol) was added in small portions over 60 min. The mixture was acidified with conc. aq. HCl (0.5 ml)

and stirred at 40 °C for 72 h. Then, the solid was filtered off. The crude product was dissolved in a minimum amount of boiling water. The solution was acidified with conc. aq. HCl (0.5 ml). After standing overnight, the white crystalline solid was filtered off, washed with ethanol and dried over P₂O₅, affording 2.8 g of the product (35%).

NMR (in D₂O/NaOD, pD ~ 12): ¹H: 3.47 (P-CH₂-N, d, 2H, ²J_{HP} = 10.4 Hz); 4.19 (N-CH₂-CO₂H, s, 4H); 7.26 (H-P, d, 1H, ¹J_{HP} = 553 Hz); ¹³C{¹H}: 53.7 (P-CH₂-N, d, ¹J_{CP} = 83 Hz); 57.5 (N-CH₂-CO₂H, s); 169.2 (COOH, s); ³¹P: 11.94 (d, ¹J_{HP} = 553 Hz). MS: (–) 209.5 (M – H)[–]. Elemental analysis: found (calculated for C₅H₁₀NO₆P) C: 28.44 (28.45), H: 4.60 (4.77), N: 6.54 (6.63), P: 14.48 (14.67).

10-({Hydroxy[N,N-bis(carboxymethyl)aminomethyl]phosphoryl}methyl)-1,4,7,10-tetraazacyclododecane-1,4,7-triacetic acid

tBu₃do3a·HBr (3.86 g, 6.5 mmol) was dissolved in a mixture of trifluoroacetic acid (40 ml) and chloroform (40 ml) and the resulting solution was refluxed for 24 h. Then, volatiles were removed under vacuum. The resulting oily residue was dissolved in water (20 ml), mixed with aq. conc. HCl (20 ml) and [N,N-bis(carboxymethyl)aminomethyl]phosphinic acid (2.73 g, 13 mmol) was added. The resulting mixture was heated at 50 °C and paraformaldehyde (0.58 g, 19 mmol) was added in small portions. The reaction mixture was stirred overnight. Volatiles were evaporated on a rotary evaporator. The oily residue was purified on a strong cation exchanger (Dowex 50, H⁺-form). Impurities were eluted with water and the product was eluted with 5% aq. ammonia. The product-containing fractions were evaporated and purified on a strong anion exchanger (Dowex 1, acetate form). Impurities were eluted with water followed by 2% aq. AcOH. The product was eluted with 6 M aq. HCl. Volatiles were evaporated and the oily residue was recrystallized from water by the addition of EtOH. The product was filtered off, washed with EtOH and dried over P₂O₅. The product (2.32 g, 63%) was obtained as a non-stoichiometric hydrate in the form of white powder.

NMR (in D₂O, pD = 6): ¹H: 3.13 (cyc_{bs}, 4H), 3.16 (P-CH₂-cyclen, d, 2H, ²J_{HP} = 4.9 Hz), 3.25 (cyc_{bs}, 4H), 3.37 (cyclen-CH₂-COOH, s, 4H), 3.41 (P-CH₂-IDA, d, 2H, ²J_{HP} = 7.3 Hz), 3.45 (cyc_{bs}, 4H), 3.50 (cyc_{bs}, bs, 4H), 3.85 (cyclen-CH₂-COOH, s, 2H), 3.92 (IDA-CH₂-COOH, s, 4H); ¹³C{¹H}: 48.4 (cyc_{bs}), 49.2 (cyc_{bs}), 51.1 (cyclen, s), 51.7 (cyc_{bs}, s), 52.7 (cyclen-CH₂-P, d, ¹J_{CP} = 98 Hz), 53.7 (IDA-CH₂-P, d, ¹J_{CP} = 79 Hz), 55.7 (cyclen-CH₂-COOH, s), 56.7 (cyclen-CH₂-COOH, s), 58.8 (IDA-CH₂-COOH, s), 171.9 (IDA-CH₂-COH, s), 172.1 (cyclen-CH₂-COOH, s), 179.0 (cyclen-CH₂-COH, s); ³¹P{¹H}: 24.98 (s). ¹H, ¹³C{¹H} and ³¹P{¹H} NMR spectra are shown in Fig. S1.† MS: (–) 568.0 (M – H)[–]. Elemental analysis: found (calculated for C₂₀H₃₆N₅O₁₂P·3.5H₂O) C: 37.93 (37.98), H: 6.50 (6.85), N: 10.80 (11.07), P: 4.78 (4.90).

Potentiometric titrations

The methodology of the potentiometric titrations and processing of the experimental data were analogous to those pre-

viously reported.^{17,31} For the detailed procedure, see the ESI.† Titrations were carried out in a vessel thermostated at 25 ± 0.1 °C at ionic strength $I = 0.1$ M (NMe₄)Cl. The ligand-to-metal ratio was 1 : 1 (and 1 : 2 or 2 : 1 in some cases) with $c_L = 4$ mM, and the pH range was 1.7–12.0 (or till precipitation of the metal hydroxide). The titrations were carried out at least three times, each consisting of about 40 points. The water ion product, $pK_w = 13.81$, and stability constants of M^{2/3+}–OH[–] systems were taken from ref. 32. The calculated overall protonation constants β_h are concentration constants and are defined by $\beta_h = [H_hL]/([H]^h \times [L])$, and consecutive protonation constants are $\log K(HL) = \log \beta_1$ and $\log K(H_hL) = \log \beta_h - \log \beta_{h-1}$. The overall stability constants are defined by $\beta_{hlm} = [H_hL_lM_m]/([H]^h \times [L]^l \times [M]^m)$. The constants (with standard deviations) were calculated with the program OPIUM.³³ Throughout the paper, pH means $-\log[H^+]$.

The stability constants of the Ln(III) complexes were obtained by the out-of-cell method. The batches (starting volume 1 ml) were prepared under an argon stream in tubes with ground joints from the ligand, metal ion and HCl/(NMe₄)Cl stock solutions and water (L : M = 1 : 0.95 molar ratio, $c_L = 0.004$ M). Then, the known amount of the (NMe₄)OH stock solution was added under Ar. The tubes were firmly closed with stoppers and the solutions were equilibrated at room temperature for 4 weeks (one batch was checked after 6 weeks and gave the same data). The titrations were performed in the pH range of 1.5–3.8 (the final pH values) with around 20 data points per titration and three titrations per system.

The solution of the pre-formed Ln(III) complexes (Ln = La, Nd, Eu, Gd and Y) was obtained by mixing a known amount of the ligand (5% molar excess) and LnCl₃ stock solutions in a glass ampoule followed by a slow portion-wise addition (2 h) of stock (NMe₄)OH solution (4 equiv.) under Ar, and the ampoule was flame-sealed and left at 80 °C overnight to fully form the in-cage complexes of the metal ions. The ampoule was opened under Ar and the aliquots of the in-cage-[Ln(do3aP^{ida})]^{3–} complex solutions were transferred into the titration vessel. Water, HCl and (NMe₄)Cl stock solutions (and in the case of the Gd(III) complex, also stock solutions of other metal chlorides) were added (to reach pH of about 1.8 and $I = 0.1$ M (H,NMe₄)Cl in the final solution, starting volume 5 mL, complex concentration ~0.004 M) and the in-cell titration was performed as above.

Kinetic studies

The experiments were carried out in the pH range of 3.5–9.0 at the temperature 25 ± 0.1 °C maintained by the Peltier block employing a spectrophotometer Specord 50 Plus (Analytik Jena AG). The kinetics was studied in 1 cm sample cells using the following non-coordinating buffers ($c = 0.2$ M): 1,4-dimethylpiperazine (pH < 5), acetic acid (pH 5–5.5), MES (pH 5.6–6.8; MES = 2-(*N*-morpholino)ethanesulfonic acid), HEPES (pH 6.8–8.2; HEPES = 2-[4-(2-hydroxyethyl)piperazin-1-yl]ethanesulfonic acid) and AMPSO (pH 8.3–9.0; AMPSO = *N*-(1,1-dimethyl-2-hydroxyethyl)-3-amino-2-hydroxypropanesulfonic acid). The

time dependence of absorbance at 314 nm was fitted with the general exponential function (eqn (1))

$$A = A_f + (A_0 - A_f)e^{-k_{\text{obs}}t} \quad (1)$$

where A is absorbance, A_f is the final absorbance, A_0 is the initial absorbance, t is time and k_{obs} is the rate constant of the reaction. The data were fitted by means of a least square fitting procedure using the Micromath Scientist program version 2.0 (Salt Lake City, UT, USA).

Formation kinetics of the in-cage Ce(III) complex was followed in the wavelength region of 270–360 nm using the pH range of 3.5–9 and the concentration ranges $c_{\text{Ce}} = 5.0 \times 10^{-4}$ – 7.5×10^{-3} M and $c_L = 5.0 \times 10^{-4}$ – 5.0×10^{-3} M. The experiments were initiated by the addition of the Ce(III) stock solution into the cell and the data acquisition started after 15 s dead time. The formation of the out-of-cage complex was monitored by obtaining UV-Vis spectra in the wavelength region of 270–360 nm immediately after mixing of the metal ion, ligand and stock buffer solutions ($c_{\text{Ce}} = 2.5 \times 10^{-3}$ M, $c_L = 0$ – 5×10^{-3} M, pH 4 and 8).

Dissociation kinetics of the in-cage [Ce(do3aP^{ida})]^{3–} complex ($c = 2.5 \times 10^{-3}$ M) was studied in HClO₄ ($c = 0.2$ – 3.0 M). The ionic strength was maintained by the addition of NaClO₄ ($I = 3$ M (H/Na)ClO₄).

X-ray diffraction studies

Single crystals of H₆do3aP^{ida}·4H₂O were obtained by a slow diffusion of EtOH vapour into an aq. solution of the ligand. Single crystals of [Cu₄(do3aP^{ida})(OH)(H₂O)₄]Cl·7.5H₂O were obtained by a slow diffusion of EtOH vapour into an aq. solution containing ligand and CuCl₂ (5 equiv.) adjusted to pH 4.1 by the addition of LiOH.

The diffraction data were collected at 150 K (Cryostream Cooler, Oxford Cryosystem) using a Nonius Kappa CCD diffractometer and Mo-K α radiation ($\lambda = 0.71073$ Å) and analysed using the HKL DENZO program package.³⁴ The structures were solved by direct methods (SIR92),³⁵ and refined by full-matrix least-squares techniques (SHELXL2014).³⁶ In general, all non-hydrogen atoms were refined anisotropically. All hydrogen atoms were located in the difference map of electron density; however, they were fixed in theoretical (C–H) or original (N–H, O–H) positions with thermal parameters $U_{\text{eq}}(\text{H}) = 1.2U_{\text{eq}}(\text{X})$ as their free refinement led to some unrealistic bond lengths. In the structure of H₆do3aP^{ida}·4H₂O, one of the water molecules was found to be disordered in two positions (one of them very close to the centre of symmetry) and was best refined with restrained occupancy of both positions 50 : 50%. In the structure of [Cu₄(do3aP^{ida})(OH)(H₂O)₄]Cl·7.5H₂O, the chloride anion was best refined disordered over three positions very close to each other; the relative occupancies of these positions were chosen to obtain comparable thermal parameters of all three atomic fragments, and were 50 : 35 : 15%; it was possible to use anisotropic refinement for all three positions. One of the water molecules lies very close to the centre of symmetry and, thus, its occupancy factor was set to 50%. Table S6† con-

tains selected crystallographic parameters for the structures reported in this paper. Complete data for the structures have been deposited with the Cambridge Crystallographic Data Centre as CCDC 1482406 and 1482407.†

Results and discussion

Ligand synthesis

A precursor of the phosphinate pendant arm of the designed ligand was prepared by reaction of iminodiacetic acid with hypophosphorous acid and paraformaldehyde at 40 °C using a modified procedure.³⁷ The resulting [*N,N*-bis(carboxymethyl)aminomethyl]phosphinic acid was consequently reacted with H₃do3a (prepared *in situ* from tBu₃do3a) and paraformaldehyde at 50 °C. The title compound was purified by ion exchange chromatography, isolated in its hexaprotonated zwitterionic form and finally crystallized from water by addition of EtOH. The solid-state structure of the ligand was determined by X-ray diffraction (Fig. 1). In the hexaprotonated ligand mole-

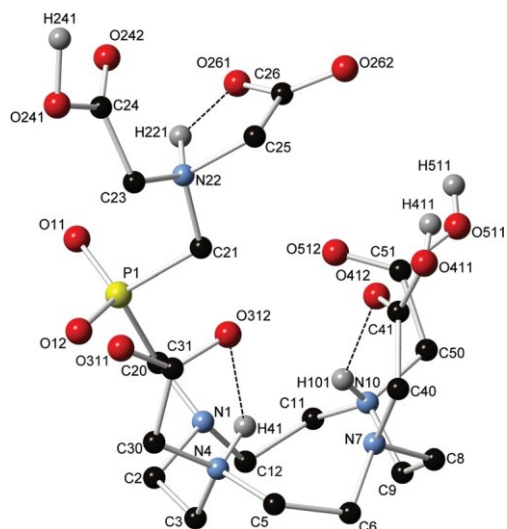


Fig. 1 The molecular structure of H₆do3aPida found in the solid-state structure of H₆do3aPida·4H₂O. The hydrogen atoms attached to the carbon atoms are not displayed for the clarity reasons. The dashed lines represent intramolecular hydrogen bonds. The data were collected at 150 K.

cule, two protons are bound to macrocycle nitrogen atoms as it is common for other cyclen-based ligands, forming the conformation of the macrocycle stabilized by intramolecular hydrogen bonds to non-protonated nitrogen atoms (N4–H41...N1, 3.018 Å and 102°; N4–H41...N7, 2.884 Å and 114°; N10–H101...N1, 3.016 Å and 105°; N10–H101...N7, 3.000 Å and 109°, for donor–acceptor distances and bond angles on the H-vertex, respectively) and pendant carboxylate oxygen atoms (N4–H41...O312, 2.685 Å and 107°; N10–H101...O412, 2.936 Å and 133°). Another proton is bound to the nitrogen atom of the IDA group that also forms an intramolecular hydrogen bond with one of the IDA acetate moieties (N22–H221...O261, 2.652 Å, 143°). The remaining three protons are bound to the carboxylate oxygen atoms – one of the IDA acetate groups (O241; involved in strong hydrogen bonding to the macrocycle-bound pendant from the neighbouring molecule, see below), and two of the acetate pendants (O411 and O511) bound to the macrocycle backbone (Fig. 1). Two molecules of H₆do3aPida are connected to the centrosymmetric head-to-head dimer through very short intermolecular hydrogen bonds ($d_{O...O}$ = 2.510 Å) between protonated IDA-carboxylate (O241) and one of the non-protonated carboxylate pendants bound to the macrocycle from the neighbouring molecule (O311). Such hydrogen bonding is reflected by the relatively long C–O bonds of both the involved oxygen atoms (1.264 and 1.309 Å for O241 and O311, respectively) and by the long distance of the related hydrogen atom from both oxygen atoms (1.219 and 1.342 Å, respectively).

Equilibrium data

The ligand contains two coordination centres, the DOTA-like macrocycle motif and the IDA-phosphinate moiety. To understand the properties of the ligand, information on how the parts communicate with each other is useful. Thus, the solution properties of the title ligand were studied by potentiometry. Seven protonation constants were determined (Tables 1 and S1†). Three protonations take place in the alkaline region and they correspond to the protonation of nitrogen atoms. The remaining four protonation constants lie in the acidic region and they correspond to the protonation of the carboxylate groups. The pH dependence of the ¹H NMR shifts of the acetate CH₂ groups (Fig. 2) indicates that the constant K_3 ($\log K_3$ = 8.13) describes the protonation of the amine in the

Table 1 Consecutive protonation constants of the discussed ligands and the pre-formed [Ln(do3aPida)]³⁻ complexes (25 °C, I = 0.1 M (NMe₄)Cl)

Constant	H ₆ do3aPida ^a	H ₄ dota ³⁸	H ₅ do3aPPrA ^{39,42}	[Ln(do3aPida)] ³⁻ ^{a,b}	H ₂ ida ⁴³
log K_1	12.85	12.93	12.68	7.67–7.95	9.32
log K_2	9.63	9.72	9.44	2.40–2.74	2.60
log K_3	8.13	4.62	5.04	1.51–1.77	—
log K_4	4.40	4.15	4.34	—	—
log K_5	3.27	2.29	2.94	—	—
log K_6	1.98	1.34	1.54	—	—
log K_7	1.58	—	—	—	—

^aFor overall equilibrium constants with experimental errors, see the ESI. ^bDetermined for pre-formed complexes with La(III), Nd(III), Eu(III), Gd(III) and Y(III) ions.

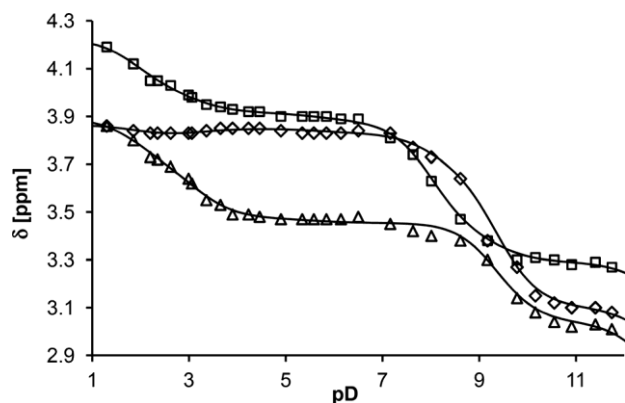


Fig. 2 ^1H NMR titration of the acetate CH_2 groups of $\text{H}_6\text{do3aP}^{\text{ida}}$ (diamonds and triangles – the DO3A group; squares – IDA group; 25°C).

IDA group and constants K_1 and K_2 correspond to the protonation of the macrocycle nitrogen atoms. All the protonations are reflected in the ^{31}P NMR titration curve (Fig. S2†) as the chemical shift gradually changes along the whole pH region of 7–10. The values of K_1 and K_2 are comparable to those of H_4dota ³⁸ or its monophosphinate analogues (e.g. $\text{H}_5\text{do3aP}^{\text{PrA}}$).³⁹ The assignment of the constant K_3 to the IDA moiety is supported also by the measurements of the first protonation constants of the pre-formed $[\text{Ln}(\text{do3aP}^{\text{ida}})]^{3-}$ complexes ($\log K_1 = 7.67\text{--}7.95$, Tables 1, 2 and S1†). In these complexes, the metal ion is bound in the macrocyclic cavity, and only the IDA group can be protonated. The protonation constant of this nitrogen atom is very similar (only slightly lower due to the charge effect of the central metal ion) to the value of the constant K_3 of the free $\text{H}_6\text{do3aP}^{\text{ida}}$. Compared to iminodiacetic acid itself, the constants of its phosphinic derivatives are by more than one order lower due to the electron withdrawing effect of the phosphinate group(s).^{40,41}

The complexation of $\text{Cu}(\text{II})$ and $\text{Zn}(\text{II})$ ions was studied by the standard potentiometric in-cell method at the 1 : 1 and 1 : 2 ligand-to-metal ratio. Both systems behave similarly and an analogous set of stability constants can be calculated (Table S2†). Under equimolar conditions, $[\text{M}(\text{L})]$ and $[\text{M}(\text{HL})]$ species are dominant in alkaline and neutral regions, respec-

tively (Fig. 3A). Values of the stability constants (Table 2) are higher by about one order in magnitude than those reported for H_4dota (Table S3†). It indicates that the metal ions are in $[\text{M}(\text{L})]$ species coordinated in the macrocyclic cavity. The mixture of the protonated species was identified in the acid region. Protons are bound to the IDA nitrogen atom or to non-coordinated carboxylates. The fact that only one carboxylate protonation was found for the $\text{Cu}(\text{II})$ complex indicates the coordination of two macrocycle carboxylate pendant arms, whereas the phosphinic group remains free. Similar coordination mode was found in the solid state (see below). Surprisingly, high abundance of the dinuclear complexes was found in the acid region even in solution with $\text{M} : \text{L} = 1 : 1$ molar ratio. The presence of the dinuclear complexes under equimolar conditions could be explained by changes of the charge-distribution associated with the coordination of the first metal ion. At low pH, the macrocyclic part is protonated on nitrogen atoms as well as on carboxylates. So, more than two protons dissociate due to the in-cage coordination of the metal ion. In the case of divalent ions, complexation leads to a decrease of the overall positive charge of the whole complex species. Consequently, coordination of the second metal ion by the IDA group is facilitated. Under the metal ion excess, dinuclear complexes are dominant along the whole pH range (Fig. 3B). As one ligand molecule does not saturate the coordination sphere of both metal ions in the dinuclear species, hydroxido-complexes are formed in the alkaline region.

The complexation of the $\text{Ln}(\text{III})$ ions is slow and, therefore, the systems were studied by the out-of-cell method in the acidic region. The out-of-cell titrations cannot be performed at $\text{pH} > 5$ due to the precipitation of lanthanide(III) hydroxides. However, at $\text{pH} < 5$, only protonated complexes $[\text{Ln}(\text{H}_3\text{L})]$, $[\text{Ln}(\text{H}_2\text{L})^-]$ and $[\text{Ln}(\text{HL})]^{2-}$ (although in in-cage binding mode, see below) are formed and, thus, full description of the systems was enabled only with the knowledge of the values of the first protonation constants (corresponding to the formation of $[\text{Ln}(\text{HL})]^{2-}$ belonging to the IDA moiety). Therefore, the acid–base titration of the pre-formed complex was performed, the protonation constant of $[\text{Ln}(\text{L})]^{3-}$ species was calculated and, consequently, the stability constant of the $[\text{Ln}(\text{L})]^{3-}$ complex was derived. As the systems were not studied in metal ion excess

Table 2 Equilibrium constants of the $\text{H}_6\text{do3aP}^{\text{ida}}$ complexes (25°C , $I = 0.1\text{ M (NMe}_4\text{)Cl}$)^a

Equilibrium ^b	$\text{Cu}(\text{II})$	$\text{Zn}(\text{II})$	$\text{La}(\text{III})$	$\text{Nd}(\text{III})$	$\text{Eu}(\text{III})$	$\text{Gd}(\text{III})$	$\text{Y}(\text{III})$
$\text{M} + \text{L} = [\text{M}(\text{L})]$	23.75	21.79	22.09	24.02	24.94	25.27	25.39
$[\text{M}(\text{HL})] = [\text{M}(\text{L})] + \text{H}^+$	8.40	8.46	7.67 ^c	7.83 ^c	7.83 ^c	7.79 ^c	7.95 ^c
$[\text{M}(\text{H}_2\text{L})] = [\text{M}(\text{HL})] + \text{H}^+$	3.84	3.76	3.20/2.58 ^c	2.94/2.46 ^c	2.95/2.40 ^c	2.60/2.74 ^c	2.40/2.57 ^c
$[\text{M}(\text{H}_3\text{L})] = [\text{M}(\text{H}_2\text{L})] + \text{H}^+$	—	2.98	2.23/1.63 ^c	2.22/1.51 ^c	2.27/1.59 ^c	2.13/1.56 ^c	2.20/1.77 ^c
$\text{M} + [\text{M}(\text{L})] = [\text{M}_2(\text{L})]$	10.96	9.59	<i>d</i>	<i>d</i>	<i>d</i>	<i>d</i>	<i>d</i>
$[\text{M}_2(\text{HL})] = [\text{M}_2(\text{L})] + \text{H}^+$	4.00	3.68	<i>d</i>	<i>d</i>	<i>d</i>	<i>d</i>	<i>d</i>
$[\text{M}_2(\text{H}_2\text{L})] = [\text{M}_2(\text{HL})] + \text{H}^+$	1.59	—	<i>d</i>	<i>d</i>	<i>d</i>	<i>d</i>	<i>d</i>
$[\text{M}_2(\text{L})] + \text{H}_2\text{O} = [\text{M}_2(\text{L})(\text{OH})] + \text{H}^+$	9.20	10.17	<i>d</i>	<i>d</i>	<i>d</i>	<i>d</i>	<i>d</i>
$[\text{M}_2(\text{L})(\text{OH})] + \text{H}_2\text{O} = [\text{M}_2(\text{L})(\text{OH})_2] + \text{H}^+$	12.05	—	<i>d</i>	<i>d</i>	<i>d</i>	<i>d</i>	<i>d</i>

^aFor overall stability constants, see the ESI. ^bCharges of complexes are omitted for clarity reasons. ^cDetermined from titrations of the pre-formed complexes. ^dThe systems were studied by the out-of-cell method and, thus, only the 1 : 1 metal-to-ligand ratio was utilized.

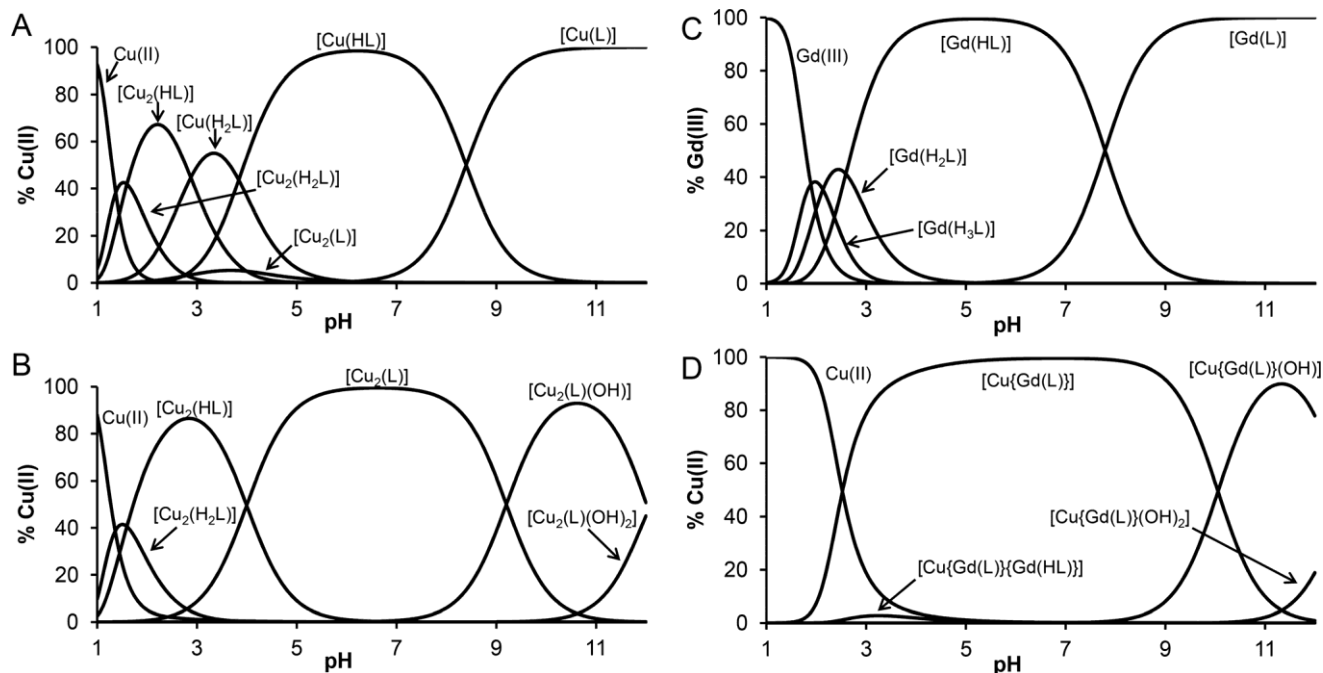


Fig. 3 Distribution diagrams of the Cu(II)–H₆do3aP^{ida} system at 1 : 1 (A) and 1 : 2 (B) ligand-to-metal ratios, Gd(III)–H₆do3aP^{ida} system at 1 : 1 ratio (C) and the ternary system Cu(II)–preformed [Gd(do3aP^{ida})]³⁻ at the 1 : 1 ratio (D) (25 °C, *I* = 0.1 M (NMe₄)Cl, *c*_L = 4 mM).

(metal hydroxide precipitation), only stability constants of the 1 : 1 complexes were obtained (Table 2). The stabilities of the complexes are slightly higher than those reported for H₄dota (Table S3†). The complexes are present in the protonated form at pH < 7 (Fig. 3C). Similarly to transition metal ion complexes, comparison of the stability constants with those of the complexes of the similar ligands (Table S3†) indicates that the [Ln(H_ndo3aP^{ida})]ⁿ⁻³ complexes (*n* = 0, 1) are in-cage species with the metal ions bound inside the macrocyclic cavity.

The presence of two different chelating centres allows the formation of heterodinuclear complexes. The coordination of Cu(II), Zn(II), Ca(II) and Eu(III) ions only by the IDA pendant arm was studied using the pre-formed [Gd(do3aP^{ida})]³⁻ complex. Lanthanide(III) complexes of the title ligand show a high kinetic inertness (see below) and, therefore, the pre-formed complex could be considered as an intact unit during

the course of in-cell potentiometric titrations and the coordination behaviour of the IDA-phosphinate moiety can be evaluated independently. The results are summarized in Table 3. The complexes with M : {Gd(L)} 1 : 1 stoichiometry are formed under the equimolar conditions (Fig. 2D, S3 and S4†) and the complexes with M : {Gd(L)} 1 : 2 stoichiometry are formed when the [Gd(do3aP^{ida})]³⁻ complex was used in excess (Fig. S3 and S4†). The first and the second consecutive stability constants describing the coordination of the [Gd(do3aP^{ida})]³⁻ unit to the Eu(III) ion are comparable, whereas the coordination of the second [Gd(do3aP^{ida})]³⁻ unit to Cu(II) or Zn(II) (already bound in [M{Gd(do3aP^{ida})]⁻ species) is more disfavoured due to the smaller size and lower positive charge of these ions. As the coordination spheres of the metal ions are not saturated, hydroxido complex species are formed in the alkaline region. The formation of the hydroxido complex in the system with

Table 3 Equilibrium constants of the metal ion–[Gd(do3aP^{ida})]³⁻ ternary complexes (25 °C, *I* = 0.1 M (NMe₄)Cl)

Equilibrium ^a	Cu(II)	Zn(II)	Ca(II)	Eu(III)
M + [Gd(L)] = [M{Gd(L)}]	10.53	8.10	5.19	8.98
[M{Gd(HL)}] = [M{Gd(L)}] + H ⁺	—	—	—	2.59
[M{Gd(L)}] + H ₂ O = [M{Gd(L)}(OH)] + H ⁺	9.06	^b	11.88	^b
[M{Gd(L)}(OH)] + H ₂ O = [M{Gd(L)}(OH) ₂] + H ⁺	11.62	^b	—	^b
[Gd(L)] + [M{Gd(L)}] = [M{Gd(L)} ₂]	4.87	5.20	—	7.33
[Gd(HL)] + [M{Gd(L)}] = [M{Gd(HL)}{Gd(L)}]	2.63	2.58	—	3.84
[M{Gd(HL)}{Gd(L)}] = [M{Gd(L)} ₂] + H ⁺	5.55	5.17	—	4.30
[M{Gd(L)} ₂] + H ₂ O = [M{Gd(L)} ₂ (OH)] + H ⁺	10.01	10.71	—	10.3
[M{Gd(L)} ₂ (OH)] + H ₂ O = [M{Gd(L)} ₂ (OH) ₂] + H ⁺	—	—	—	12.4

^aCharges of the complexes are omitted for clarity reasons. ^bThe constant cannot be determined due to the precipitation of metal hydroxide in the neutral region when metal excess was used.

Ca(II) ions might be explained by the dissociation of the proton from the water molecule coordinated to the Gd(III) ion that is facilitated by the Ca(II) ion coordinated in the proximity. The stability constants are similar to or slightly higher than those reported for the parent ligand, H₂ida (Table S5†), despite the lower basicity of the nitrogen atom in the [Gd(do3aP^{ida})]³⁻ complex. It originates from the higher denticity of the IDA-phosphinate coordination site, where the phosphinate group could be coordinated to both metal ions in the bridging mode. Thus, the IDA-phosphinate moiety behaves as a tetradentate ligand even if the phosphinate group is already bound to the metal ion which is located inside the macrocyclic cavity.

The values of protonation and stability constants show that both coordination sites – DOTA-like macrocycle and IDA-phosphinate – behave similarly to the parent ligands, H₄dota and H₂ida, respectively, and almost independently of each other, despite the presence of the very short and mutually shared spacer (Tables S3 and S5†).

Solid-state structure of the Cu(II) complex

Despite the numerous attempts to crystallize the Cu(II)–H₆do3aP^{ida} system, single-crystals suitable for the X-ray diffraction study were obtained only when the ligand was crystallized in the presence of a high excess of Cu(II) ions. The independent unit of the formed crystals has the composition [Cu₄(do3aP^{ida})(OH)(H₂O)₄]Cl·7.5H₂O, but two asymmetric units form a centrosymmetric dimer with the overall formula [Cu₈(do3aP^{ida})₂(OH)₂(H₂O)₈]Cl₂·15H₂O. The structure of the complex dimer is shown in Fig. 4 and coordination distances are summarized in Table S7.† Each of the four symmetrically independent Cu(II) ions exhibits different ligand coordination modes. The Cu1 ion is coordinated in the macrocyclic cavity (Fig. S5†) and its coordination mode is analogous to that in the Cu(II) complexes of H₄dota and related ligands.² The central metal ion is coordinated by four nitrogen atoms of the macrocycle and two oxygen atoms of the acetate pendants, forming a *cis*-N₄O₂ coordination environment. However, one of the oxygen atoms is coordinated with a relatively long distance (2.49 Å) and, thus, the complex geometry could be alternatively viewed also as a deformed square pyramid. In addition, the detailed coordination geometry in [Cu(do3aP^{ida})]⁴⁻ is somewhat different from those previously reported in the octahedral structures of Cu(II) complexes with H₄dota^{44–47} and related ligands,^{48–50} where the coordination sphere was usually axially elongated with the N₂O₂ equatorial base (typical equatorial bond lengths around $d_{\text{Cu-N}} \sim 2.0\text{--}2.1$ Å and $d_{\text{Cu-O}} \sim 1.9\text{--}2.0$ Å) and the remaining two nitrogen atoms of the macrocycle coordinated in more distant axial positions ($d_{\text{Cu-N}} \sim 2.3$ Å). In contrast, all nitrogen atoms in the [Cu(do3aP^{ida})]⁴⁻ unit are coordinated with short bond distances in a narrow range of 2.06–2.10 Å, and both *cis*-oxygen atoms of two acetate pendants are bound in more distant positions (2.22 and 2.49 Å). The Cu2 ion is coordinated in the square-planar environment with two additional very weak axial interactions (Fig. S6†). The nitrogen atom and both IDA carboxylates are coordinated in

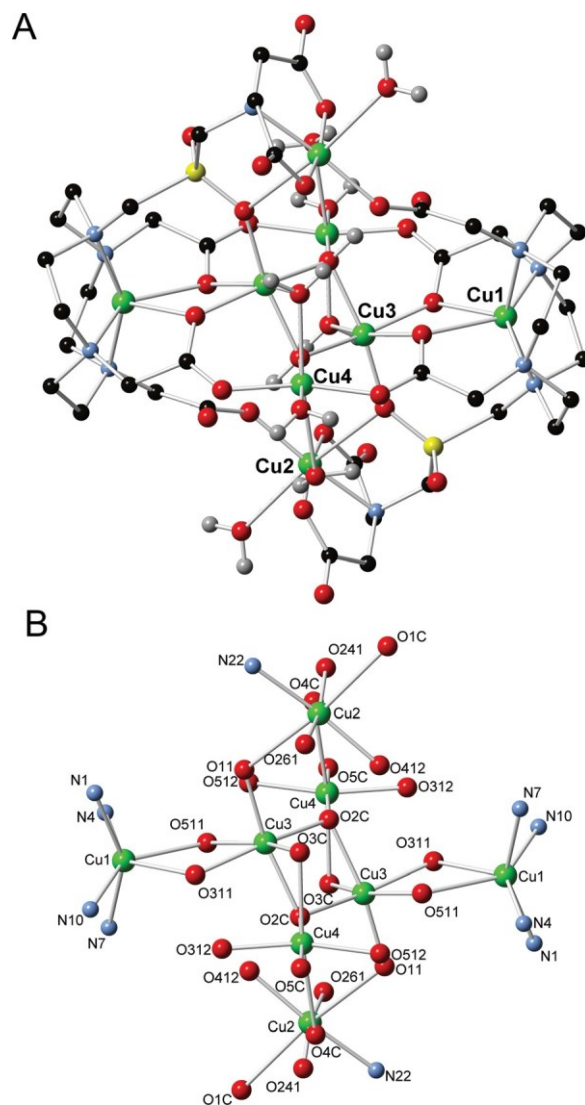


Fig. 4 Molecular structure of the dimeric [Cu₈(do3aP^{ida})₂(OH)₂(H₂O)₈]²⁺ cation found in the crystal structure of [Cu₄(do3aP^{ida})(OH)(H₂O)₄]Cl·7.5H₂O (A; hydrogen atoms attached to the carbon atoms are not displayed for the clarity reasons) and the coordination environment of the dimeric Cu₈ cluster (B; only the copper-coordinated atoms are displayed for the clarity reasons). The data were collected at 150 K.

the equatorial plane, and the fourth equatorial position is occupied by a carboxylate of the DO3A-group from the second (symmetrically related) ligand molecule. All equatorial distances are in a narrow range of 1.9–2.0 Å. The axial positions are significantly Jahn–Teller deformed and occupied by a water molecule (2.50 Å) and by a phosphinate oxygen atom (2.70 Å). The coordination spheres of the two remaining copper(II) ions are also very irregular and could be viewed as significantly axially elongated octahedrons. The two symmetrically associated Cu3 ions are bridged by two hydroxide anions coordinated in the distances ~ 1.98 Å (Fig. S7†). Another two coordination sites of each Cu3 ion are occupied by the two carboxylate oxygen atoms that are simultaneously coordinated

to Cu1. One of them is placed in the equatorial position (1.97 Å) and the other one is in the axial position (2.38 Å). The fourth equatorial site is occupied by the phosphinate oxygen atom (1.93 Å) already bound to Cu2 and the remaining axial position is occupied by the water molecule (2.49 Å, bridging to Cu4). The Cu4 ion bridges the two ligand molecules (Fig. S8†) through the macrocycle acetate pendants coordinated in the equatorial plane (1.92 and 1.94 Å). Another equatorial position is occupied by the hydroxide anion bridging to two Cu3 ions (2.04 Å). The remaining equatorial position (2.01 Å) and both axial positions (2.26 and 2.41 Å) are occupied by water molecules, one of them bridging to the Cu3 ion. The whole molecule is a complicated Cu₈ cluster bridged by carboxylate, phosphinate, hydroxide and water oxygen atoms (Fig. 4). The shortest distances are those between Cu3...Cu3 (2.95 Å) and Cu3...Cu4 (3.16 Å) which are bridged by the tricoordinated μ₃-hydroxido ligand.

Formation kinetics of the Ce(III) complex

The formation of the complexes of DOTA-like ligands is mostly described as a two-step process.^{8–17} An out-of-cage complex (indicated in formulas below with superscript "oc") is swiftly formed in the first step. In the complex, donor atoms of the pendant arms are coordinated and two macrocyclic amines are protonated and the protons block the macrocyclic cavity. In the next (rate-determining) step, nitrogen atoms of the macro- cycle are deprotonated and the metal ion is simultaneously transferred into the macrocyclic cavity forming the in-cage complex (indicated in formulas below with superscript "ic") where, in the case of lanthanide(III) ions, all donor atoms of the ligands are coordinated. Recently, we have shown that different types of the out-of-cage complexes are formed if ligand or metal ion excesses are used in the reaction of lanthanide(III) ions and H₄dota.¹⁴ With metal ion excess, the out-of-cage complex has the structure discussed above where oxygen atoms of four acetate pendant arms are bound together with some water molecules. However with the ligand excess, two ligand molecules are coordinated through their pendant arms to the metal ion in the out-of-cage complex. The title ligand, H₆do3aP^{ida}, was designed to stabilize the out-of-cage complex through the coordination of the IDA moiety. Therefore, the local concentration of the metal ion close to the macrocyclic cavity would be increased and the overall complexation reaction should be possibly faster. On the other hand, too strong binding in the out-of-cage mode would decrease the complex formation rate. To distinguish between these limits, a set of complex formation experiments was performed.

The formation of the [Ce(do3aP^{ida})]³⁻ complex was studied by UV-Vis spectroscopy. Spectra of the in-cage complex and out-of-cage complexes are shown in Fig. S9 and S10.† The in-cage complex shows similar spectra under all applied experimental conditions. The spectra are similar to those reported for the [Ce(dota)]⁻ complex.¹³ The change in the maximum could be ascribed to the coordination of the phosphinate group in the title ligand. In contrast, the spectra of out-of-cage complexes are strongly dependent on the applied conditions.

The spectra obtained under the ligand excess remain unchanged along the whole studied pH range and they are similar to those reported for the Ce(III)–H₄dota system.¹³ The spectra obtained under the ligand excess are pH dependent and they indicate the formation of various out-of-cage species (see also lower).

The out-of-cage complexes are formed immediately (during the 15 s dead time). The results of potentiometry (see above) show that the IDA group is a strongly complexing group and the out-of-cage complexes are formed quantitatively even in the equimolar mixture along the whole studied pH range. Thus, the changes in the UV-Vis spectra describe the rearrangement of the out-of-cage species into the in-cage product. Such a process is the first order reaction and, so, the dependence of the absorbance at 314 nm (λ_{\max} of the in-cage product) on time was fitted with the general exponential function (eqn (1)). The changes of the spectra in the course of the reaction and the corresponding fits of the data are shown in Fig. S11.†

As the labelling with a metal radioisotope is commonly done with the ligand excess, kinetic experiments were performed under both the metal and the ligand excesses at pH 5.9, 6.5, 7.0 and 8.0. The obtained rate constants k_{obs} were plotted against the metal-to-ligand or ligand-to-metal ratio (Fig. 5). Under the metal ion as well as the ligand excess, the curves show a saturation shape. The different mutual shape of the curves is a result of the presence of the different reaction intermediates. As mentioned above, the IDA group is a strongly complexing group and, so, the [ML]^{oc} species is quantitatively formed in the equimolar mixture in the studied pH range. So, the saturation shape of the curve under the metal ion excess indicates the formation of the [M₂L]^{oc} complex. Under the ligand excess, the reaction rate is progressively decreased to a limiting value. It might be rationalized by the formation of the [ML₂]^{oc} intermediate with a decreased reaction rate of the sub-

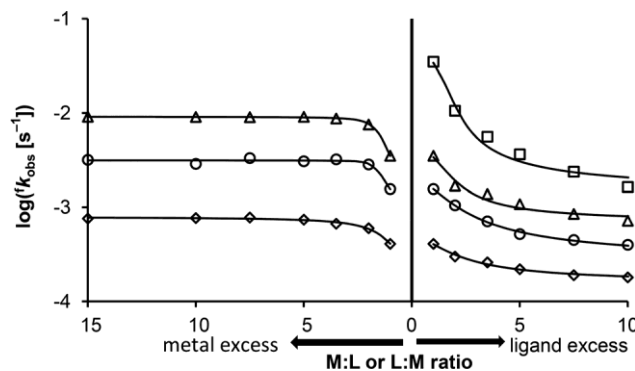


Fig. 5 Complex formation in the Ce(III)–H₆do3aP^{ida} system performed at 25 °C under the Ce(III) ion excess (left part, $c_L = 5 \times 10^{-4}$ M) and the ligand excess (right part, $c_{Ce} = 5 \times 10^{-4}$ M) at pH = 5.9 (diamonds), 6.5 (circles), 7.0 (triangles) and 8.0 (squares). The highest pH value was not used in the experiments employing the metal excess due to the precipitation of Ce(III) hydroxide. The curves represent the best fit according to eqn (2)–(5).

sequent in-cage complexation. The presence of multiple reaction intermediates is also evidenced by the UV-Vis spectra of the $\text{Ce(III)}\text{-H}_6\text{do3aP}^{\text{ida}}$ system obtained immediately after mixing at pH 4 and 8 (Fig. 6). Keeping constant Ce(III) concentration at pH 4, the first absorbance maximum is reached at 300 nm at the 2 : 1 metal-to-ligand ratio (Fig. 6B). With more ligand added, the absorbance further increases with gradual shifting of the maximum to 314 nm until the ~ 1 : 1 metal-to-ligand ratio is reached, where the out-of-cage $[\text{ML}]^{\text{oc}}$ complex is fully formed. It indicates the formation of two different intermediates with $[\text{ML}]^{\text{oc}}$ and $[\text{M}_2\text{L}]^{\text{oc}}$ stoichiometry. At pH 8, the spectra are changing even more dramatically. The intensity

of the absorption band at 314 nm gradually increases and reaches maximum at the ~ 1 : 1 metal-to-ligand ratio (Fig. 6C and E) that corresponds to the $[\text{ML}]^{\text{oc}}$ intermediate and the spectra are similar to those observed at pH 4. At a higher ligand concentration, the absorbance at 314 nm decreases and a new band at 291 nm is observed (Fig. 6C and E). These changes in the spectra could be ascribed to the formation of the $[\text{ML}_2]^{\text{oc}}$ intermediate. Based on these observations, the overall system can be described as shown in Scheme 1.

Due to the high complexing ability of the IDA group, a mixed coordination by both the IDA group and macrocycle pendant arms is expected for the $[\text{ML}]^{\text{oc}}$ complex. In the

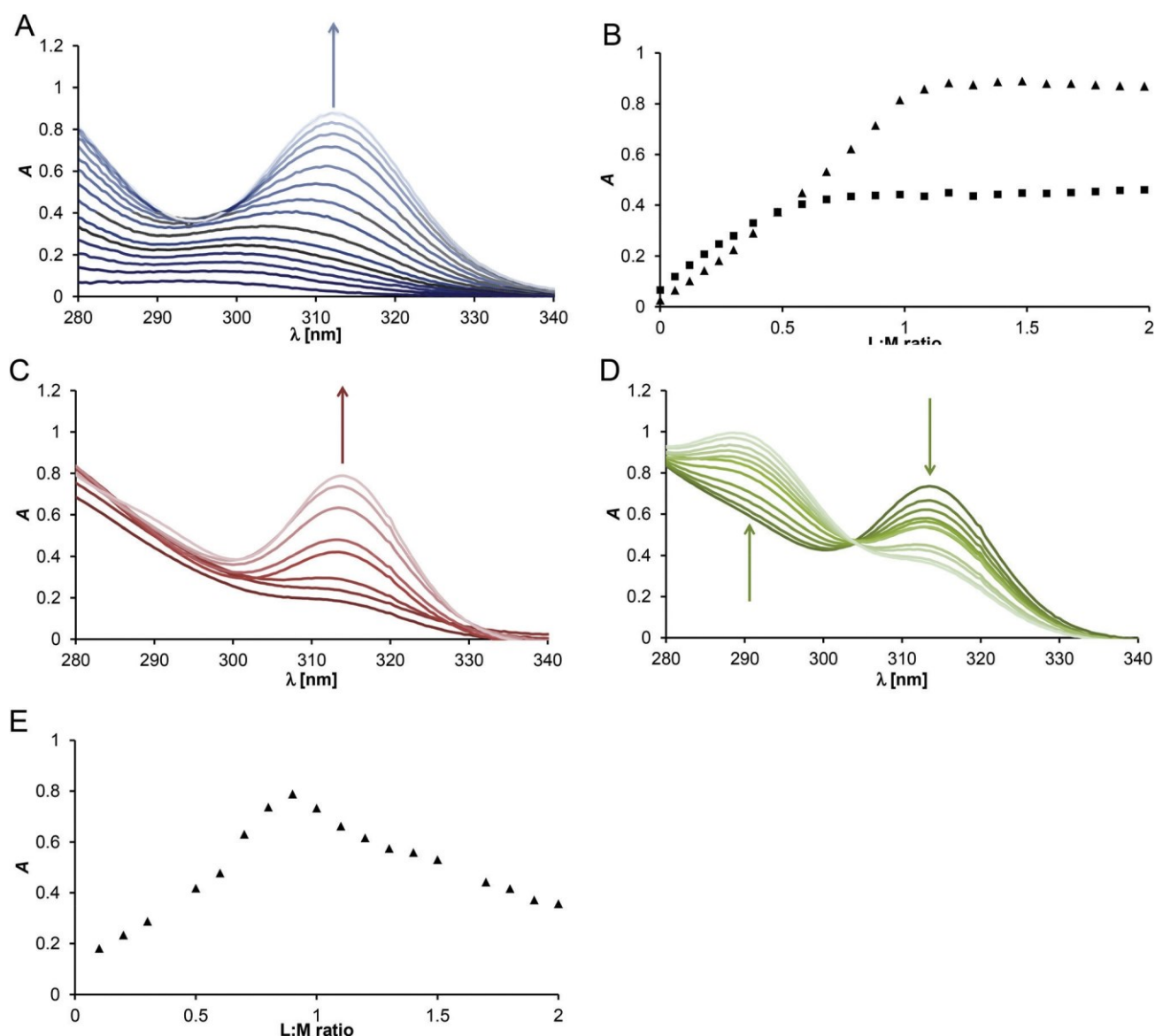
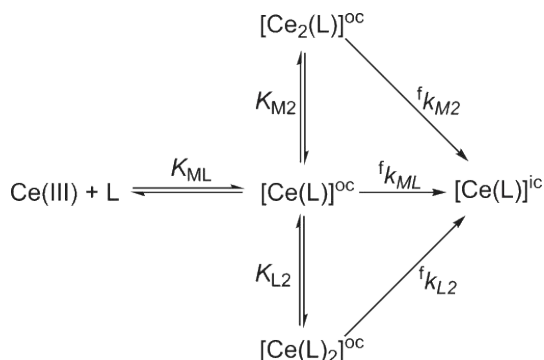


Fig. 6 UV-Vis spectra of the $\text{Ce(III)}\text{-H}_6\text{do3aP}^{\text{ida}}$ out-of cage complexes at pH 4 (A, $c_{\text{M}} = 2.5 \times 10^{-3}$ M, $c_{\text{L}} = 0\text{--}5 \times 10^{-3}$ M) and the corresponding changes of the absorbance at 300 nm (squares) and 314 nm (triangles) with increasing metal-to-ligand ratio (B). UV-Vis spectra of the $\text{Ce(III)}\text{-H}_6\text{do3aP}^{\text{ida}}$ out-of cage complexes at pH 8 at low ligand concentrations (C, $c_{\text{M}} = 2.5 \times 10^{-3}$ M, $c_{\text{L}} = 0\text{--}2.5 \times 10^{-3}$ M) and high ligand concentration (D, $c_{\text{M}} = 2.5 \times 10^{-3}$ M, $c_{\text{L}} = 2.5\text{--}5 \times 10^{-3}$ M) and the corresponding changes of the absorbance at 314 nm with increasing metal-to-ligand ratio (E). The arrows indicate the increasing ligand concentration.



Scheme 1 Mechanism of complexation in the Ce(III)–H₆do3aP^{ida} system.

[M₂L]^{oc} complex, each coordination unit – the IDA group and macrocycle acetate arms – binds independently one metal ion. In contrast, in the [ML₂]^{oc} species, the metal ion is probably

coordinated by two IDA groups originating from two different ligand molecules.

According to the mechanism suggested in Scheme 1, the rate of the whole complexation reaction to form the in-cage complex can be expressed as a sum of contributions given by transformation of all expected out-of-cage intermediates (eqn (2)).

$$\frac{d[\text{ML}]^{\text{ic}}}{dt} \approx \frac{1}{4} f_{k_2} [\text{L}]_{\text{tot}} [\text{M}]_{\text{tot}} + \frac{1}{4} f_{k_{\text{ML}}} [\text{ML}]^{\text{oc}} + \frac{1}{4} f_{k_{\text{L}_2}} [\text{ML}_2]^{\text{oc}} + \frac{1}{4} f_{k_{\text{M}_2}} [\text{M}_2\text{L}]^{\text{oc}}$$

where f_{k_2} is a second-order rate constant of the bimolecular reaction and can be calculated from the observed pseudo-first-order rate constant $f_{k_{\text{obs}}}$ by $f_{k_2} = f_{k_{\text{obs}}} / [\text{M}]_{\text{tot}}$ or $f_{k_2} = f_{k_{\text{obs}}} / [\text{L}]_{\text{tot}}$ for the metal excess and the ligand excess, respectively. Eqn (2) must be combined with metal and ligand mass balance equations and with the formula for the stability constants of the reaction intermediates (eqn (3)–(5))

$$[\text{ML}]^{\text{oc}} \approx \frac{1}{4} K_{\text{ML}} [\text{M}] [\text{L}] \quad (3)$$

$$[\text{ML}_2]^{\text{oc}} \approx \frac{1}{4} K_{\text{L}_2} [\text{ML}] [\text{L}] \quad (4)$$

$$[\text{M}_2\text{L}]^{\text{oc}} \approx \frac{1}{4} K_{\text{M}_2} [\text{ML}] [\text{M}] \quad (5)$$

where K_{ML} , K_{L_2} and K_{M_2} are the conditional stability constants of the out-of-cage intermediates (see Scheme 1), $[\text{L}]$ is the concentration of the free ligand and $[\text{M}]$ is the concentration of the free metal ion. The constant K_{ML} is excessively high and

cannot be rigorously determined from the acquired data. So, the value had to be fixed and the same results were obtained for all values $\log K_{\text{ML}} > 6$. Finally, the data were treated with the set of eqn (2)–(5) and using fixed $\log K_{\text{ML}} = 8$ in order to fulfil the minimization condition for the overall fit.

The results are shown in Fig. 5 and summarized in Table 4. The conditional stability constant K_{L_2} describing the coordination of the second ligand molecule is pH dependent as the imino-diacetate group is (partially) protonated in the studied pH range. Its values are comparable to the stability constant describing the consecutive coordination of the second ligand to form the [Eu(ida)₂][−] complex (Table S5†). From a relatively sharp break in Fig. 5 at the L : M 1 : 2 ratio, one can conclude that the conditional stability constant K_{M_2} describing the coordination of the second metal ion is high. This suggestion is supported also by a break in absorbance at 300 nm (Fig. 6B). Calculations confirmed that this assumption and the values of the conditional stability constant K_{M_2} are about one order of magnitude higher than those of K_{L_2} . However, the values of K_{M_2} were determined with a large error due to a too sharp break shown in Fig. 5 mentioned above.

To get detailed information about the pH dependence of the complexation process, the formation reaction was studied under pseudo-first order conditions using 10-fold ligand or metal ion excess at various pH values. The excess was chosen to reach the quantitative formation of the [ML₂]^{oc} or [M₂L]^{oc} complexes, respectively. The results are depicted in Fig. 7. Both the series of experiments show a linear increase of the formation rate with a higher concentration of OH[−] ions. It is in agreement with the generally accepted mechanism of the formation of lanthanide(III) complexes of DOTA-like ligands^{8–17} where the rate-determining step is the hydroxide ion-assisted deprotonation of the ring nitrogen atoms in the out-of-cage complex coupled with the transfer of the Ln(III) ion into the macrocyclic cavity. Therefore, the rate constant $f_{k_{\text{obs}}}$ could be also expressed as general eqn (6)

$$f_{k_{\text{obs}}} \approx \frac{1}{4} {}^{\text{OH}}k_0 + \frac{1}{4} {}^{\text{OH}}k_1 [\text{OH}^-] \quad (6)$$

where ${}^{\text{OH}}k_0$ and ${}^{\text{OH}}k_1$ are rate constants characterizing the OH[−]-independent and OH[−]-dependent transformation of the out-of-cage intermediate into the final in-cage complex.¹⁰

Under the excess of H₆do3aP^{ida}, linearity is not maintained at pH < 5 (see Fig. 7, inset B). It might be ascribed to an additional protonation of the out-of-cage complex or to an incomplete coordination of the second ligand molecule. However, the data do not allow one to distinguish between

Table 4 The rate constants of individual pathways for the formation of the [Ce(do3aP^{ida})₃]^{3−} complex and the conditional stability constants of the corresponding out-of-cage intermediates (25 °C)

pH	$f_{k_{\text{ML}}} [\text{M}^{-1} \text{s}^{-1}]$	$f_{k_{\text{M}_2}} [\text{M}^{-2} \text{s}^{-1}]$	$f_{k_{\text{L}_2}} [\text{M}^{-2} \text{s}^{-1}]$	K_{M_2}	K_{L_2}
5.9	$(4.1 \pm 0.2) \times 10^{-5}$	$(7.9 \pm 0.2) \times 10^{-4}$	$(1.5 \pm 0.2) \times 10^{-4}$	$(3 \pm 1) \times 10^3$	$(1.8 \pm 0.6) \times 10^3$
6.5	$(1.5 \pm 0.2) \times 10^{-3}$	$(3.1 \pm 0.1) \times 10^{-3}$	$(2.6 \pm 0.3) \times 10^{-4}$	$(6 \pm 10) \times 10^4$	$(2.2 \pm 0.2) \times 10^3$
7.0	$(3.5 \pm 0.1) \times 10^{-3}$	$(9.15 \pm 0.05) \times 10^{-3}$	$(6 \pm 3) \times 10^{-4}$	$(2.1 \pm 0.3) \times 10^4$	$(5 \pm 3) \times 10^3$
8.0	$(3.4 \pm 0.1) \times 10^{-2}$	—	$(1.4 \pm 2) \times 10^{-3}$	—	$(1.2 \pm 0.6) \times 10^4$

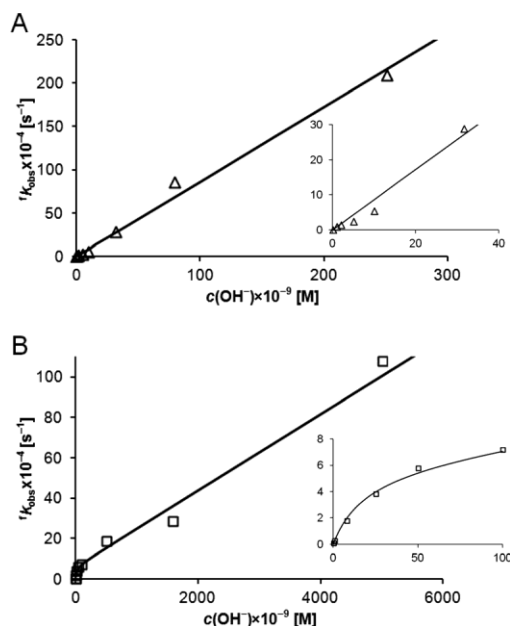


Fig. 7 The pH dependence of the formation rate constant values in the Ce(III)–H₆do3aP^{ida} system using the metal excess (A, 25 °C, $c_{Ce} = 5 \times 10^{-3}$ M, $c_L = 5 \times 10^{-4}$ M) and the ligand excess (B, 25 °C, $c_{Ce} = 5 \times 10^{-4}$ M, $c_L = 5 \times 10^{-3}$ M). The insets show the data obtained in the low-pH region. The solid lines correspond to the best fits obtained according to eqn (6). The line in the inset B is a guide for eyes only.

these two options, so the nonlinear region was not included in the further data treatment. It also means that the constant ${}^{OH}k_0$ has no chemical sense (inset in Fig. 7B). Fitting the data acquired at metal ion excess using eqn (6) shows that the contribution described by the OH⁻-independent term is negligible. Thus, only the rate constant for the hydroxide-assisted pathway could be determined and values of the ${}^{OH}k_1$ are $(8.6 \pm 0.3) \times 10^4 \text{ M}^{-1} \text{ s}^{-1}$ and $(1.9 \pm 0.2) \times 10^3 \text{ M}^{-1} \text{ s}^{-1}$ for the metal ion and the ligand excess, respectively. The direct comparison of reaction rates shows steeper pH dependence under metal ion excess than that under ligand excess (Fig. 8). Thus, the [M₂L]^{oc} complex shows higher reactivity than the [ML₂]^{oc} species

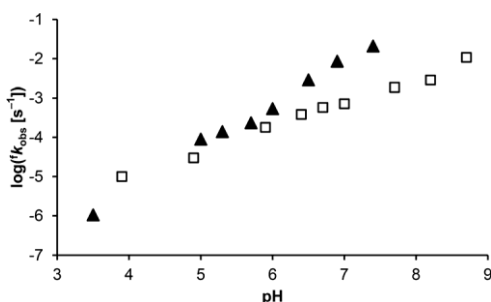


Fig. 8 pH dependence of the rate constants for the formation of the in-cage [Ce(do3aP^{ida})]³⁻ complex at 25 °C under the metal excess (full triangles, $c_{Ce} = 5 \times 10^{-3}$ M, $c_L = 5 \times 10^{-4}$ M) and the ligand excess (open squares, $c_{Ce} = 5 \times 10^{-4}$ M, $c_L = 5 \times 10^{-3}$ M).

rearranges faster than [M₂L]^{oc}. The differences might be ascribed to the different basicity of the macrocycle nitrogen atoms of the [ML₂]^{oc} and [M₂L]^{oc} species as well as differences in their structures. The metal ion in the [ML₂]^{oc} complex is dominantly coordinated by the IDA-groups and only weak interaction between the metal ion and macrocycle acetate pendants could be expected. In contrast, one metal ion in the [M₂L]^{oc} species is bound to the macrocycle acetate pendants. The coordination of pendants to the positively charged metal ion leads to a decreased basicity of macrocycle nitrogen atoms. These effects result in a bigger slope of k_{obs} dependence on pH.

The comparison of the presented results with those for H₄dota and H₅do3aP (Table 5) shows a significant decrease of the complexation rate when the IDA group is attached to the phosphorus atom of the pendant arm in H₆do3aP^{ida}. This is highly important information for the design of new chelators for radiomedical applications. Recently, we have shown that the pendant arms containing weakly chelating units such as hydroxomethylphosphinate,¹⁹ 2-carboxyethylphosphinate¹⁸ or methylene-bis(phosphinate)²⁰ accelerate the in-cage complexation of the metal ions. In contrast, the results presented here indicate that the presence of a more strongly complexing group in the pendant arm is not advantageous for the fast in-cage complexation. The complexation rate is governed by two factors – the stability of the out-of-cage intermediates and the rate of the into-cage transfer. The low stability of out-of-cage complexes leads to low abundance of these intermediate species and, consequently, to low concentration of the metal ion in the vicinity of the macrocyclic cage and, thus, slow in-cage complexation. The presented results show that the too

Table 5 The rate constants of formation and dissociation reactions of the discussed Ce(III) complexes ($t = 25$ °C)

Ligand	Formation (half-life at pH 7)	Dissociation ^a (half-life at pH 0)
H ₆ do3aP ^{ida}	${}^{OH}k_1 = 8.6 \times 10^4 \text{ M}^{-1} \text{ s}^{-1}$ $t_{1/2} = 81 \text{ s}$ (This work ^b) ${}^{OH}k_1 = 1.9 \times 10^3 \text{ M}^{-1} \text{ s}^{-1}$ $t_{1/2} = 1 \text{ h}$ (This work ^c)	$d k_1 = 6.9 \times 10^{-4} \text{ M}^{-1} \text{ s}^{-1}$ $t_{1/2} = 23 \text{ min}$ (This work)
H ₅ do3aP	${}^{OH}k_1 = 9.6 \times 10^5 \text{ M}^{-1} \text{ s}^{-1}$ $t_{1/2} = 7 \text{ s}$ (ref. 17 ^b)	$d k_1 = 1.22 \times 10^{-3} \text{ M}^{-1} \text{ s}^{-1}$ $t_{1/2} = 10 \text{ min}$ (ref. 17)
H ₄ dota	${}^{OH}k_1 = 2.7 \times 10^6 \text{ M}^{-1} \text{ s}^{-1}$ $t_{1/2} = 3 \text{ s}$ (ref. 13 ^b) ${}^{OH}k_1 = 3.5 \times 10^6 \text{ M}^{-1} \text{ s}^{-1}$ $t_{1/2} = 2 \text{ s}$ (ref. 10 ^d)	$d k_1 = 8 \times 10^{-4} \text{ M}^{-1} \text{ s}^{-1}$ $d k_2 = 2 \times 10^{-3} \text{ M}^{-2} \text{ s}^{-1}$ $t_{1/2} = 4 \text{ min}$ (ref. 10) $d k_1 = 3.4 \times 10^{-4} \text{ M}^{-1} \text{ s}^{-1}$ $d k_2 = 1.6 \times 10^{-3} \text{ M}^{-2} \text{ s}^{-1}$ $t_{1/2} = 6 \text{ min}$ (ref. 54)

^a $k_{obs} = d k_1 [H^+] + d k_2 [H^+]^2$. ^b10-times metal excess. ^c10-times ligand excess. ^d20-times metal excess.

high stability of the out-of-cage complexes is also undesirable as it leads to a slow transfer of the metal ion into the macrocyclic cavity due to mutual competition of both sites for the metal ion. Only literature precedence for such slow complexation is the transfer of Cu(II) into the cyclam cavity when tris(2-aminoethyl)amine (tren) was used as a pendant arm.⁵¹ The in-cage transfer rate is dependent on the nature of both out-of-cage and in-cage chelation centres and, recently, we have shown that the spacer connecting the macrocycle part with coordinating groups in the pendants is also very important.¹⁴ Moreover, the protonable groups in the pendant arms might assist the proton transfer from the macrocyclic nitrogen atoms to the surrounding environment. In the out-of-cage complex, the pendants are coordinated to the metal ion.^{52,53} Consequently, the formation of highly stable out-of-cage complex blocks the pendant-assisted proton transfer and the complex formation rate is decreased. Thus, the stability of the out-of-cage intermediates must be kept in a narrow range to reach the optimal complexation rate for in-cage complexation and it should be combined with an appropriate spacer. However, the kinetic data are mostly reported for “chemical” conditions, *i.e.* for the millimolar concentration range. The complexation of radioisotopes is mostly performed at concentrations that are several orders of magnitude lower (“radiochemical” conditions). Furthermore, various metallic impurities originating from the radioisotope production are present in the samples. As a result, the above mentioned parameters might be of different importance and the formation of the out-of-cage complexes might become highly dominant for the overall complexation rate. Thus, design of the pendant arms must be tuned for each metal ion–ligand system, and the complexation/labelling ability of such ligands should be evaluated under both “chemical” and “radiochemical” conditions.

Dissociation kinetics of the Ce(III) complex

The acid-assisted decomplexation of the $[\text{Ce}(\text{do3aP}^{\text{ida}})]^{3-}$ complex was studied in 0.2–3.0 M HClO₄ (Fig. 9). The dependence of the observed reaction rate constant ${}^d k_{\text{obs}}$ on the

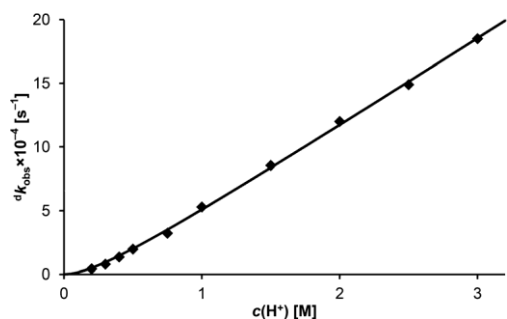


Fig. 9 Acid-assisted dissociation of the $[\text{Ce}(\text{do3aP}^{\text{ida}})]^{3-}$ complex (25 °C, $I = 3 \text{ M (Na/H)ClO}_4$). The curve represents the best fit according to eqn (8).

proton concentration is almost linear. However, there is a significant negative intercept on the y -axis. It indicates that the kinetically active species is present in two different protonation states in the studied pH range. There are three protonation constants of the Ln(III) complexes determined by potentiometry. As the studied pH range is below the range covered by potentiometry, $\{\text{M}(\text{H}_3\text{L})\} = \{\text{M}(\text{H}_4\text{L})\}^+$ is very probably the kinetically important equilibrium that is described by the dissociation constant K_a . The less protonated species, $\{\text{M}(\text{H}_3\text{L})\}$, does not contribute to the overall dissociation. The $\{\text{M}(\text{H}_4\text{L})\}^+$ species might dissociate spontaneously (rate constant ${}^d k_0$) or *via* the proton-assisted pathway (rate constant ${}^d k_1$). The dissociation rate is then expressed as given by eqn (7)

$$v = \frac{{}^d k_0 [\text{comp}]_{\text{tot}} + {}^d k_1 [\text{M}(\text{H}_4\text{L})]^+}{1 + \frac{[\text{H}^+]}{K_a}}$$

where $[\text{comp}]_{\text{tot}}$ is the total concentration of the complex. Taking into account the protonation equilibrium suggested above, ${}^d k_{\text{obs}}$ can be expressed by eqn (8)

$${}^d k_{\text{obs}} = \frac{{}^d k_0 + \frac{{}^d k_1 [\text{H}^+]}{K_a}}{1 + \frac{[\text{H}^+]}{K_a}}$$

Fitting of the data according to eqn (8) gave ${}^d k_1 = (6.9 \pm 0.1) \times 10^{-4} \text{ M}^{-1} \text{ s}^{-1}$ and $K_a = 0.36 \pm 0.05$. The value of ${}^d k_0$ is negligible and this indicates very slow spontaneous dissociation of the $[\text{M}(\text{H}_4\text{L})]^+$ species. Values of the rate constant ${}^d k_1$ are comparable to those reported for the Ce(III) complexes of H₄dota and H₅do3aP (Table 5). It shows a very high kinetic inertness of the studied complex and a negligible role of the IDA-group in the dissociation process.

Conclusions

The title ligand combines the macrocyclic DOTA-like unit with the pendant IDA group and the groups are connected through a phosphinate spacer. Determined protonation and stability constants show that each group behaves as an independent chelating unit and their coordinating abilities are similar to those reported for each group as an individual molecule. The close proximity of the groups in the molecule is important for the overall complexation mechanism and significantly influences the in-cage complexation rate. In the first step, the metal ion is complexed by the IDA group in the out-of-cage mode. Several out-of-cage complexes with 2 : 1, 1 : 1 and 1 : 2 ligand-to-metal ratios were identified. The strong complexing ability of the IDA group blocks the transfer of the metal ion into the macrocyclic cavity and, thus, the title ligand shows significantly slower in-cage complexation compared to that of the parent H₄dota. It is a significant finding as it indicates that the coordination ability of the groups in the pendant arms must be properly tuned to reach the faster chelation which is among the most important properties of ligands for the radio-medical applications. The strongly chelating pendant arm stabilizes the out-of-cage complexes too much and, thus, a suitable chelating group for the faster in-cage complexation should have only weak coordination ability.

Acknowledgements

The support from the Grant Agency of Charles University (No. 272314) EU program COST Action 15209 (LTC17067) is acknowledged. We thank Dr I. Čiřarov for the collection of the X-ray diffraction data.

References

- 1 E. Merbach, L. Helm and . Tth, *The Chemistry of Contrast Agents in Medical Magnetic Resonance Imaging*, John Wiley & Sons, Chichester, 2013.
- 2 T. J. Wadas, E. H. Wong, G. R. Weisman and C. J. Anderson, *Chem. Rev.*, 2010, 110, 2858–2902.
- 3 R. E. Mewis and S. J. Archibald, *Coord. Chem. Rev.*, 2010, 254, 1686–1712.
- 4 S. Cutler, H. M. Hennkens, N. Sisay, S. Huclier-Markai and S. S. Jurisson, *Chem. Rev.*, 2013, 113, 858–883.
- 5 E. W. Price and C. Orvig, *Chem. Soc. Rev.*, 2014, 43, 260–290.
- 6 S. Faulkner, S. J. A. Pope and B. P. Burton-Pye, *Appl. Spectrosc. Rev.*, 2005, 40, 1–31.
- 7 X. Wang, H. Chang, J. Xie, B. Zhao, B. Liu, S. Xu, W. Pei, N. Ren, L. Huang and W. Huang, *Coord. Chem. Rev.*, 2014, 273–274, 201–212.
- 8 J. Moreau, E. Guillon, J.-C. Pierrard, J. Rimbault, M. Port and M. Aplincourt, *Chem. – Eur. J.*, 2004, 10, 5218–5232.
- 9 S. L. Wu and W. D. Horrocks, *Inorg. Chem.*, 1995, 34, 3724–3732.
- 10 . Tth, E. Brucher, I. Lzr and I. Tth, *Inorg. Chem.*, 1994, 33, 4070–4076.
- 11 E. Brucher, G. Laurency and Z. Makra, *Inorg. Chim. Acta*, 1987, 139, 141–142.
- 12 X. Wang, T. Jin, V. Comblin, A. Lopez-Mut, E. Merciny and J. F. Desreux, *Inorg. Chem.*, 1992, 31, 1095–1098.
- 13 L. Burai, I. Fbin, R. Kirly, E. Szilgyi and E. Brucher, *J. Chem. Soc., Dalton Trans.*, 1998, 243–248.
- 14 S. Prochzkov, J. Hranek, V. Kubiek and P. Hermann, *Polyhedron*, 2016, 111, 143–149.
- 15 P. Tborsk, I. Svobodov, P. Lubal, Z. Hnatejko, S. Lis and P. Hermann, *Polyhedron*, 2007, 26, 4119–4130.
- 16 P. Tborsk, I. Svobodov, Z. Hnatejko, P. Lubal, S. Lis, M. Frsterov, P. Hermann, I. Lukeř and J. Havel, *J. Fluoresc.*, 2005, 15, 507–512.
- 17 P. Tborsk, P. Lubal, J. Havel, J. Kotek, J. Rudovsk, P. Hermann and I. Lukeř, *Collect. Czech. Chem. Commun.*, 2005, 70, 1909–1942.
- 18 J. Notni, P. Hermann, J. Havlikov, J. Kotek, V. Kubiek, J. Plutnar, N. Loktionova, P. J. Riss, F. Rsch and I. Lukeř, *Chem. – Eur. J.*, 2010, 16, 7174–7185.
- 19 J. řimeek, M. Schulz, J. Notni, J. Plutnar, V. Kubiek, J. Havlikov and P. Hermann, *Inorg. Chem.*, 2012, 51, 577–590.
- 20 T. David, V. Kubiek, O. Gutten, P. Lubal, J. Kotek, H.-J. Pietzsch, L. Ruliřek and P. Hermann, *Inorg. Chem.*, 2015, 54, 11751–11766.
- 21 H.-S. Chong, S. Lim, K. E. Baidoo, D. E. Milenic, X. Ma, F. Jia, H. A. Song, M. W. Brechbiel and M. R. Lewis, *Bioorg. Med. Chem. Lett.*, 2008, 18, 5792–5795.
- 22 M. Dadwal, C. S. Kang, H. A. Song, X. Sun, A. Dai, K. E. Baidoo, M. W. Brechbiel and H.-S. Chong, *Bioorg. Med. Chem. Lett.*, 2011, 21, 7513–7515.
- 23 H.-S. Chong, X. Sun, Y. Chen, I. Sin, C. S. Kang, M. R. Lewis, D. Liu, V. C. Ruthengael, Y. Zhong, N. Wu and H. A. Song, *Bioorg. Med. Chem.*, 2015, 23, 1169–1178.
- 24 H. A. Song, C. S. Kang, K. E. Baidoo, D. E. Milenic, Y. Chen, A. Dai, M. W. Brechbiel and H. S. Chong, *Bioconjugate Chem.*, 2011, 22, 1128–1135.
- 25 S. Kang, X. Sun, F. Jia, H. A. Song, Y. Chen, M. Lewis and H.-S. Chong, *Bioconjugate Chem.*, 2012, 23, 1775–1782.
- 26 I. Mamedov, N. K. Logothetis and G. Angelovski, *Org. Biomol. Chem.*, 2011, 9, 5816–5824.
- 27 G. Angelovski, T. Chauvin, R. Pohmann, N. K. Logothetis and . Tth, *Bioorg. Med. Chem.*, 2011, 19, 1097–1105.
- 28 B. McMahon, P. Mauer, C. P. McCoy, T. C. Lee and T. Gunnlaugsson, *J. Am. Chem. Soc.*, 2009, 131, 17542–17543.
- 29 M. Surender, S. Comby, S. Martyn, B. Cavanagh, T. C. Lee, D. F. Brougham and T. Gunnlaugsson, *Chem. Commun.*, 2016, 52, 10858–10861.
- 30 A. Dadabhoy, S. Faulkner and P. G. Sammes, *J. Chem. Soc., Perkin Trans. 2*, 2002, 348–357.
- 31 V. Kubiek, J. Havlikov, J. Kotek, G. Tircs, P. Hermann, . Tth and I. Lukeř, *Inorg. Chem.*, 2010, 49, 10960–10969.
- 32 C. F. Baes Jr. and R. E. Mesmer, *The Hydrolysis of Cations*, Wiley, New York, 1976.
- 33 M. Kvala and I. Lukeř, International Conference, Chemometrics '95, Pardubice, Czech Republic, 1995, p. 63, full version of "OPIUM" is available (free of charge) on <http://www.natur.cuni.cz/~kyvala/opium.html>.
- 34 (a) Z. Otwinovski and W. Minor, *HKL DENZO and Scalepack Program Package*, Nonius BV, Delft, 1997; (b) Z. Otwinovski and W. Minor, Processing of X-ray diffraction data collected in oscillation mode, *Methods Enzymol.*, 1997, 276, 307–326.
- 35 A. Altomare, G. Casciarano, C. Giacovazzo, A. Guagliardi, M. C. Burla, G. Polidori and M. Camalli, "SIR92", *J. Appl. Crystallogr.*, 1994, 27, 435–436.
- 36 G. M. Sheldrick, *SHELXL-2014/7. Program for Crystal Structure Refinement from Diffraction Data*, University of Gttingen, Gttingen, 2014.
- 37 G. Tircs, A. Bnyei, R. Kirly, I. Lzr, R. Pl and E. Brucher, *Eur. J. Inorg. Chem.*, 2007, 701–713.
- 38 M. Pniok, V. Kubiek, J. Havlikov, J. Kotek, A. Sabatie-Gogov, J. Plutnar, S. Huclier-Markai and P. Hermann, *Chem. – Eur. J.*, 2014, 20, 7944–7955.
- 39 M. Frsterov, I. Svobodov, P. Lubal, P. Tborsk, J. Kotek, P. Hermann and I. Lukeř, *Dalton Trans.*, 2007, 535–549.
- 40 S. Prochzkov, Z. Bhmov, V. Kubiek, J. Kotek, P. Hermann and I. Lukeř, *Phosphorus, Sulfur Silicon Relat. Elem.*, 2014, 189, 933–945.
- 41 I. Lukeř, J. Kotek, P. Vojtřek and P. Hermann, *Coord. Chem. Rev.*, 2001, 217–218, 287–312.

- 42 R. Kerdjoudj, M. Pniok, C. Alliot, V. Kubiček, J. Havlíčková, F. Rösch, P. Hermann and S. Huclier-Markai, *Dalton Trans.*, 2016, 45, 1398–1409.
- 43 A. E. Martell and R. M. Smith, *Critical Stability Constants*, Plenum Press, New York, 1974–1989, vol. 1–6; *NIST Standard Reference Database 46 (Critically Selected Stability Constants of Metal Complexes)*, version 5.0, 1994.
- 44 A. Riesen, M. Zehnder and T. A. Kaden, *J. Chem. Soc., Chem. Commun.*, 1985, 1336–1338.
- 45 A. Riesen, M. Zehnder and T. A. Kaden, *Helv. Chim. Acta*, 1986, 69, 2067–2073.
- 46 A. Riesen, M. Zehnder and T. A. Kaden, *Helv. Chim. Acta*, 1986, 69, 2074–2080.
- 47 J. Albalad, J. Arinez-Soriano, J. Vidal-Gancedo, V. Lioveras, J. Juanhuix, I. Imaz, N. Aliaga-Alcalde and D. MasPOCH, *Chem. Commun.*, 2016, 52, 13397–13400.
- 48 P. Barbaro, C. Bianchini, G. Capannesi, L. Di Luca, F. Laschi, D. Petroni, P. A. Salvadori and A. Vacca, *J. Chem. Soc., Dalton Trans.*, 2000, 2393–2401.
- 49 A. Takacs, R. Napolitano, M. Purgel, A. C. Bényei, L. Zekány, E. Brücher, I. Tóth, Z. Barányai and S. Aime, *Inorg. Chem.*, 2014, 53, 2858–2872.
- 50 K. Kumar, M. F. Tweedle, M. F. Malley and J. Z. Gougoutas, *Inorg. Chem.*, 1995, 34, 6472–6480.
- 51 L. Siegfried, M. Honecker, A. Schlageter and T. A. Kaden, *Dalton Trans.*, 2003, 3939–3948.
- 52 P. A. Stenson, A. L. Thomson and D. Parker, *Dalton Trans.*, 2006, 3291–3293.
- 53 J. Šimeček, P. Hermann, J. Havlíčková, E. Herdtweck, T. G. Kapp, N. Engelbogen, H. Kessler, H.-J. Wester and J. Notni, *Chem. – Eur. J.*, 2013, 19, 7748–7757.
- 54 A. Chang and Y.-L. Liu, *J. Chin. Chem. Soc.*, 2000, 47, 1001–1006.

DOTA analogue with phosphinate-iminodiacetate pendant arm: modification of complex formation rate with a strongly chelating pendant

Soňa Procházková, Vojtěch Kubíček,* Zuzana Böhmová, Kateřina Holá, Jan Kotek and Petr Hermann

Department of Inorganic Chemistry, Faculty of Science, Charles University, Hlavova 2030, 128 40 Prague 2, Czech Republic; email: kubicek@natur.cuni.cz; tel.: +420 221951436; fax: +420 22191253

Table of content

Potentiometry - the detailed procedure

Figure S1. ^1H , $^{13}\text{C}\{^1\text{H}\}$ and $^{31}\text{P}\{^1\text{H}\}$ NMR spectra of $\text{H}_6\text{do3aP}^{\text{ida}}$.

Table S1. The experimentally determined overall protonation constants $\log\beta_n^a$ of $\text{H}_6\text{do3aP}^{\text{ida}}$ and the pre-formed $[\text{Ln}(\text{do3aP}^{\text{ida}})]^{3-}$ complexes.

Table S2. The experimentally determined overall stability constants $\log\beta_{\text{hlm}}^a$ of the $\text{H}_6\text{do3aP}^{\text{ida}}$ complexes.

Table S3. Comparison of the stability constants $\log K_{011}^a$ of the discussed complexes.

Table S4. The overall stability constants $\log K$ of the ternary complexes with pre-formed $[\text{Gd}(\text{do3aP}^{\text{ida}})]^{3-}$ complex.

Table S5. Comparison of the consecutive stability constants $\log K_{011}$ and $\log K_{021}^a$ of the ternary complexes of $[\text{Gd}(\text{do3aP}^{\text{ida}})]^{3-}$ with those of the complexes of H_2ida .

Figure S2. ^{31}P NMR titration of $\text{H}_6\text{do3aP}^{\text{ida}}$.

Figure S3. Distribution diagram of $\text{Cu}(\text{II})$ – $[\text{Gd}(\text{H}_n\text{do3aP}^{\text{ida}})]^{n-3}$ system.

Figure S4. Distribution diagram of $\text{Eu}(\text{III})$ – $[\text{Gd}(\text{H}_n\text{do3aP}^{\text{ida}})]^{n-3}$ system.

Table S6. Experimental data of the reported crystal structures.

Table S7. The coordination distances found in the crystal structure of $[\text{Cu}_4(\text{do3aP}^{\text{ida}})(\text{OH})(\text{H}_2\text{O})_4]\text{Cl}\cdot 7.5\text{H}_2\text{O}$.

Figure S5. The coordination mode of the Cu1 ion in the crystal structure of $[\text{Cu}_4(\text{do3aP}^{\text{ida}})(\text{OH})(\text{H}_2\text{O})_4]\text{Cl}\cdot 7.5\text{H}_2\text{O}$.

Figure S6. The coordination mode of the Cu2 ion in the crystal structure of $[\text{Cu}_4(\text{do3aP}^{\text{ida}})(\text{OH})(\text{H}_2\text{O})_4]\text{Cl}\cdot 7.5\text{H}_2\text{O}$.

Figure S7. The coordination mode of the Cu3 ion in the crystal structure of $[\text{Cu}_4(\text{do3aP}^{\text{ida}})(\text{OH})(\text{H}_2\text{O})_4]\text{Cl}\cdot 7.5\text{H}_2\text{O}$.

Figure S8. The coordination mode of the Cu4 ion in the crystal structure of $[\text{Cu}_4(\text{do3aP}^{\text{ida}})(\text{OH})(\text{H}_2\text{O})_4]\text{Cl}\cdot 7.5\text{H}_2\text{O}$.

Figure S9. UV-Vis spectra at the beginning of measurement, corresponding to the *out-of-cage* complex, and at the end of measurement, corresponding to the *in-cage* complex, performed under the 10-fold metal excess.

Figure S10. UV-Vis spectra at the beginning of measurement, corresponding to the *out-of-cage* complex and at the end of measurement, corresponding to the *in-cage* complex, performed under the 10-fold ligand excess.

Figure S11. Changes of absorption spectra in the course of complexation and time dependences of absorbance at 314 nm.

Potentiometry - the detailed procedure

The stock solution of hydrochloric acid (~0.03 M) was prepared from 35 % aqueous solution (puriss, Fluka). Commercial (NMe₄)Cl (99 %, Fluka) was recrystallized from boiling *i*-PrOH and the solid salt was dried over P₂O₅ in vacuum to constant weight (this dried form of the salt is extremely hygroscopic). Carbonate-free (NMe₄)OH solution (~0.2 M) was prepared from (NMe₄)Cl using ion exchanger Dowex 1 in the OH⁻-form (elution with carbonate-free water, under argon). The hydroxide solution was standardized against potassium hydrogen phthalate and the HCl solution against the ca. 0.2 M (NMe₄)OH solution. Stock solutions of the individual metal cations were prepared by dissolving hydrates of metal chlorides and the metal ions contents were determined by titration with a standard Na₂H₂edta solution. Analytical concentration of a stock solution of the ligand was determined together with refinement of protonation constants using OPIUM software package (see below). The in-cell titrations were carried out in a vessel thermostatted at 25.0 ± 0.1 °C, at ionic strength $I = 0.1$ M ((NMe₄)Cl; with $pK_w = 13.81$) and in the presence of extra HCl using a PHM 240 pH-meter, a 2-ml ABU 900 automatic piston burette and a GK 2401B combined electrode (all Radiometer, Denmark). The in-cell titrations were carried out in pH range 1.7–12.0 with at least 40 points per titration and four parallel titrations ($c_L = 0.004$ M, $c_M = 0.004$ M or 0.002 M or 0.008 M).

The stability constants of the Ln(III) complexes were obtained by the out-of-cell method. The batches (starting volume 1 ml) were prepared under Ar stream in tubes with ground joints from ligand, metal ion and HCl/(NMe₄)Cl stock solutions and water ($c_L = c_M \sim 0.004$ M, 5% ligand excess). Then a known amount of (NMe₄)OH standard solution was added under Ar. The tubes were firmly closed with stoppers and the solutions were equilibrated at room temperature for 4 weeks (one batch was checked after 6 weeks and gave the same data). Titrations were performed in the pH ranges 1.5–3.8 (final pH values) with around 20 data points per whole titration and three titrations per system.

The pre-formed Ln(III) complexes in solution were obtained by mixing of the ligand stock solution (5 % molar excess) with Ln(III) ion stock solution in a glass ampoule and a slow portion-wise addition (2 h) of standard (NMe₄)OH solution (just to neutralize the ligand amount) under Ar. The ampoule was flame-sealed and left at 80 °C overnight to fully complex the metal ion. The ampoules were opened under Ar and aliquots of the solutions of the Ln(III) complexes were transferred into a titration vessel. Water and excess of HCl, metal ion stock solution and (NMe₄)Cl solutions were added (to reach a pH of about 1.8 and $I = 0.1$ M (NMe₄)Cl in the final solution, starting volume 5 ml, the preformed complex concentration ~0.004 M) and the solution was immediately titrated with a standard (NMe₄)OH solution at 25.0 °C acquiring at least 40 data points per each of three titrations.

The constants (with standard deviations) were calculated with program OPIUM.¹ The program minimizes the criterion of the generalized least-squares method using the calibration function

$$E = E_0 + S \times \log[H^+] + j_1 \times [H^+] + j_2 \times K_w / [H^+]$$

where the additive term E_0 contains the standard potentials of the electrodes used and contributions of inert ions to the liquid-junction potential, S corresponds to the Nernstian slope, the value of which should be close to the theoretical value and the $j_1[H^+]$ and $j_2[OH^-]$ terms are the contributions of the H⁺ and OH⁻ ions to the liquid-junction potential. The calibration parameters were determined from titration of standard HCl with standard (NMe₄)OH before and after

¹Kývala, M.; Lukeš, I. *International Conference, Chemometrics '95*; Pardubice, Czech Republic, 1995; p 63; full version of "OPIUM" is available (free of charge) on <http://www.natur.cuni.cz/~kyvala/opium.html>.

each ligand or ligand–metal titration to give pairs of calibration/titration, which was used for calculations of the constants. The overall protonation constants β_n are concentration constants, defined by $\beta_n = [H_nL]/([H]_n[L])$ (they were transformed to dissociation constants as $pK_1 = \log\beta_1$ and $pK_n = \log\beta_n - \log\beta_{n-1}$). The (concentration) stability constant are defined by $\beta_{hlm} = [H_hL_lM_m]/([H]^h[L]^l[M]^m)$.

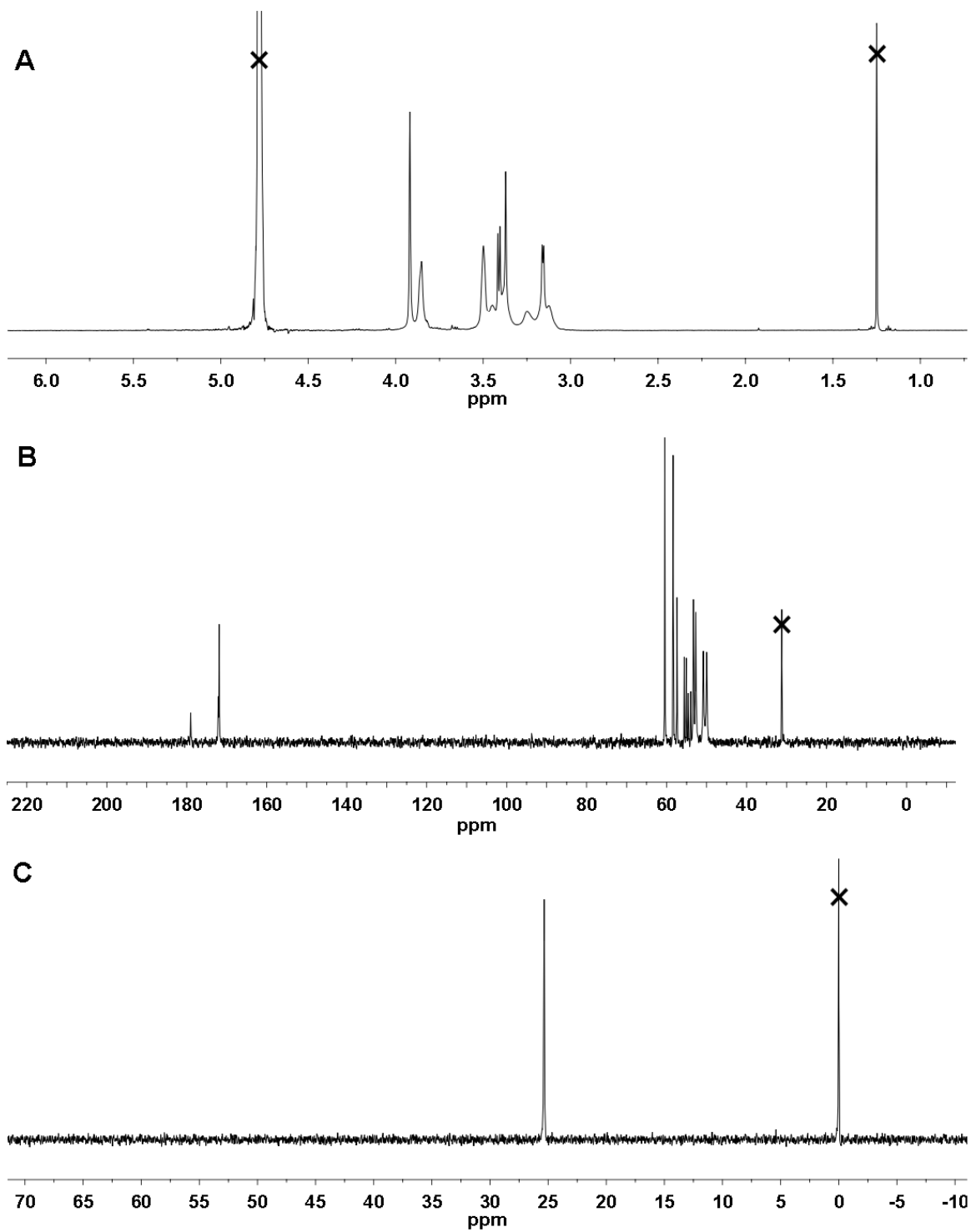


Figure S1. 1H (A), $^{13}C\{^1H\}$ (B) and $^{31}P\{^1H\}$ (C) NMR spectra of H_6do3aP^{ida} (25 °C, pD = 6). Signals of solvent and standards are labeled with crosses.

Table S1. The experimentally determined overall protonation constants $\log\beta_h^a$ of H_6do3aP^{ida} and the pre-formed $[Ln(do3aP^{ida})]^{3-}$ complexes (25 °C, $I = 0.1$ M (NMe₄)Cl).

h	H_6do3aP^{ida}	$[La(do3aP^{ida})]^{3-}$	$[Nd(do3aP^{ida})]^{3-}$	$[Eu(do3aP^{ida})]^{3-}$	$[Gd(do3aP^{ida})]^{3-}$	$[Y(do3aP^{ida})]^{3-}$
1	12.85(4)	7.67(2)	7.83(3)	7.83(1)	7.79(2)	7.95(1)
2	22.48(4)	10.25(3)	10.29(4)	10.23(1)	10.53(2)	10.52(1)
3	30.61(4)	11.88(3)	11.80(4)	11.82(1)	12.09(2)	12.29(1)
4	35.01(4)	–	–	–	–	–
5	38.28(4)	–	–	–	–	–
6	40.26(5)	–	–	–	–	–
7	41.85(5)	–	–	–	–	–

^a For the free ligand, $\beta_h = [H_hL] / ([H]^h \times [L])$. For the pre-formed complexes, $\beta_h = [H_h(ML)] / ([H]^h \times [ML])$.

Table S2. The experimentally determined overall stability constants $\log\beta_{hm}^a$ of the H_6do3aP^{ida} complexes (25 °C, $I = 0.1$ M (NMe₄)Cl).

Species ^b	Cu(II)	Zn(II)	La(III)	Nd(III)	Eu(III)	Gd(III)	Y(III)
[M(L)]	23.75(3)	21.79(2)	22.09 ^c	24.02 ^c	24.94 ^c	25.27 ^c	25.39 ^c
[M(HL)]	32.15(2)	30.25(1)	29.76(3)	31.85(3)	32.77(3)	33.06(9)	33.34(5)
[M(H ₂ L)]	35.99(2)	34.01(2)	32.96(5)	34.79(2)	35.72(2)	35.66(9)	35.74(7)
[M(H ₃ L)]	–	36.99(1)	36.19(2)	37.01(3)	37.99(3)	37.79(11)	37.94(7)
[M ₂ (L)]	34.71(3)	31.37(1)	^d	^d	^d	^d	^d
[M ₂ (HL)]	38.71(2)	35.05(1)	^d	^d	^d	^d	^d
[M ₂ (H ₂ L)]	40.30(3)	–	^d	^d	^d	^d	^d
[M ₂ (L)(OH)]	25.51(3)	21.20(2)	^d	^d	^d	^d	^d
[M ₂ (L)(OH) ₂]	13.46(4)	–	^d	^d	^d	^d	^d

^a $\beta_{hm} = [H_hL_lM_m] / ([H]^h \times [L]^l \times [M]^m)$. ^b Charges are omitted for clarity reasons. ^c Calculated using the protonation constants determined for the pre-formed complexes. ^d The systems were studied by out-of-cell method and, thus, only in 1:1 metal-to-ligand ratio was utilized.

Table S3. Comparison of the stability constants $\log K_{011}^a$ of the discussed complexes.

Ligand	Cu(II)	Zn(II)	La(III)	Nd(III)	Eu(III)	Gd(III)	Y(III)
H ₄ dota ²	22.3	20.8	22.0	23.7	23.0	24.0	24.0
H ₆ do3aP ^{ida}	23.75	21.79	22.09	24.02	24.94	25.27	25.39
H ₅ do3aP ^{PrA} ³	–	–	23.1	–	25.3	25.04	24.63

$$^a K_{011} = [M(L)] / ([L] \times [M]).$$

Table S4. The overall stability constants $\log K$ of the ternary complexes with pre-formed [Gd(do3aP^{ida})]³⁻ complex (25 °C, $I = 0.1$ M (NMe₄)Cl).

Equilibrium ^a	Cu(II)	Zn(II)	Ca(II)	Eu(III)
$M + \{Gd(L)\} = [M\{Gd(L)\}]$	10.53(1)	8.10(3)	5.19(5)	8.98(2)
$M + \{Gd(L)\} + H^+ = [M\{Gd(HL)\}]$	–	–	–	11.57(3)
$M + \{Gd(L)\} + H_2O = [M\{Gd(L)\}(OH)] + H^+$	1.47(3)	–	-6.69(5)	–
$M + \{Gd(L)\} + 2H_2O = [M\{Gd(L)\}(OH)_2] + 2H^+$	-10.15(4)	–	–	–
$M + 2\{Gd(L)\} = [M\{Gd(L)\}_2]$	15.40(7)	13.30(7)	–	16.31(8)
$M + 2\{Gd(L)\} + H^+ = [M\{Gd(HL)\}\{Gd(L)\}]$	20.95(4)	18.47(8)	–	20.61(2)
$M + 2\{Gd(L)\} + H_2O = [M\{Gd(L)\}_2(OH)] + H^+$	5.39(7)	2.59(9)	–	6.0(1)
$M + 2\{Gd(L)\} + 2H_2O = [M\{Gd(L)\}_2(OH)_2] + 2H^+$	–	–	–	-6.4(1)

^a Charges are omitted for clarity reasons.

Table S5. Comparison of the consecutive stability constants $\log K_{011}$ and $\log K_{021}^a$ of the ternary complexes of [Gd(do3aP^{ida})]³⁻ with those of the complexes of H₂ida.²

Species ^b	Cu ²⁺		Zn ²⁺		Ca ²⁺		Eu ³⁺	
	[Gd(do3aP ^{ida})]	H ₂ ida	[Gd(do3aP ^{ida})]	H ₂ ida	[Gd(do3aP ^{ida})]	H ₂ ida	[Gd(do3aP ^{ida})]	H ₂ ida
[M(X)]	10.53	10.6	8.10	7.03	5.19	2.59	8.98	6.2
[M(X) ₂]	4.87	5.7	5.20	5.4	–	–	7.33	4.5

^a $K_{011} = [M(X)] / ([X] \times [M])$ and $K_{021} = [M(X)_2] / ([X] \times [M(X)])$, where X = [Gd(do3aP^{ida})]³⁻ or X = ida²⁻. ^b Charges are omitted for clarity reasons.

² A. E. Martell, R. M. Smith, *Critical Stability Constants*, Plenum Press, New York, 1974–1989, vol. 1–6; *NIST Standard Reference Database 46 (Critically Selected Stability Constants of Metal Complexes)*, version 5.0, 1994.

³ M. Försterová, I. Svobodová, P. Lubal, P. Táborský, J. Kotek, P. Hermann, I. Lukeš *Dalton Trans.*, 2007, 535–549.

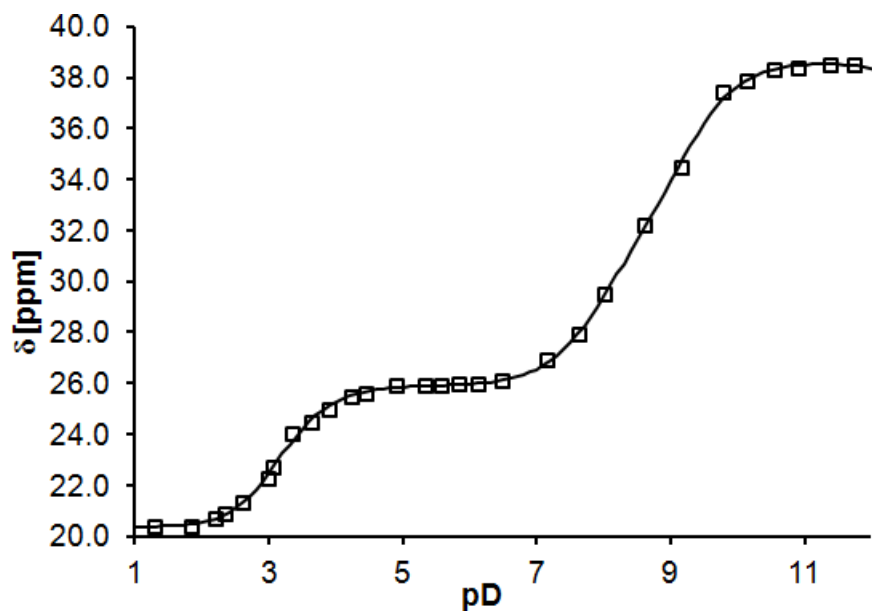


Figure S2. ^{31}P NMR titration of $\text{H}_6\text{do3aP}^{\text{ida}}$.

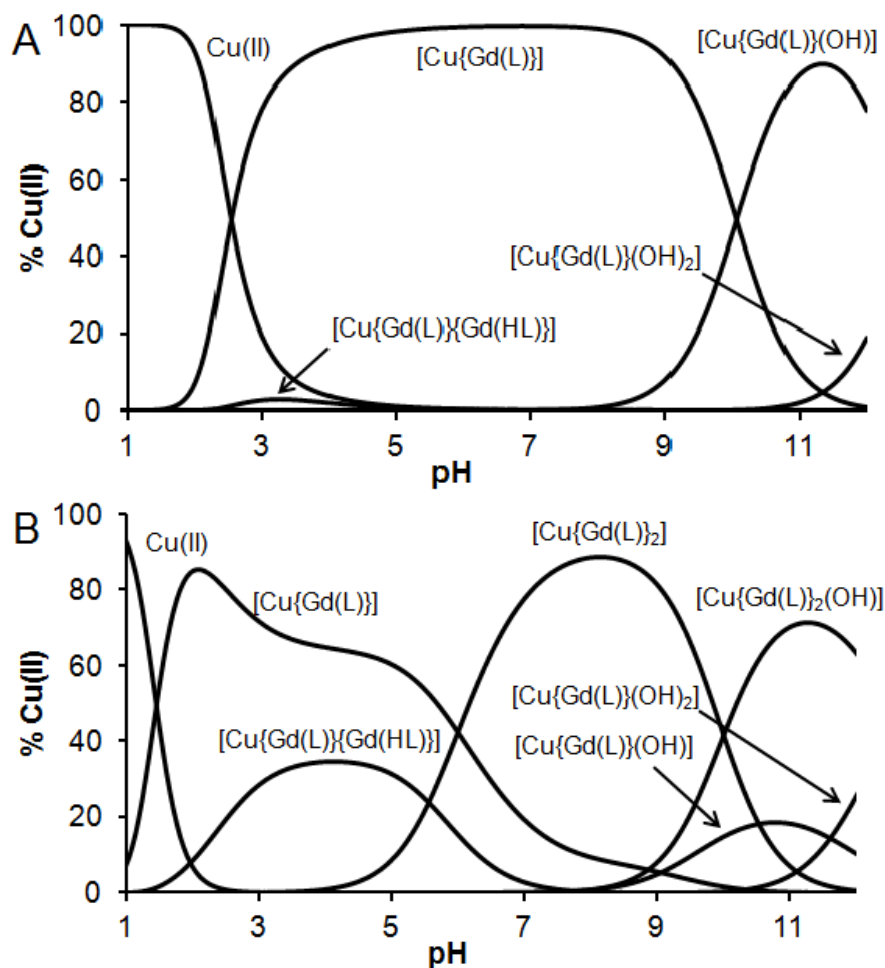


Figure S3. Distribution diagram of $\text{Cu(II)}\text{-}[\text{Gd}(\text{H}_n\text{do3aP}^{\text{ida}})]^{n-3}$ system ($25\text{ }^\circ\text{C}$, $I = 0.1\text{ M (NMe}_4\text{)Cl}$, $c_{\text{GdL}} = 4\text{ mM}$, $c_{\text{M}} = 4\text{ mM}$ (A) $c_{\text{M}} = 2\text{ mM}$ (B)). Charges are omitted for clarity reasons.

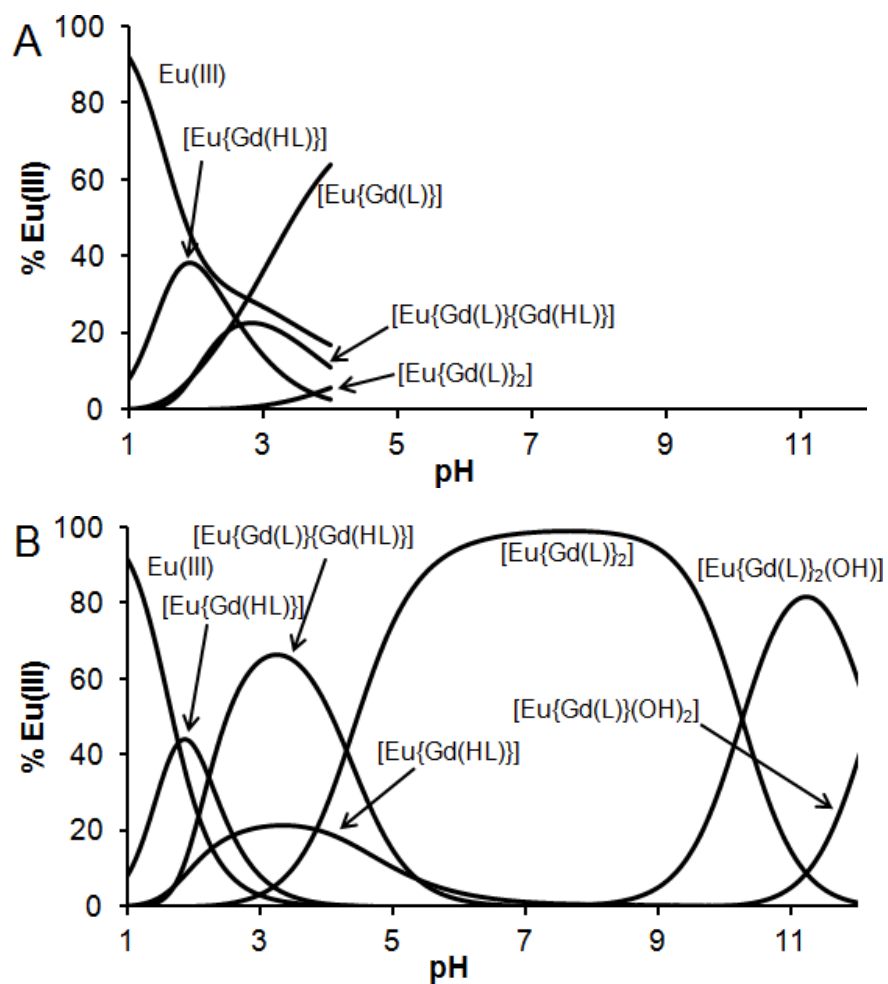


Figure S4. Distribution diagram of Eu(III)–[Gd(H_ndo3aP^{ida})]^{n–3} system (25 °C, *I* = 0.1 M (NMe₄)Cl, *c*_{GdL} = 4 mM, *c*_M = 4 mM (A) *c*_M = 2 mM (B)). Charges are omitted for clarity reasons.

Table S6. Experimental data of the reported crystal structures.

Compound	H ₆ do3aP ^{ida} ·4H ₂ O	[Cu ₄ (do3aP ^{ida})(OH)(H ₂ O) ₄]Cl·7.5H ₂ O
Formula	C ₂₀ H ₃₆ N ₅ O ₁₂ P·4H ₂ O	C ₂₀ H ₃₉ Cu ₄ N ₅ O ₁₇ PCl·7.5H ₂ O
<i>M_r</i>	641.57	1077.26
Colour	colorless	blue
Shape	prism	prism
Dimensions (mm)	0.35×0.13×0.10	0.30×0.25×0.21
Crystal system	triclinic	triclinic
Space group	<i>P</i> ₋₁	<i>P</i> ₋₁
<i>a</i> (Å)	9.5462(4)	12.0847(5)
<i>b</i> (Å)	10.7017(7)	12.4493(5)
<i>c</i> (Å)	16.0510(10)	12.9847(5)
α (°)	100.877(2)	85.606(2)
β (°)	95.356(4)	78.603(2)
γ (°)	112.760(3)	86.931(2)
<i>V</i> (Å ³)	1459.66(15)	1907.87(13)
<i>Z</i>	2	2
<i>D_c</i> (g·cm ⁻³)	1.460	1.875
μ (mm ⁻¹)	0.176	2.407
<i>F</i> (000)	684	1106
Reflections unique; observed (<i>I</i> ₀ > 2σ(<i>I</i>))	5679; 3638	7764; 8790
Parameters	388	523
G-o-f on <i>F</i> ²	1.057	1.125
<i>R</i> ; <i>R'</i> (all data)	0.0728; 0.1119	0.0404; 0.0489
<i>wR</i> ; <i>wR'</i> (all data)	0.2071; 0.2370	0.0977; 0.1042
Difference max; min (e Å ⁻³)	1.329; 0.474	1.675; 1.146

Table S7. The coordination distances found in the crystal structure of [Cu₄(do3aP^{ida})(OH)(H₂O)₄]Cl·7.5H₂O.

Bond	Distance [Å]	Bond	Distance [Å]
Cu1–N1	2.066(3)	Cu2–O241	1.946(3)
Cu1–N4	2.101(3)	Cu2–O261	1.951(3)
Cu1–N7	2.059(3)	Cu2–N22	2.018(3)
Cu1–N10	2.089(3)	Cu2–O412 ^a	1.930(3)
Cu1–O311	2.489(2)	Cu2–O1C	2.497(4)
Cu1–O511	2.216(3)	Cu2–O11	2.697(3)
Bond	Distance [Å]	Bond	Distance [Å]
Cu3–O11	1.927(2)	Cu4–O512 ^a	1.919(3)
Cu3–O311	1.972(2)	Cu4–O312	1.939(3)
Cu3–O2C	1.977(2)	Cu4–O5C	2.005(3)
Cu3–O2C ^b	1.976(2)	Cu4–O2C ^b	2.042(2)
Cu3–O511	2.376(2)	Cu4–O3C	2.268(3)
Cu3–O3C	2.491(3)	Cu4–O4C	2.412(3)

^a Symmetrically-associated ligand molecule. ^b Symmetrically-associated hydroxido ligand.

Figure S5. The coordination mode of the Cu1 ion in the crystal structure of $[\text{Cu}_4(\text{do3aP}^{\text{ida}})(\text{OH})(\text{H}_2\text{O})_4]\text{Cl}\cdot 7.5\text{H}_2\text{O}$. The hydrogen atoms attached to the carbon atoms are not displayed for the clarity reasons.

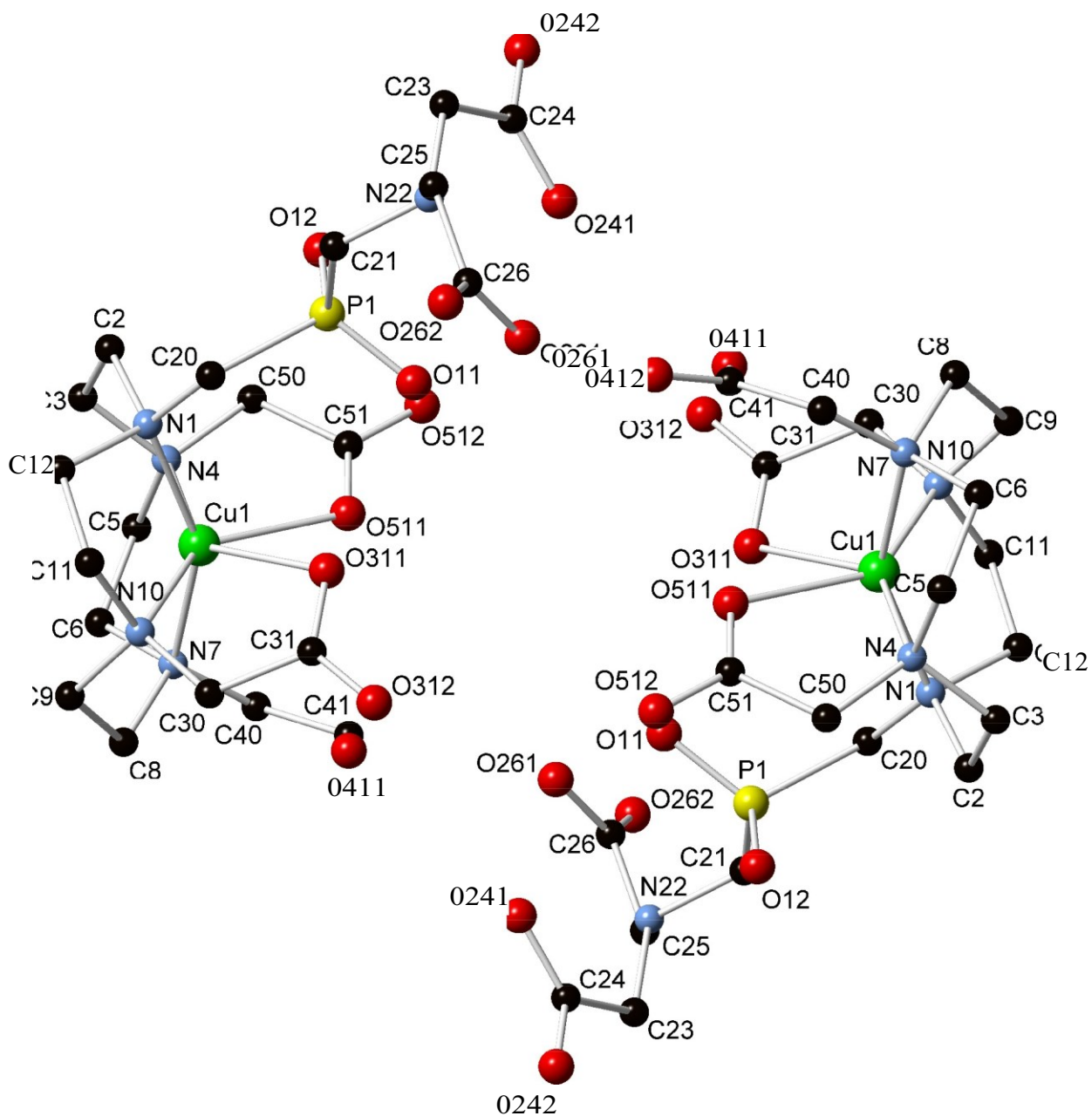


Figure S6. The coordination mode of the Cu2 ion in the crystal structure of $[\text{Cu}_4(\text{do3aP}^{\text{ida}})(\text{OH})(\text{H}_2\text{O})_4]\text{Cl}\cdot 7.5\text{H}_2\text{O}$. The hydrogen atoms attached to the carbon atoms are not displayed for the clarity reasons.

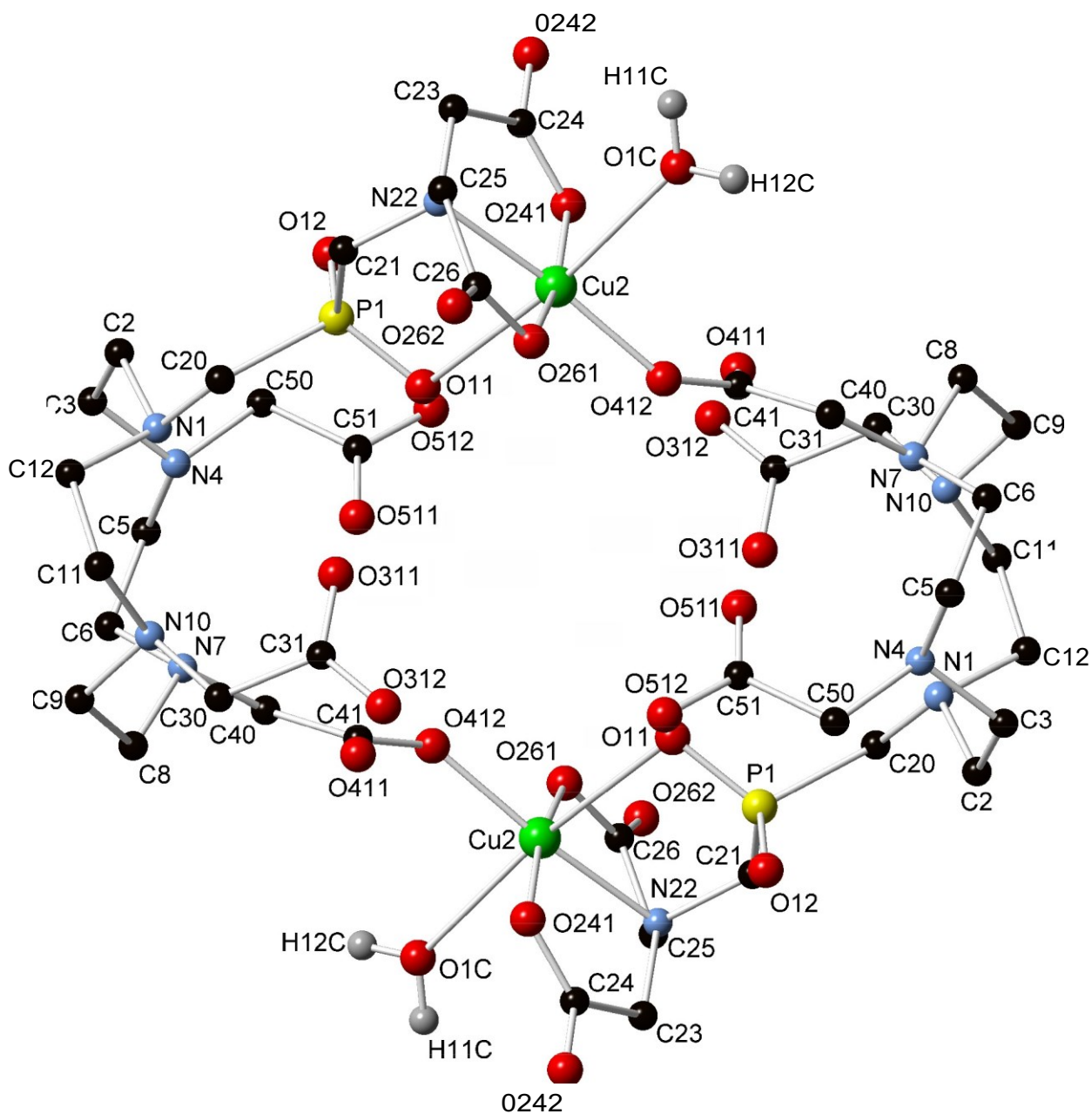


Figure S7. The coordination mode of the Cu3 ion in the crystal structure of $[\text{Cu}_4(\text{do3aP}^{\text{ida}})(\text{OH})(\text{H}_2\text{O})_4]\text{Cl}\cdot 7.5\text{H}_2\text{O}$. The hydrogen atoms attached to the carbon atoms are not displayed for the clarity reasons.

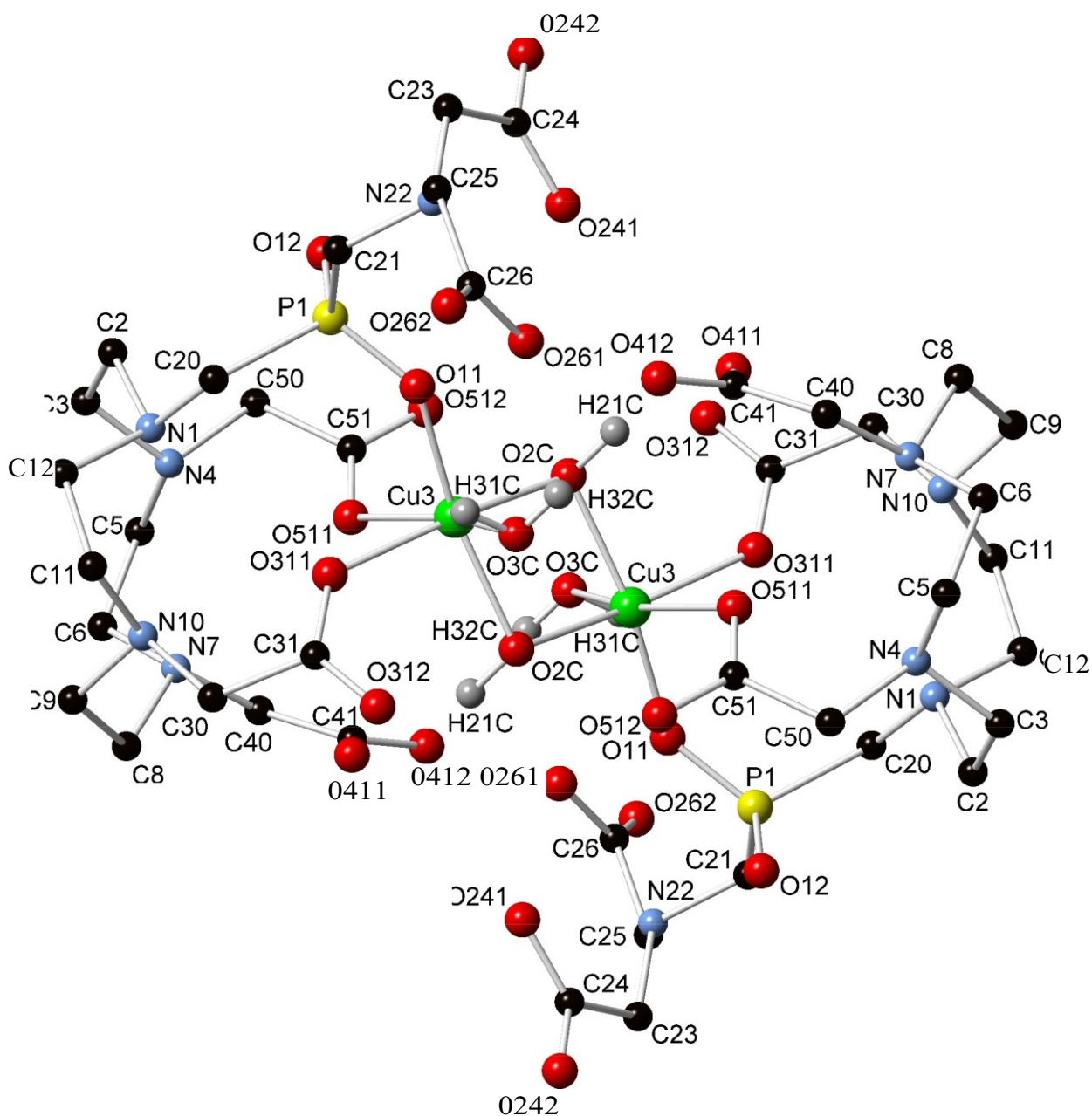


Figure S8. The coordination mode of the Cu₄ ion in the crystal structure of [Cu₄(do3aP^{ida})(OH)(H₂O)₄]Cl·7.5H₂O. The hydrogen atoms attached to the carbon atoms are not displayed for the clarity reasons.

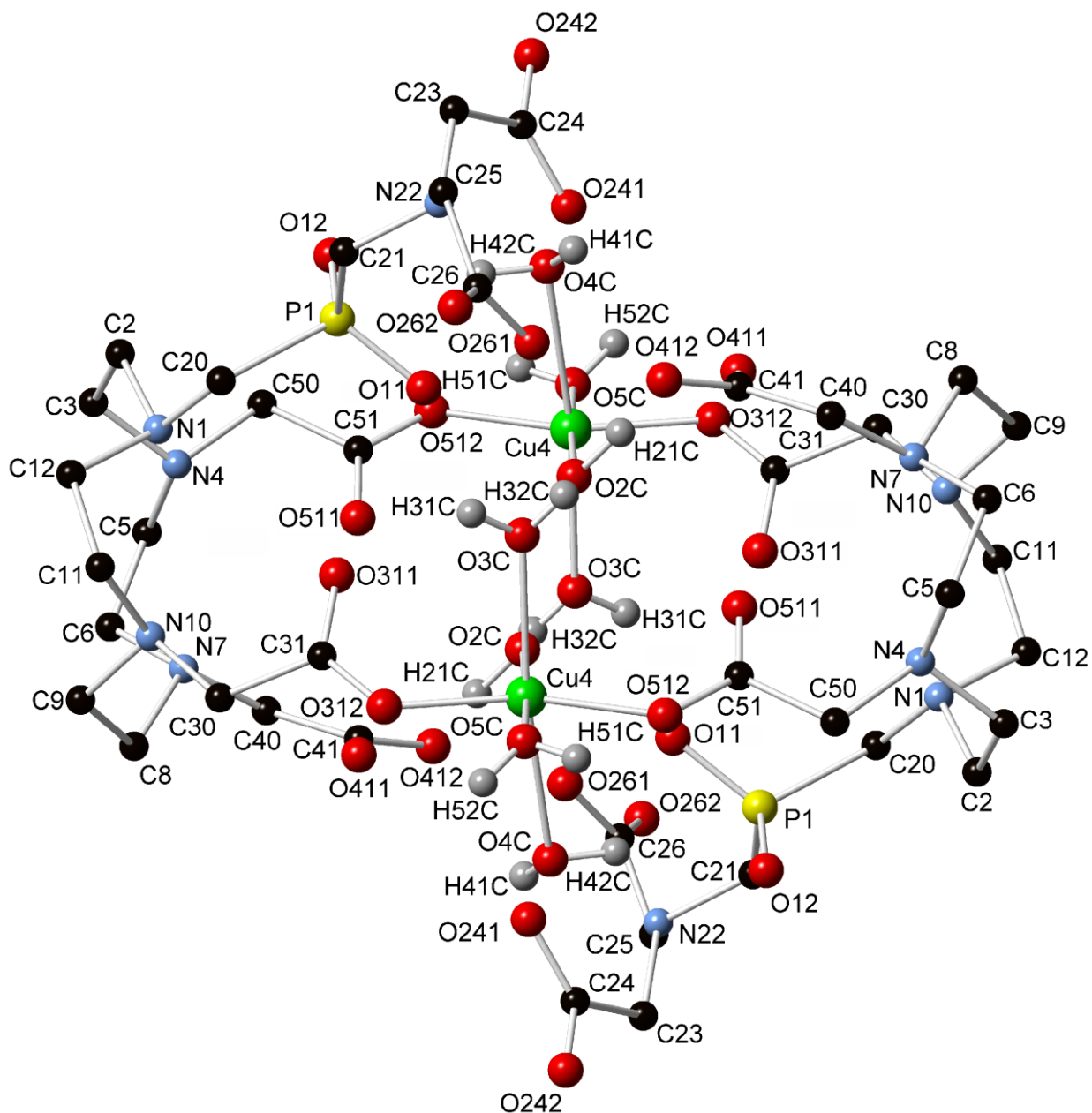


Figure S9. UV-Vis spectra at the beginning of measurement, corresponding to the *out-of-cage* complex (blue), and at the end of measurement, corresponding to the *in-cage* complex (red), performed under the 10-fold metal excess (pH = 6.5, $c_{Ce} = 5.0 \cdot 10^{-3}$ M, $c_L = 5.0 \cdot 10^{-4}$ M, 25 °C). The increasing absorbance at short wavelengths results from the Ce(III) ion excess. Similar spectra were observed along the whole studied pH range.

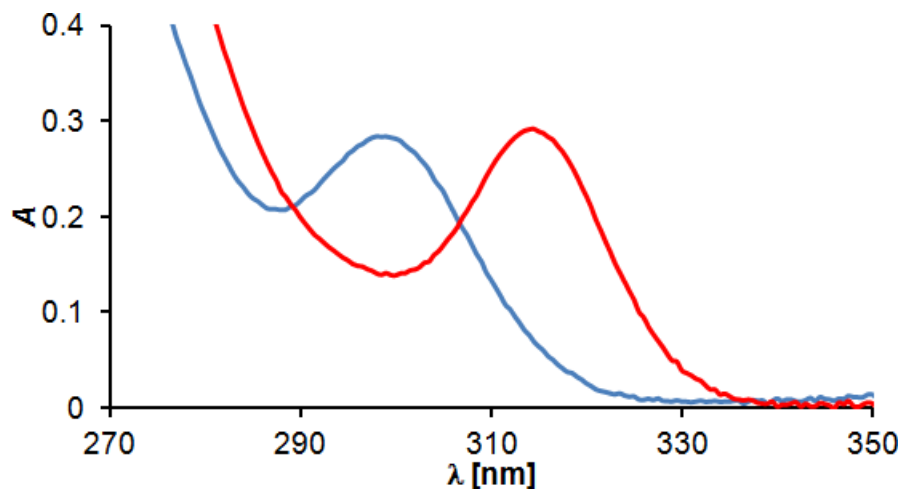


Figure S10. UV-Vis spectra at the beginning of measurement, corresponding to the *out-of-cage* complex (**A**, the spectra change with pH), and at the end of measurement, corresponding to the *in-cage* complex (**B**, pH = 6.5, similar spectra were observed along the whole studied pH range), performed under the 10-fold ligand excess ($c_{Ce} = 5.0 \cdot 10^{-4}$ M, $c_L = 5.0 \cdot 10^{-3}$ M, 25 °C).

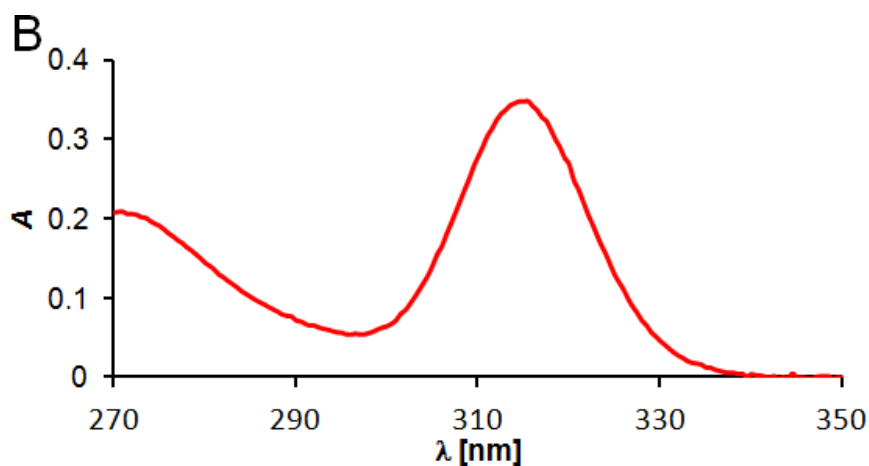
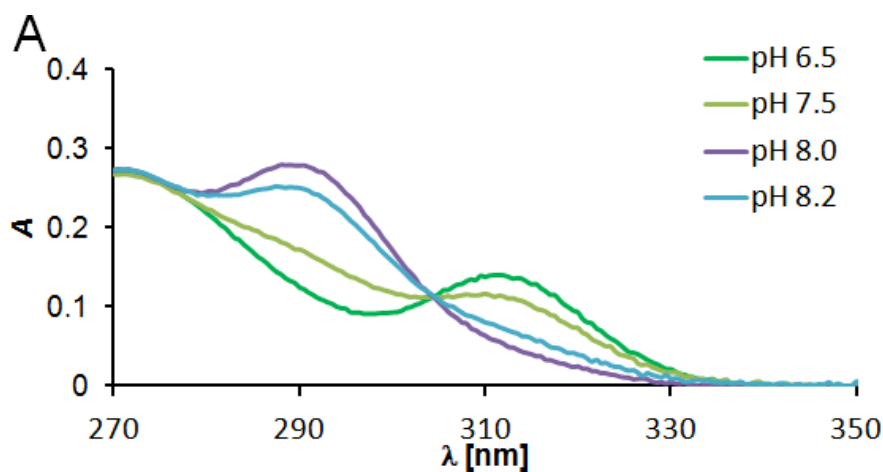
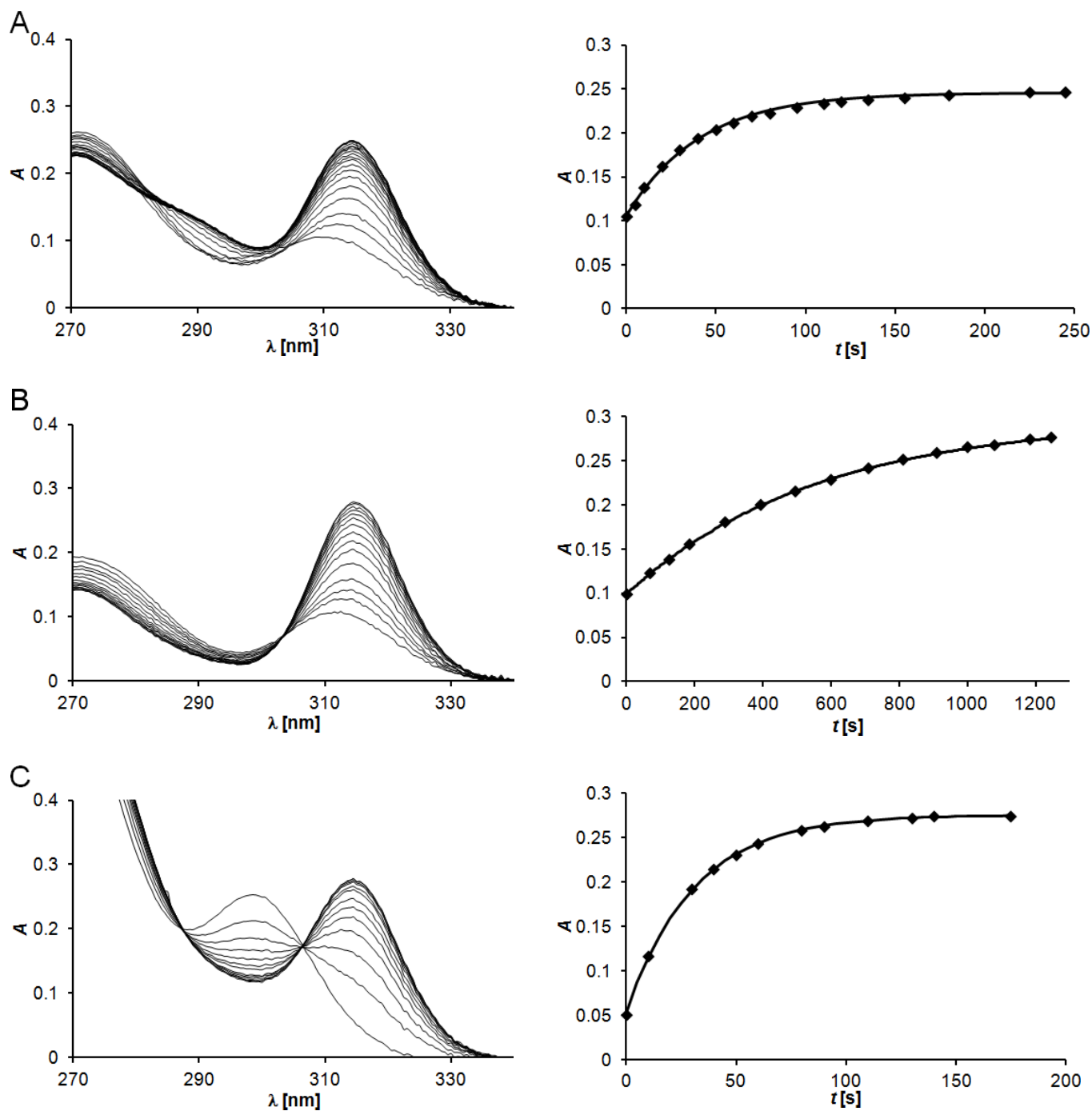


Figure S11. Changes of absorption spectra in the course of complexation (left, pH = 6, 25 °C) and time dependences of absorbance at 314 nm (right). The curves represent the best fit according to Equation 1. **A:** $c_{Ce} = 5.0 \cdot 10^{-4}$ M, $c_L = 5.0 \cdot 10^{-4}$ M; **B:** $c_{Ce} = 5.0 \cdot 10^{-4}$ M, $c_L = 5.0 \cdot 10^{-3}$ M; **C:** $c_{Ce} = 5.0 \cdot 10^{-3}$ M, $c_L = 5.0 \cdot 10^{-4}$ M.



Cite this: *Dalton Trans.*, 2018, 47, 13006Lanthanide(III) complexes of monophosphinate/
monophosphonate DOTA-analogues: effects of
the substituents on the formation rate and
radiolabelling yield†Soňa Procházková,^a Vojtěch Kubíček,^{a*} Jan Kotek,^a Adrienn Vágner,^{‡b}
Johannes Notni,^c and Petr Hermann^a

H₄dota and its analogues are routinely used for complexation of lanthanide radioisotopes in nuclear medicine. Many of the radioisotopes have short half-lives and, thus, the complexation rate plays an important role. Notwithstanding that, the relationship between ligand structures and complexation rates is not well understood. Here we report a complexation study of H₄dota and its analogues bearing one phosphonate or phosphinate pendant arm. The substituents on the phosphinate group were non-coordinating (–H) or contained another coordinating group (–CH₂N(CH₂COOH)₂, –CH₂PO₂H₂ or –CH₂NH₂). The basicity of ligands, stability of reaction intermediates, formation rates of Ce^{III} complexes, and ¹⁷⁷Lu^{III} radiolabelling were studied. The complexation rates and labelling yields do not show any correlation with ligand basicity. In contrast, the additional chelating group attached to the pendant arm plays an important role. A decreased complexation rate and lower labelling yield were found for compounds bearing an additional amino group, whereas improved properties were found for the compound bearing a geminal bis(phosphinate) pendant arm. It indicates that the introduction of chelating pendant arms with acidic coordinating groups might be a promising strategy to improve radiolabelling of macrocyclic carriers with metal radioisotopes.

Received 26th June 2018,
Accepted 13th August 2018

DOI: 10.1039/c8dt02608d

rsc.li/dalton

Introduction

Macrocyclic ligands are used as metal ion carriers in various medical imaging techniques such as Magnetic Resonance Imaging (MRI), Single-Photon Emission Computed Tomography (SPECT), Positron Emission Tomography (PET) or Optical Imaging (OI), and in radiotherapy.^{1–7}

For a long time, significant interest has been focused on their lanthanide(III) complexes as Gd^{III} ions are dominantly used in MRI contrast agents and several lanthanide radio-

isotopes such as ¹⁵³Sm, ¹⁶⁶Ho, or ¹⁷⁷Lu are used in nuclear medicine. In these applications, the metal ions must be bound in a thermodynamically stable and kinetically inert complex to prevent toxicity of free metal ions or nonspecific deposition in tissues. The octadentate macrocyclic ligand H₄dota (Chart 1) and its analogues are ligands that are ideal for producing stable lanthanide(III) complexes for biomedical applications.

One of the most important parameters in the development of metal-based radiopharmaceuticals is the complex formation rate. The complex formation rate is the limiting factor mainly for the short living radioisotopes. Thus, radiolabelling is often performed at a high temperature to accelerate complexation and achieve high labelling yields. However, many of the newly developed radiopharmaceuticals are conjugates with biomolecules to ensure desired biodistribution. The biomolecules are often sensitive compounds (*e.g.* oligopeptides or antibodies) and, thus, labelling cannot be performed under harsh conditions. Therefore, development of new chelators enabling fast and efficient complexation under mild conditions is still in the centre of interest.

Formation of the dota-like complexes proceeds in two steps.^{8–15} In the first step, the metal ion is coordinated by the pendant arm oxygen atoms forming an *out-of-cage* complex,

^aDepartment of Inorganic Chemistry, Faculty of Science, Charles University, Hlavova 2030, 128 43 Prague 2, Czech Republic. E-mail: kubicek@natur.cuni.cz; Fax: +420 221951253; Tel: +420 221951436

^bDepartment of Inorganic and Analytical Chemistry, University of Debrecen, Debrecen, Egyetem tér 1, H-4032, Hungary

^cLehrstuhl für Pharmazeutische Radiochemie, Technische Universität München, Walther-Meissner-Strasse 3, D-85748 Garching, Germany

† Electronic supplementary information (ESI) available: Crystal packing of Eu^{III}-do3aP^H, molecular structure of do3a-lactame, experimental data of crystal structures, overall protonation constants, absorption spectra of Ce^{III} complexes, formation rate constants. CCDC 1846694–1846696. For ESI and crystallographic data in CIF or other electronic format see DOI: 10.1039/c8dt02608d

‡ Present address: Scanomed Ltd, Debrecen, Hungary.

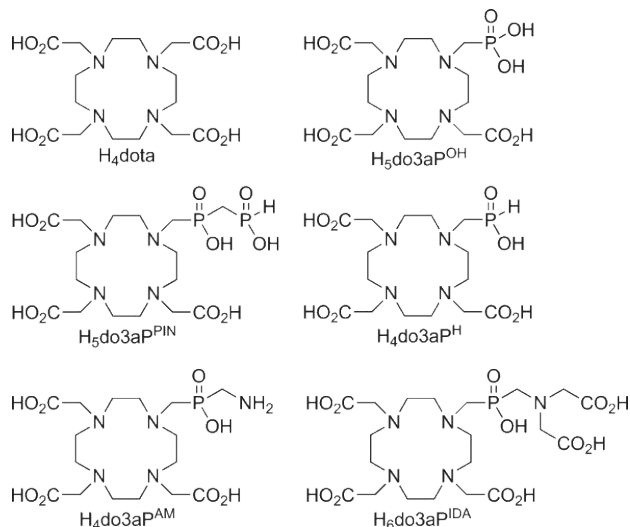


Chart 1 Structures of the studied ligands.

whereas the macrocycle amino groups are protonated. The rate-determining step of the complexation is deprotonation of the ring nitrogen atoms and simultaneous formation of the *in-cage* complex with the metal ion coordinated by four nitrogen and four oxygen atoms. The complexation rate could be modified by the introduction of pendant arms bearing various coordinating groups such as amides, amines, phenols, thiols, pyridines, and phosphonic or phosphinic acids. We have shown that the phosphonate and/or phosphinate pendants may change the complexation rate in positive as well as in negative ways.^{16–21} The improvement was observed mainly for phosphinate derivatives bearing an additional coordinating group in the pendant arm. However, recently, we have shown that the introduction of a strongly complexing pendant such as bis (phosphonate) or imino-diacetate groups leads to a decrease of the *in-cage* complex formation rate due to an excessive stabilization of the *out-of-cage* intermediate.^{15,22} To better understand the effect of the pendant arm structure on the complexation rate, we present here a comparative complex formation and radiolabelling study on the series of monophospho(i)nate dota-analogues (Chart 1). In order to find the relationship between the ligand structure and complexation rate, we show a comparison of the ligand basicity, stability of *out-of-cage* complexes, formation rates of Ce^{III} *in-cage* complexes under “chemical” conditions and formation of ¹⁷⁷Lu^{III} complexes under “radiochemical” (low concentration) conditions.

Experimental part

Materials and methods

Commercially available chemicals were used as received. *t*Bu₃do3a·HBr (H₃do3a = 1,4,7,10-tetraazacyclododecane-1,4,7-triacetic acid) (ref. 23), H₄dota (ref. 24), H₅do3aP (ref. 25), H₆do3aP^{IDA} (ref. 22) and H₄do3aP^{AM} (ref. 26) were synthesized according to the published procedures. The ¹H (400 or

300 MHz), ¹³C (100 or 75 MHz) and ³¹P (162 or 122 MHz) NMR spectra were acquired at 25 °C (unless stated otherwise) with Varian Unity Inova-400 and -300 spectrometers, respectively. For the ¹H and ¹³C NMR measurements in D₂O, the methyl signals of *t*BuOH were used as an internal standard ($\delta = 1.2$ and 31.2 ppm for ¹H and ¹³C NMR, respectively). The ³¹P chemical shifts were measured with respect to 1% H₃PO₄ in D₂O as an external reference. ESI-MS spectra were recorded on a Bruker Esquire 3000 spectrometer equipped with an electrospray ion source and an ion-trap detection system. ¹⁷⁷Lu^{III} for radiolabelling was obtained from Isotope Technologies Garching (Garching, Germany) as a ¹⁷⁷Lu^{III} chloride solution in 0.05 M HCl. Elemental analyses were performed at the Institute of Organic Chemistry and Biochemistry (Prague, Czech Republic).

Synthesis

Synthesis of H₄do3aP^H. *t*Bu₃do3a (3.00 g, 5.0 mmol) was dissolved in CF₃COOH (30 ml) and CHCl₃ (30 ml). The solution was refluxed for 6 h and then evaporated. The residue – H₃do3a, intermediate 1 – was dissolved in 6 M aq. HCl (100 ml), 50% aq. H₃PO₂ (2.78 g, 21 mmol) was added and the solution was heated to 60 °C. Paraformaldehyde (0.126 g, 4.2 mmol) was added portion-wise for 1 h. The mixture was stirred for 2 d at 60 °C. Volatiles were evaporated and the residue was purified on a strong cation exchange resin (Dowex 50, H⁺-form). Impurities were eluted with water, and the product was eluted with 10% aq. pyridine. The crude product was purified on a strong anion exchange resin (Amberlite IRA, acetate-form). Impurities were eluted with water and 2% aq. acetic acid, and the product was eluted with 20% aq. acetic acid. The fractions containing the pure product were evaporated and the residue was co-evaporated with water three times. The obtained colourless oil was dissolved in a minimum amount of water and the product was crystallized by the addition of EtOH. The white crystalline powder was filtered and dried under vacuum over P₂O₅ (1.66 g, 83% based on paraformaldehyde).

NMR (D₂O + NaOD, pD ≥ 12): ¹H: 2.2–2.6 (*ctc*, 16H), 2.71 (N–CH₂–P, bs, 2H), 2.95 (N–CH₂–COOH, bs, 6H), 6.37 (P–H₂d, ¹J_{PH} = 522 Hz); ¹³C{¹H}: 60.1 (*ctg* s, 2C), 61.0 (*cgle* s, 2C), 62.0 (*cycle* s, 4C), 64.1 (N–CH₂–P, d, ¹J_{CP} = 88 Hz, 1C), 64.8 (N–CH₂–COOH, s, 2C), 65.7 (N–CH₂–COOH, s, 1C), 183.5 (CH₂–COOH, s, 2C), 183.8 (CH₂–COOH, s, 1C) ³¹P: 20.5 (d, ¹J_{PH} = 525 Hz); MS-ESI: (–) 439.1 (M – H)[–]; EA: calculated for C₁₅H₂₉N₄O₈·3H₂O (*M*_r = 478.4): C, 37.7; H, 7.4; N, 11.7; found C, 37.5; H, 7.5; N, 12.0.

Late fractions of the ion exchange workup contained DO3A lactam and its structure was determined by X-ray diffraction analysis (Fig. S3†).

Synthesis of 4. Cyclen 2 (2.40 g, 14 mmol) and methylenebis(phosphinic acid) 3 (1.00 g, 7.0 mmol) were dissolved in 6 M aq. HCl (50 ml) and the mixture was heated to 40 °C. Paraformaldehyde (0.10 g, 3.3 mmol) was added portion-wise for 1 h. The mixture was stirred for 2 d at 40 °C. Volatiles were evaporated and the residue was purified on a strong cation

exchange resin (Dowex 50, H⁺-form). Impurities were eluted with water and the product was eluted with 5% aq. ammonia. The crude product was purified on a strong anion exchange resin (Amberlite IRA, OH⁻-form). Impurities were eluted with water and the product was eluted with 6 M aq. HCl. Evaporation yielded a colourless residue that was dried under vacuum at 80 °C. The product was obtained as a white powder (1.08 g, 73% based on paraformaldehyde).

NMR (D₂O + NaOD, pD ≥ 12): ¹H δ 2.04 (P-CH₂-P, t, 2H, ²J_{HP} = 17 Hz); 2.61 (cyle, m, 4H); 2.65 (cyl, m, 4H); 2.76 (cycle, m, 8H); 2.76 (N-CH₂-P, d, 2H, ²J_{HP} = 8 Hz); 7.15 (P-H, d, 1H, ¹J_{HP} = 530 Hz); ¹³C{¹H} δ 35.8 (P-CH₂-P, dd, ¹J_{CP} = 77 Hz, ¹J_{CP} = 74 Hz, 1C); 44.3 (cycle, s, 2C); 45.2 (cyls, 2C); 45.7 (cyle, s, 2C); 53.1 (CH₂-N-CH₂-P, d, ³J_{CP} = 7 Hz, 2C); 56.3 (N-CH₂-P, d, ¹J_{CP} = 109 Hz, 1C); ³¹P δ 19.4 (P-H, dtd, 2P, ¹J_{PH} = 530 Hz, ²J_{PH} = 17 Hz, ²J_{PP} = 6 Hz); 32.6 (P-CH₂-N, m, 2P); MS-ESI: (-) 327.5 [M - H]⁻; EA: calculated for C₁₀H₂₆N₄O₄P₂·2.5H₂O·2HCl (M_r = 446.2): C, 26.9; H, 7.5; N, 12.6; found C, 26.7; H, 7.7; N, 12.4.

Synthesis of H₅do3aP^{PH}. Hydrochloride of 4 (0.50 g, 1.1 mmol), chloroacetic acid (0.21 g, 22 mmol) and LiOH (2.35 g, 56 mmol) were dissolved in water (100 ml). The mixture was heated at 70 °C for 6 h. Volatiles were evaporated and the resulting oil was purified on a strong cation exchange resin (Dowex 50, H⁺-form). Impurities were eluted with water. The product was eluted with 10% aq. pyridine and was further purified on a weak cation exchange resin (Amberlite CG50, H⁺-form) by elution with water. Volatiles were evaporated and the residue was slowly added dropwise into anhydrous EtOH. The precipitate was filtered off and dried under vacuum over P₂O₅. The product was obtained as a white crystalline powder (0.32 g, 49% based on 4).

NMR (D₂O + NaOD, pD ≥ 12): ¹H: 2.33 (P-CH₂-P, t, 2H, ²J_{PH} = 17 Hz), 3.21 (cylcbs, 8H), 3.4–3.7 (cycleβH), 3.53 (N-CH₂-P, d, 2H, ²J_{PH} = 6 Hz), 3.78 (N-CH₂-COOH, s, 4H), 4.00 (N-CH₂-COOH, s, 2H), 7.16 (P-H, d, ¹J_{PH} = 552 Hz), ¹³C{¹H}: 38.9 (P-CH₂-P, t, ¹J_{CP} = 94 Hz, 1C), 47.2 (cyl, 2C), 50.3 (cylc, s, 2C), 51.0 (cyls, 2C), 52.6 (cycle, s, 2C), 53.7 (N-CH₂-P, d, ¹J_{CP} = 104 Hz, 1C), 56.1 (N-CH₂-COOH, s, 2C), 56.5 (N-CH₂-COOH, s, 1C), 178.1 (CH₂-COH, s, 2C), 182.2 (CH₂-COH, s, 1C), ³¹P: 20.5 (P-H, dtd, ¹J_{PH} = 556 Hz, ²J_{PH} = 18 Hz, ²J_{PP} = 4 Hz), 23.1 (CH₂-PCH₂, bs); MS-ESI: (-) 501.3 (M - H)⁻; EA: calculated for C₁₆H₃₂N₄O₁₀P₂·2H₂O (M_r = 583.4): C, 35.7; H, 6.7; N, 10.4; found C, 35.6; H, 6.9; N, 10.1.

X-ray diffraction studies

Single-crystals of (H₆do3aP^{PH})Cl₂·THF·3H₂O were grown by vapour diffusion of THF into a solution of H₄do3aP^{PH} in 6 M aq. HCl. A solution of the Eu^{III}-H₄do3aP^{PH} complex was prepared by mixing equimolar amounts of EuCl₃ and H₄do3aP^{PH} in water followed by pH adjustment with NaOH solution (final pH ≈ 5). From this solution, the single-crystals of composition Na[Eu(do3aP^{PH})(H₂O)]·2NaCl·7.125H₂O were grown by vapour diffusion of EtOH.

The diffraction data were collected at 150 K (Cryostream Cooler, Oxford Cryosystem) using a Nonius Kappa CCD diffr-

actometer and Mo-K_α radiation (λ = 0.71073 Å) and were analysed using the HKL DENZO software package.²⁷ The structures were solved by direct methods (SIR92)²⁸ and refined by full-matrix least-squares techniques (SHELXL2014).²⁹ All non-hydrogen atoms were refined anisotropically. Almost all hydrogen atoms were localized in a difference density map; however, those bound to the carbon atoms were placed in theoretical positions with thermal parameters U_{eq}(H) = 1.2U_{eq}(C) to keep the number of refinement parameters low. Hydrogen atoms bound to heteroatoms (O, N) were usually fully refined.

In the crystal structure of (H₆do3aP^{PH})Cl₂·THF·3H₂O, the THF molecule was found to be disordered in two positions, sharing the oxygen atom, which is involved as an acceptor in the hydrogen bond with one of the protonated carboxylate moieties. The occupancy of both positions was refined as 55 : 45%. In the crystal structure of Na[Eu(do3aP^{PH})(H₂O)]·2NaCl·7.125H₂O, no disorder was found. Two of Na^I ions are placed in general positions and other two independent Na^I ions occupy special positions with 50% occupancies. A large electronic maximum present in specially occupied positions (with an occupancy factor of 0.5) was best interpreted as 0.125 of water molecules to keep its thermal parameter comparable to other water molecules of crystallization. Except for this low-occupied water molecule, all hydrogen atoms were found in the difference density map. Table S1† contains selected crystallographic parameters for the structures reported in this paper. Complete data for the structures have been deposited at the Cambridge Crystallographic Data Centre as CCDC 1846694–1846696.†

Potentiometric titrations

Methodology of the potentiometric titrations and processing of the experimental data were analogous to those previously reported.^{18,30} Titrations were carried out in a vessel thermostatted at 25 ± 0.1 °C at an ionic strength I = 0.1 M (NMe₄)Cl, and the pH range used was 1.7–12.0. The titrations were carried out at least three times, each consisting of about 40 points. The water ion product (pK_w = 13.81) was taken from the literature.³¹ The calculated overall protonation constants β_n are concentration constants and are defined by β_n = [H_nL]/([H]ⁿ[L]), and consecutive protonation constants are log K(HL) = log β₁ and log K(H_nL) = log β_n - log β_{n-1}. The constants (with standard deviations) were calculated with the OPIUM software package.³²

Formation kinetics studies

The experiments were carried out in the pH range 3.5–7.5 employing a Specord 50 Plus spectrophotometer (Analytik Jena AG). The temperature was 25 ± 0.1 °C maintained using a Peltier block. The kinetics was studied in 1 cm sample cells using the following non-coordinating buffers (c = 0.2 M): 1,4-dimethylpiperazine (pH 3.5–5.1), MES (pH 5.4–6.8; MES = 2-(N-morpholino)ethanesulfonic acid), and HEPES (pH 6.8–7.5; HEPES = 2-[4-(2-hydroxyethyl)piperazin-1-yl]ethanesulfonic acid). Constant ionic strength was maintained by adding a cal-

culated amount of KCl (final concentration was 0.5 M). Formation of the *in-cage* Ce^{III} complex was followed in the wavelength region 270–360 nm employing Ce^{III}:ligand molar ratios of 1:10 ($\alpha_{\text{Ce}} = 4.0 \times 10^{-4}$ M, $\alpha_{\text{L}} = 4.0 \times 10^{-3}$ M) and 10:1 ($\alpha_{\text{Ce}} = 4.0 \times 10^{-3}$ M, $\alpha_{\text{L}} = 4.0 \times 10^{-4}$ M). Examples of time changes of spectra are shown in Fig. S7.† The experiments were initiated by the addition of a Ce^{III} stock solution into the cell and the data acquisition started after 15 s dead time. Time changes of absorbance at the wavelength of the absorption band maximum (312–316 nm) were fitted with the general exponential function (eqn (1)):

$$A_t = A_f + (A_0 - A_f) e^{-k_{\text{obs}} t}$$

where A_t is the absorbance at time t , A_f is the final absorbance, A_0 is the initial absorbance and k_{obs} is the rate constant of the reaction. The data were fitted by means of a least-squares fitting procedure using the Micromath Scientist program version 2.0 (Salt Lake City, UT, USA).

Stability of *out-of-cage* complexes

The formation of the *out-of-cage* complex was studied by UV-Vis spectroscopy in the wavelength region 270–360 nm at pH \approx 0.5–5 and 10:1, 1:1 and 1:10 metal-to-ligand ratios ($\alpha_{\text{Ce}} = 4.0 \times 10^{-4}$ or 4.0×10^{-3} M, $\alpha_{\text{L}} = 4.0 \times 10^{-4}$ or 4.0×10^{-3} M).

The spectra were recorded immediately after mixing of the stock solutions. Examples of spectra are shown in Fig. S5.† Examples of absorbance measured at the wavelength of the absorption band maximum (298–305 nm) as a function of pH are shown in Fig. S6.†

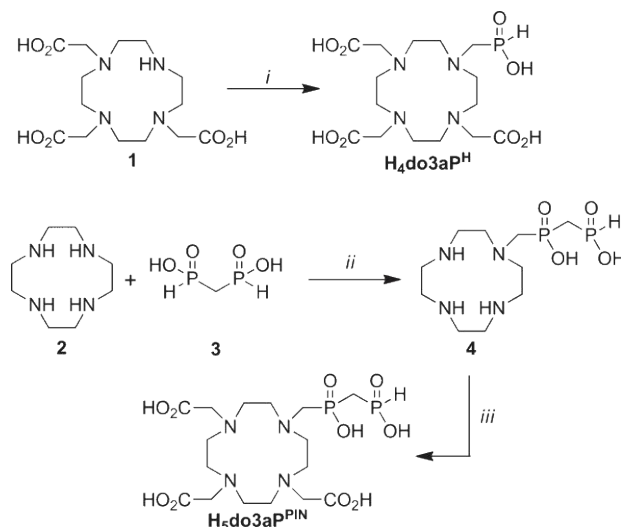
Labelling with ¹⁷⁷Lu

10 MBq of ¹⁷⁷Lu^{III} in 0.04 M aq. HCl (1.8–3.4 μ L) were transferred into Eppendorf vials containing stock solutions of the ligand (ranging from 0.01 nmol to 0.2 nmol) and 90 μ L of aq. NH₄OAc (1 M, pH 6.6). Radiolabelling was performed for 30 min, while the temperature was maintained at 95 °C by placing the closed Eppendorf vials into a thermostated water bath. Radiolabeling as a function of pH (ranging from 2 to 6.6) was studied using 0.1 nmol of the respective chelators and the pH of the reaction solutions was adjusted with 1 M aq. HCl (monitored with a Seven-Easy pH-meter Mettler-Toledo). The ¹⁷⁷Lu^{III} incorporation was evaluated by radio-TLC (stationary phase: silica impregnated glass fibre sheets (ITLC® by Agilent); mobile phase: 0.1 M aq. trisodium citrate solution, pH 8) where labelled chelators stay close to the origin ($R_f = 0.2$) and non-incorporated ¹⁷⁷Lu^{III} moves with the solvent front ($R_f > 0.8$).

Results and discussion

Ligand synthesis

H₄dota (ref. 24), H₅do3aP^{OH} (ref. 25), H₆do3aP^{DA} (ref. 22) and H₄do3aP^{AM} (ref. 26) were prepared according to the published procedures. H₄do3aP^H and H₅do3aP^{PIN} were synthesized by a Mannich-type reaction (Scheme 1). H₄do3aP^H was synthesized



Scheme 1 Synthesis of H₄do3aP^H and H₅do3aP^{PIN}: (i) H₃PO₂, paraformaldehyde, 6 M aq. HCl, 60 °C; (ii) paraformaldehyde, 6 M aq. HCl, 40 °C; and (iii) ClCH₂CO₂H, LiOH, H₂O, 70 °C.

in 83% yield by the reaction of H₃do3a (1) with paraformaldehyde and hypophosphorous acid in 6 M aq. HCl. The amount of formaldehyde used was sub-molar with respect to H₃do3a, because in the presence of an equimolar (or higher) amount, hydroxymethylation of the P–H bond in the H₄do3aP^H molecule was observed by ³¹P NMR spectroscopy. When old batches of H₃do3a were used (especially when stored in a semi-solid form obtained by evaporation from acid media after deesterification), some amount of lactam H₂do3a^{lac} was isolated as a late fraction of the ion exchange workup of the reaction mixture. To minimize the lactam formation, a deesterification of tBu₃do3a to H₃do3a was performed immediately before the synthesis of H₄do3aP^H. The lactam by-product was separated from the reaction mixture by ion exchange chromatography and isolated in the form of dihydrochloride (H₄do3a^{lac}) Cl₂·2H₂O, and the identity of this compound was confirmed by X-ray diffraction analysis (Fig. S3†).

Ligand H₅do3aP^{PIN} was synthesized in two steps. First, cyclen (2) was treated with methylene-bis(phosphinic acid) (3) and paraformaldehyde. Cyclen and methylene-bis(phosphinic acid) were used in excess to avoid the formation of multiply substituted products and hydroxymethylation of the P–H bond of the intermediate 4. The excess of reagents was easily removed using an ion exchange resin. The monosubstituted product 4 was isolated in 73% yield. Subsequently, the cyclen secondary amino groups were alkylated using chloroacetic acid. The compound H₅do3aP^{PIN} was obtained in 49% yield (related to 4).

X-ray diffraction studies

(H₆do3aP^H)Cl₂·THF·3H₂O. The hexaprotonated ligand molecule adopts the most common conformation of cyclen derivatives with all the pendant arms pointing to the same side of the macrocyclic plane.³³ Two macrocycle nitrogen atoms

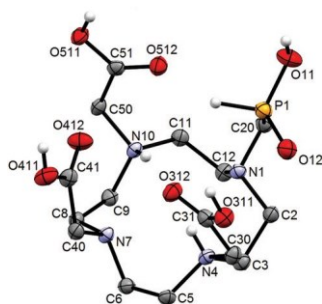


Fig. 1 Molecular structure of the $(\text{H}_6\text{do3aP}^{\text{H}})^{2+}$ cation found in the crystal structure of $(\text{H}_6\text{do3aP}^{\text{H}})\text{Cl}_2 \cdot \text{THF} \cdot 3\text{H}_2\text{O}$. Carbon-bound hydrogen atoms are omitted for clarity.

(those bearing mutually *trans* acetate groups) as well as all four pendant arms are protonated (Fig. 1). The macrocycle ring conformation is stabilized by medium–strong intramolecular hydrogen bonds between protonated and non-protonated amino groups ($d_{\text{N}\cdots\text{N}} \approx 2.88\text{--}2.97 \text{ \AA}$). All protons belonging to the pendant arms are involved in strong hydrogen binding to water molecules of crystallization ($d_{\text{O}\cdots\text{O}} \approx 2.51\text{--}2.58 \text{ \AA}$) and to a molecule of THF ($d_{\text{O}\cdots\text{O}} = 2.62 \text{ \AA}$), and all protons belonging to the water molecules serve as sources of hydrogen bridges to chloride counter anions ($d_{\text{O}\cdots\text{Cl}} \approx 3.01\text{--}3.18 \text{ \AA}$).

$\text{Na}[\text{Eu}(\text{do3aP}^{\text{H}})(\text{H}_2\text{O})] \cdot 2\text{NaCl} \cdot 7.125\text{H}_2\text{O}$. To confirm the suggested molecular structures of the studied complexes, we attempted to prepare several representative Ln^{III} complexes for determination of their crystal structures, and we were successful only in the case of the $\text{Eu}^{\text{III}}\text{--H}_4\text{do3aP}^{\text{H}}$ complex. The Eu^{III} ion is *in-cage* complexed by four nitrogen and four oxygen atoms forming mutually parallel N_4 and O_4 -planes, and its coordination sphere is completed to nona-coordination by an apically bound water molecule (Fig. 2). The same sign of the twist angles of $\text{N}\text{--}\text{C}\text{--}\text{C}\text{--}\text{N}$ macrocyclic chelate rings and of $\text{N}\cdots\text{NQ}\cdots\text{OQ}\cdots\text{O}$ pendant torsions (where NQ and OQ are centroids of the N_4 and O_4 -planes) reveals a twisted-square-anti-prismatic geometry of the complex species (TSA, *i.e.* formation of the $\Delta\delta\delta\delta\delta/\Lambda\Lambda\Lambda\Lambda$ enantiomeric pair).³⁴ The value of the $\text{N}\cdots\text{NQ}\cdots\text{OQ}\cdots\text{O}$ torsion ($25.6\text{--}27.8^\circ$) and separation of the N_4 and O_4 -planes (2.52 \AA) are in the range typical of the TSA

species.^{35,36} The “opening” angles (*trans*- $\text{O}\text{--}\text{Eu}\text{--}\text{O}$ angles) are 134.6 and 139.5° and they are in agreement with the presence of the apically coordinated water molecule but at a relatively long coordination distance (2.56 \AA), as the smaller opening angle is just at the border value of $\approx 135^\circ$ needed to preserve enough space for the apical coordination.^{35,36} Other coordination bond lengths ($\text{Eu}\text{--}\text{N} \approx 2.62\text{--}2.73 \text{ \AA}$; $\text{Eu}\text{--}\text{O} \approx 2.32\text{--}2.42 \text{ \AA}$) are in the range common for the related compounds.

The $[\text{Eu}(\text{do3aP}^{\text{H}})(\text{H}_2\text{O})]^-$ units form a 2-D coordination polymer interconnected by Na^{I} cations bound to oxygen atoms of carboxylate and phosphinate pendant arms (Fig. S1†). Some of the water molecules of crystallization fill the coordination spheres of the Na^{I} ions. The water molecule coordinated to the central Eu^{III} ion serves as a coordination bridge to one of the Na^{I} ions ($d_{\text{Na}\text{--}\text{O}} = 2.41 \text{ \AA}$, $d_{\text{Eu}\cdots\text{Na}} = 3.77 \text{ \AA}$). To this Na^{I} ion, one of the charge-compensating chloride anions is coordinated. The other chloride anion and uncoordinated water molecules are present in the space between the layers formed by the 2-D coordination polymer (Fig. S2†).

Ligand protonation constants

Ligand protonation constants were determined by potentiometry. Since dota-like ligands form weak complexes with alkali metal ions, such as Na^{I} and K^{I} , which influences their protonation constant values, the potentiometric measurements were performed in the presence of non-coordinating tetramethylammonium cations. The results are summarized in Tables 1 and S2.† All ligands show the protonation scheme typical of dota-like compounds. The values of $\log K(\text{HL})$ and $\log K(\text{H}_2\text{L})$ are found in the alkaline region and correspond to the protonation of the macrocycle nitrogen atoms. The basicities of the macrocycles mostly follow the common order phosphinate < carboxylate < phosphonate.³⁷ However, the phosphinate derivatives bearing an additional functional group with an electron-donating character show increased basicity ($\log K(\text{HL}) + \log K(\text{H}_2\text{L})$) comparable with that of H_4dota (Table 1). The third protonation process ($\log K(\text{H}_3\text{L})$) corresponds to the protonation of the phosphonate pendant group in $\text{H}_5\text{do3aP}^{\text{OH}}$ or the protonation of the pendant amino group in $\text{H}_4\text{do3aP}^{\text{AM}}$ and $\text{H}_6\text{do3aP}^{\text{IDA}}$ and occurs in the neutral or weakly alkaline region. The remaining constants correspond to

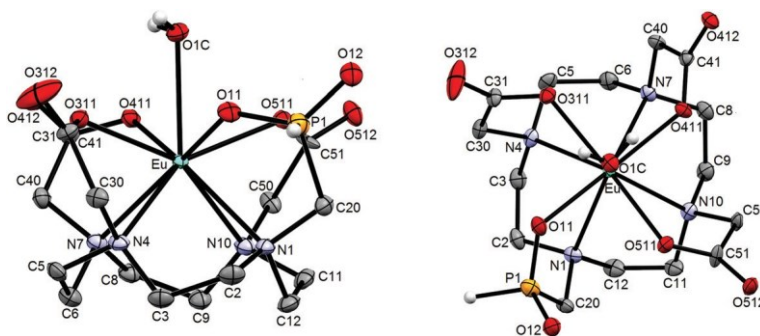


Fig. 2 Molecular structure of the $[\text{Eu}(\text{do3aP}^{\text{H}})(\text{H}_2\text{O})]^-$ complex found in the crystal structure of $\text{Na}[\text{Eu}(\text{do3aP}^{\text{H}})(\text{H}_2\text{O})] \cdot 2\text{NaCl} \cdot 7.125\text{H}_2\text{O}$. Carbon-bound hydrogen atoms are omitted for clarity.

Table 1 Protonation constants of the studied ligands ($I = 0.1 \text{ M NMe}_4\text{Cl}$, $25 \text{ }^\circ\text{C}$). The values of overall protonation constants $\log \beta$ and standard deviations are given in Table S2

	H ₄ dota ^a	H ₅ do3aP ^{OH} ^b	H ₄ do3aP ^H	H ₅ do3aP ^{Pin}	H ₄ do3aP ^{AM}	H ₆ do3aP ^{IDA} ^c
$\log K(\text{HL})$	12.9	13.83	12.43	12.46	13.29	12.85
$\log K(\text{H}_2\text{L})$	9.72	10.35	9.10	9.40	9.56	9.63
$\log K(\text{H}_3\text{L})$	4.62	6.54 ^d	4.33	4.55	8.45 ^e	8.13 ^e
$\log K(\text{H}_4\text{L})$	4.15	4.34	2.78	3.42	4.11	4.40
$\log K(\text{H}_5\text{L})$	2.29	3.09	1.45	2.06	1.86	3.27
$\log K(\text{H}_6\text{L})$	1.34	1.63	—	—	0.98	1.98
$\log K(\text{H}_7\text{L})$	—	—	—	—	—	1.58
$\log K_1 + \log K_2$	22.30	24.18	21.53	21.86	22.85	22.48

^a Ref. 38. ^b Ref. 18. ^c Ref. 22. ^d The constant corresponds to the protonation of the phosphonate group. ^e The constant corresponds to the protonation of the pendant amino group.

the subsequent protonation of oxygen atoms of carboxylate, phosphonate or phosphinate groups.

Stabilities of Ce^{III} *out-of-cage* complexes

The complexation of Ln^{III} ions by dota-like ligands proceeds in two steps. An *out-of-cage* intermediate is formed in the very fast first step, whereafter it slowly rearranges to the *in-cage* complex during the second step, which is furthermore associated with the removal of protons from two protonated ring amino groups. In terms of the overall complexation reaction, the kinetics of formation of the *out-of-cage* complex does not play an important role because the species is formed immediately. However, the *out-of-cage* complex stability is of high importance because the formation rates of the *in-cage* complexes are directly proportional to the concentration of the *out-of-cage* intermediates. Hence, the conditional stabilities were studied in strongly acidic media ($\text{pH} \approx 0\text{--}3$). It could not be studied at higher pH values due to fast formation of the *in-cage* complex.

The geometry of a typical *in-cage* complex is shown in the solid-state structure of the [Eu(do3aP^H)(H₂O)]⁻ anion (see above). In the *out-of-cage* complex, two nitrogen atoms of the macrocycle are protonated.¹⁴ The formation of the *out-of-cage* complex is described by thermodynamic equilibrium (charges are omitted): $\text{Ln} + \text{H}_{n+2}\text{L} \leftrightarrow [\text{Ln}(\text{H}_2\text{L})] + n\text{H}$.

For this equilibrium, the conditional stability constant K^{oc} can be formulated with eqn (2):

$$K^{\text{oc}} = \frac{1}{4} \frac{[\text{OC}] \times [\text{H}]^n}{[\text{Ln}] \times [\text{L}]} \quad (2)$$

where [OC] is the concentration of the *out-of-cage* complex, [Ln] is the concentration of the unbound Ln^{III} ion and [L] is the concentration of the non-complexed ligand. The UV-spectra of Ce^{III} ions are highly sensitive towards changes in the coordination sphere and, thus, they are significantly different for the free aqua ion, the *out-of-cage* complex, and the *in-cage* complex (Fig. S4†). To study the stability of the *out-of-cage* reaction intermediates, the UV-spectra of Ce^{III} complexes were recorded immediately after mixing of the components at variable pH (representative spectra are shown in Fig. S5†).

Recently, we have shown that *out-of-cage* complexes of different stoichiometry might be formed under an equimolar concentration or under ligand or metal ion excess.^{15,22} Thus, the spectra were also recorded at 10 : 1 and 1 : 10 metal-to-ligand ratios. The absorbances at the absorption band maximum as a function of pH were fitted with eqn (2) (Fig. S6†). Since it is not possible to determine the number of protons released in the course of *out-of-cage* complex formation, this parameter (n) was not fixed in order to obtain the best possible fit. However, the value represents the overall number of released protons, as the fitted data cover typically 2 units of the pH scale. The calculated number of released protons is $n = 1\text{--}2$ for phosphonate and phosphinate derivatives, whereas it is higher for H₄dota ($n = 2\text{--}3$). However, the calculated values of conditional stability constants K^{oc} cannot be directly compared because the parameter n is different for each of the studied systems and is calculated just as the best parameters of the fits shown in Fig. S6.† Nevertheless, the more stable complex is generally formed at lower pH. Thus, the pH values corresponding to 50% abundance of the *out-of-cage* complex were chosen as the reference values for a comparison of the studied systems (Fig. 3). The *out-of-cage* complex of H₄dota shows the lowest stability which is similar to the H₄do3aP^{AM} complex. Stabilities of H₅do3aP^{OH}, H₄do3aP^H and H₆do3aP^{IDA} complexes are higher and mutually comparable. In addition, the stability of H₆do3aP^{IDA} is slightly increased under ligand

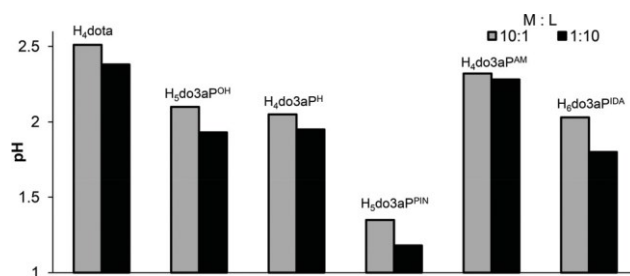


Fig. 3 Conditional stabilities of Ce^{III} *out-of-cage* complexes. The values correspond to the pH at which 50% of the *out-of-cage* complex is formed ($25 \text{ }^\circ\text{C}$; Ce^{III} excess: $c_{\text{Ce}} = 4.0 \times 10^{-3} \text{ M}$, $c_{\text{L}} = 4.0 \times 10^{-4} \text{ M}$; ligand excess: $c_{\text{Ce}} = 4.0 \times 10^{-4} \text{ M}$, $c_{\text{L}} = 4.0 \times 10^{-3} \text{ M}$).

excess, while formation of species with different M : L stoichiometry (probably ML_2) is apparently preferred in view of a significantly lower absorbance limit (plateau) observed in the M : L = 1 : 10 experiment when compared to M : L = 10 : 1 (Fig. S6†). A similar finding is in accordance with a previously published study.²² However, the highest stability was observed for H_5do3aP^{PIN} complexes.

All phospho(i)nate ligands show higher stabilities than H_4dota resulting from the higher acidity of the phospho(i)nic acid group. The stability of H_5do3aP^{OH} is comparable to that of H_4do3aP^H because the phosphonate group is monoprotonated in the studied pH range. A positive charge of the protonated amino group in H_4do3aP^{AM} apparently hampers the formation of the *out-of-cage* complex. The negative effect of the protonated amino group in H_6do3aP^{IDA} is compensated by the two additional carboxylates. Thus, the stability of its *out-of-cage* complex is comparable to those of H_5do3aP^{OH} and H_4do3aP^H . The highest stability, found for H_5do3aP^{PIN} , can be explained by a high acidity and a good chelating ability of the geminal bis(phosphinate) group which forms a stable six-membered chelate ring.³⁹

Formation kinetics of Ce^{III} complexes

The formation of Ce^{III} *in-cage* complexes was studied by UV-Vis spectroscopy using a 10-fold ligand excess or a 10-fold metal ion excess. In the studied pH range (3.5–7.5), the *out-of-cage* complexes are formed immediately and quantitatively (see above), while *out-of-cage* to *in-cage* transformation proceeds with first-order kinetics. Thus, the temporal changes of absorbance at the wavelength of the absorption band maximum was fitted by a first-order kinetic equation (eqn (1)); representative spectra and fits are shown in Fig. S7†).

The rate-determining step in the formation of lanthanide(III) complexes of dota-like ligands^{8–15} is the hydroxide ion-assisted deprotonation of the ring nitrogen atoms in the *out-of-cage* complex, associated with the transfer of the Ln^{III} ion into the macrocyclic cavity. Therefore, the first-order rate constant k_{obs} on $[OH^-]$ could be expressed as eqn (3)

$$^f k_{obs} \approx \frac{1}{4} k_0 + k_1 [\text{OH}^-] + k_2 [\text{OH}^-]^2 \quad (3)$$

where k_0 is the rate constant characterizing the OH^- -independent and k_1 and k_2 are rate constants characterizing the OH^- -dependent pathways of transformation of the *out-of-cage* intermediate into the final *in-cage* complex.¹⁰ The values of k_0 were negligible and were loaded by high ESDs indicating a negligible contribution of the OH^- -independent pathway and, thus, this rate constant was omitted from the fitting. Apart from the Ce^{III} – H_4do3aP^{AM} system, all $\log(^f k_{obs})$ as a function of pH were linear. Thus, only the processes driven by the k_1 pathway were considered. In the case of the Ce^{III} – H_4do3aP^{AM} system, a non-linear curve fitting the data indicated that the complexation process is influenced also by the k_2 -related process. It reflects the presence of an additional amino group in the pendant arm, while the nonlinearity is probably associated with the pendant amine deprotonation. The evaluation of the

Ce^{III} – H_6do3aP^{IDA} system was complicated by the protonation of the pendant arm and by the formation of highly stable *out-of-cage* complexes having various stoichiometry. Consequently, the formation rate of Ce^{III} – H_6do3aP^{IDA} as a function of pH observed under ligand excess could not be described by eqn (3). Hence, the rate constant was adopted from the original literature.²² The calculated formation rate constants as a function of pH with all ligands are shown in Fig. 4 (fitting of the experimental data is shown in Fig. S8†) and the calculated values of the k_1 and k_2 constants are summarized in Table 2.

Most of the studied ligands show very similar pH profiles for the formation rates under metal excess and under ligand excess (Fig. S8†). A slightly faster complexation under ligand excess was observed for H_4dota , which is in agreement with data previously reported for the Eu^{III} – H_4dota system.¹⁵ Even larger differences were observed for H_5do3aP^{PIN} . It might be rationalized by the formation of several *out-of-cage* species with various metal-to-ligand ratios. On the other hand, H_6do3aP^{IDA} shows a decreased complexation rate under ligand excess due to the formation of the highly stable $[ML_2]$ *out-of-cage* complex through coordination of two pendant imino-diacetic moieties belonging to two ligand molecules.²²

The fastest complexation was observed for H_4dota , followed by H_5do3aP^{OH} and H_5do3aP^{PIN} . The two derivatives contain

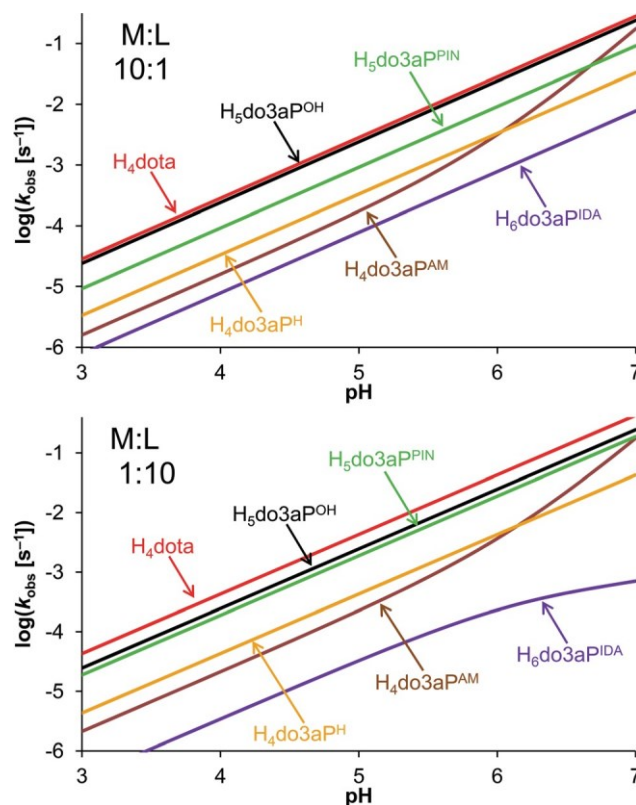


Fig. 4 The plot of calculated formation rate constants as a function of pH (25 °C) under Ce^{III} excess (top; $c_{Ce} = 10^{-3}$ M, $c_L = 10^{-4}$ M) and under ligand excess (bottom; $c_{Ce} = 10^{-4}$ M, $c_L = 10^{-3}$ M). The lines correspond to the best fits of the experimental data (see Fig. S8†) according to eqn (3). The fits for H_6do3aP^{IDA} were adopted from the literature.²²

Table 2 The formation rate constants of the *in-cage* Ce^{III} complexes of the studied ligands ($t = 25\text{ }^{\circ}\text{C}$) determined under metal excess ($c_{\text{Ce}} = 10^{-3}\text{ M}$, $c_{\text{L}} = 10^{-4}\text{ M}$) and ligand excess ($c_{\text{Ce}} = 10^{-4}\text{ M}$, $c_{\text{L}} = 10^{-3}\text{ M}$)

	Metal excess		Ligand excess	
	$k_1 \times 10^5 [\text{s}^{-1} \text{ mol}^{-1} \text{ dm}^3]$	$k_2 \times 10^{12} [\text{s}^{-1} \text{ mol}^{-2} \text{ dm}^6]$	$k_1 \times 10^5 [\text{s}^{-1} \text{ mol}^{-1} \text{ dm}^3]$	$k_2 \times 10^{12} [\text{s}^{-1} \text{ mol}^{-2} \text{ dm}^6]$
H ₄ dota	28 ± 2 35 ^a	—	43 ± 7	—
H ₅ do3aP ^{OH}	24.1 ± 0.3 9.56 ^b	—	24.5 ± 0.7	—
H ₄ do3aP ^H	3.3 ± 0.5	—	4.29 ± 0.04	—
H ₅ do3aP ^{PIN}	9.2 ± 0.2	—	18.8 ± 0.1	—
H ₄ do3aP ^{AM}	1.6 ± 0.2	16 ± 2	2.1 ± 0.6	16 ± 2
H ₆ do3aP ^{IDA}	0.86 ^c	—	0.019 ^c	—

^a Ref. 10. ^b Ref. 18. ^c Ref. 22.

easily protonable pendant groups which serve as acceptors of the hydrogens strongly bound to macrocycle amino groups. In the present case, the pendant groups can mediate a proton transfer from the macrocycle to the bulk solution. Generally, the phosphinate group forms much weaker hydrogen bonds. Thus, the proton transfer to H₄do3aP^H is not well supported and its complexation is significantly slower. A protonated pendant amino group in H₄do3aP^{AM} is probably involved in hydrogen bonding with the phosphinate oxygen atom. Thus, the phosphinate group does not mediate the proton transfer. However, at neutral or alkaline pH, the pendant amino group is deprotonated. Thus, it does not compete with the hydrogen bonding between the phosphinate group and macrocycle amines and can even enhance the proton transfer into the bulk solution. Thus, the complexation of H₄do3aP^{AM} at pH > 6 is accelerated in comparison with other ligands. The slowest complexation was found for H₆do3aP^{IDA} due to the presence of a strongly complexing group in the pendant arm, resulting in the formation of excessively stable *out-of-cage* complexes.²² Surprisingly, the formation rates neither show any clear correlation with the basicity of ligands, nor with the conditional stabilities of the *out-of-cage* complexes. Recently, a complexation kinetic study of H₄dota with trivalent metal ions was published.⁴⁰ The results show that the complexation rate increases with the increase in the amount of EtOH or other organic solvents in the solution as a result of the decreased basicity of the macrocycle in the presence of an organic modifier. However, our results show that the correlation of the complexation rate with the basicity of the macrocycle cannot be done for different ligands. It might be ascribed to the fact that the nature of the pendant arms also plays an important role in the complexation mechanism.

Radiolabelling with ¹⁷⁷Lu^{III}

Labelling with ¹⁷⁷Lu^{III} was chosen to evaluate the effects of the chelator concentration and pH on the radiochemical yield (Fig. 5). H₄dota, H₅do3aP^{OH} and H₅do3aP^{PIN} require the lowest molar amount of ligand ($\approx 0.07\text{ nmol}$) for quantitative labelling at pH 6.6 (30 min, 95 °C), followed by H₄do3aP^H and H₆do3aP^{IDA} requiring only a slightly higher amount ($\approx 0.1\text{ nmol}$). H₄do3aP^{AM} shows significantly worse labelling

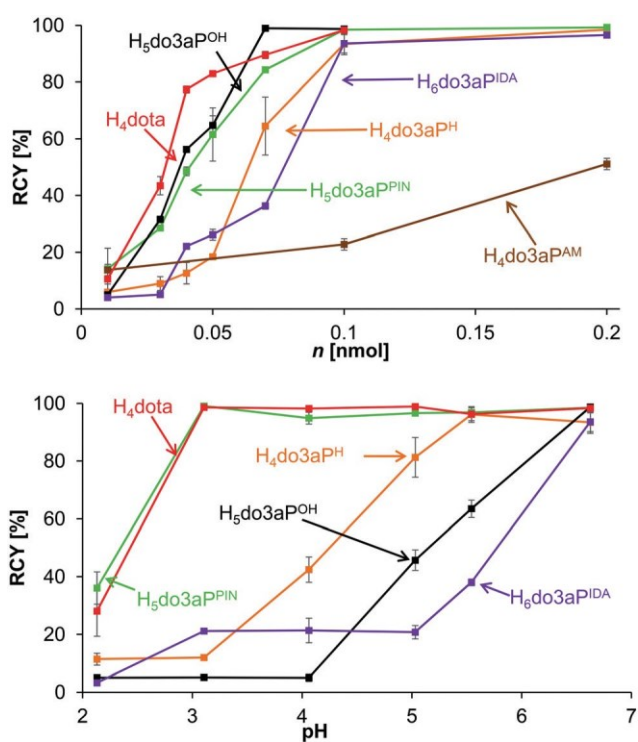


Fig. 5 Radiochemical yield of labelling with ¹⁷⁷Lu^{III} as a function of the ligand amount (top; 10 MBq, pH 6.6, 95 °C, 30 min) and pH (bottom; 10 MBq, $n_{\text{L}} = 0.1\text{ nmol}$, 95 °C, 30 min).

properties and reaches less than 50% labelling even using 0.2 nmol. Larger differences were observed when labelling was evaluated as a function of pH ($n_{\text{L}} \approx 0.1\text{ nmol}$, 30 min, 95 °C). Comparable pH profiles were found for H₄dota and H₅do3aP^{PIN}. The two ligands show quantitative labelling at pH ≈ 3 . Other ligands require significantly higher pH for quantitative labelling, namely, pH ≈ 5.5 for H₄do3aP^H and pH ≈ 6.6 for H₅do3aP^{OH} and H₆do3aP^{IDA}. Since H₄do3aP^{AM} does not show quantitative labelling even at pH 6.6, it was not studied at lower pH.

H₅do3aP^{PIN} shows the best labelling at low pH among all phospho(i)nate derivatives. This is in good agreement with the above reported conditional stabilities of the *out-of-cage* com-

plexes. On the other hand, the radiochemical yields neither show any clear correlation with the ligand basicity nor with the formation rates of *in-cage* complexes. These results suggest that the stabilities of the *out-of-cage* complexes determine the efficiency of radionuclide incorporation. The *out-of-cage* complex formation is the rate-determining factor due to the low concentrations of reactants (nanomolar scale) and the presence of various competing metal ions under radiochemical complexations. It indicates that the presence of an additional chelating group in the pendant arm is a promising strategy to improve radiolabelling. However, the design of this chelating group must be chosen carefully because an excessively strong coordination^{22,41} or an inappropriate choice of the spacer between the chelating group and the macrocycle¹⁵ could result in lower overall complexation rates. The results indicate that the presence of an amino group in the pendant arm is not desirable. The pendant coordination moiety should preferably be an acidic structural element, such as phosphinates in H₅do3aP^{Pin}. Likewise, promising properties of a bis(phosphinate) pendant were reported also for cyclam-based ligands intended for complexation of copper radioisotopes.²¹

Conclusions

We found that the complexation rates of lanthanide(III) ions with macrocyclic analogues of H₄dota bearing a phosphorous-acid pendant arm do not show any correlation with the ligand basicity. On the other hand, the additional coordinating groups in the phosphinate pendant arms play an important role in the radiolabelling process and significantly influence complexation yields, as they increase the stabilities of the respective *out-of-cage* reaction intermediates. However, the correlation between the stability of the intermediates and the labelling yield is not straightforward. An improved ¹⁷⁷Lu^{III} radiolabelling yield was found for ligands bearing bis(phosphinate) pendants that form stable intermediates under acidic conditions. On the other hand, an additional amino group in the pendant arm does not improve the conditional stability in acidic media, probably due to electrostatic repulsion between the metal ion and the protonated amino group. However, the ligand bearing imino-diacetate pendant that forms excessively stable *out-of-cage* intermediates shows a significantly decreased complexation rate. It indicates that the stability of *out-of-cage* complexes must be carefully tuned, and optimal coordinating pendant arms might be those bearing highly acidic chelating groups such as bis(phosphinate). However, the stabilities of the *out-of-cage* complexes do not explain the observed different labelling behaviour of H₄dota and its phospho(i)nate analogues.

Conflicts of interest

There are no conflicts to declare.

Acknowledgements

The investigations were supported by the European Regional Development Fund (GINOP-2.3.2-15-2016-00008), the Grant Agency of Charles University (No. 272314) and Ministry of Education of the Czech Republic (LTC 170607), and this project is connected to the EU COST CA15209 Action. We thank I. Cisařová for the collection of the X-ray diffraction data, Z. Böhmová for potentiometric measurements and P. Urbanovský for providing H₄do3aP^{AM}.

References

- 1 A. E. Merbach, L. Helm and É. Tóth, *The Chemistry of Contrast Agents in Medical Magnetic Resonance Imaging*, John Wiley & Sons, Chichester, 2013.
- 2 T. J. Wadas, E. H. Wong, G. R. Weisman and C. J. Anderson, *Chem. Rev.*, 2010, 110, 2858–2902.
- 3 R. E. Mewis and S. J. Archibald, *Coord. Chem. Rev.*, 2010, 254, 1686–1712.
- 4 C. S. Cutler, H. M. Hennkens, N. Sisay, S. Huclier-Markai and S. S. Jurisson, *Chem. Rev.*, 2013, 113, 858–883.
- 5 E. W. Price and C. Orvig, *Chem. Soc. Rev.*, 2014, 43, 260–290.
- 6 S. Faulkner, S. J. A. Pope and B. P. Burton-Pye, *Appl. Spectrosc. Rev.*, 2005, 40, 1–31.
- 7 X. Wang, H. Chang, J. Xie, B. Zhao, B. Liu, S. Xu, W. Pei, N. Ren, L. Huang and W. Huang, *Coord. Chem. Rev.*, 2014, 273–274, 201–212.
- 8 J. Moreau, E. Guillon, J.-C. Pierrard, J. Rimbault, M. Port and M. Aplincourt, *Chem. – Eur. J.*, 2004, 10, 5218–5232.
- 9 S. L. Wu and W. D. Horrocks, *Inorg. Chem.*, 1995, 34, 3724–3732.
- 10 É. Tóth, E. Brücher, I. Lázár and I. Tóth, *Inorg. Chem.*, 1994, 33, 4070–4076.
- 11 E. Brücher, G. Laurenczy and Z. Makra, *Inorg. Chim. Acta*, 1987, 139, 141–142.
- 12 X. Wang, T. Jin, V. Comblin, A. Lopez-Mut, E. Merciny and J. F. Desreux, *Inorg. Chem.*, 1992, 31, 1095–1098.
- 13 L. Burai, I. Fábrián, R. Király, E. Szilágyi and E. Brücher, *J. Chem. Soc., Dalton Trans.*, 1998, 243–248.
- 14 J. Šimeček, P. Hermann, J. Havlíčková, E. Herdtweck, T. G. Kapp, N. Engelbogen, H. Kessler, H.-J. Wester and J. Notni, *Chem. – Eur. J.*, 2013, 19, 7748–7757.
- 15 S. Procházková, J. Hraníček, V. Kubiček and P. Hermann, *Polyhedron*, 2016, 111, 143–149.
- 16 P. Táborský, I. Svobodová, P. Lubal, Z. Hnatejko, S. Lis and P. Hermann, *Polyhedron*, 2007, 26, 4119–4130.
- 17 P. Táborský, I. Svobodová, Z. Hnatejko, P. Lubal, S. Lis, M. Försterová, P. Hermann, I. Lukeš and J. Havel, *J. Fluoresc.*, 2005, 15, 507–512.
- 18 P. Táborský, P. Lubal, J. Havel, J. Kotek, J. Rudovský, P. Hermann and I. Lukeš, *Collect. Czech. Chem. Commun.*, 2005, 70, 1909–1942.
- 19 J. Notni, P. Hermann, J. Havlíčková, J. Kotek, V. Kubiček, J. Plutnar, N. Loktionova, P. J. Riss, F. Rösch and I. Lukeš, *Chem. – Eur. J.*, 2010, 16, 7174–7185.

- 20 J. Šimeček, M. Schulz, J. Notni, J. Plutnar, V. Kubiček, J. Havlíčková and P. Hermann, *Inorg. Chem.*, 2012, 51, 577–590.
- 21 T. David, V. Kubiček, O. Gutten, P. Lubal, J. Kotek, H.-J. Pietzsch, L. Rulišek and P. Hermann, *Inorg. Chem.*, 2015, 54, 11751–11766.
- 22 S. Procházková, V. Kubiček, Z. Böhmová, K. Holá, J. Kotek and P. Hermann, *Dalton Trans.*, 2017, 46, 10484–10497.
- 23 A. Dadabhoy, S. Faulkner and P. G. Sammes, *J. Chem. Soc., Perkin Trans. 2*, 2002, 348–357.
- 24 J. F. Desreux, *Inorg. Chem.*, 1980, 19, 1319–1324.
- 25 J. Rudovský, P. Cígler, J. Kotek, P. Hermann, P. Vojtíšek, I. Lukeš, J. A. Peters, L. Vander Elst and R. N. Muller, *Chem. – Eur. J.*, 2005, 11, 2373–2383.
- 26 P. Urbanovský, MSc. Thesis, Charles University, Prague, 2015.
- 27 (a) Z. Otwinovski and W. Minor, *HKL DENZO and Scalepack Program Package*, Nonius BV, Delft, 1997; (b) Z. Otwinovski and W. Minor, Processing of X-ray diffraction data collected in oscillation mode, *Methods Enzymol.*, 1997, 276, 307–326.
- 28 A. Altomare, G. Cascarano, C. Giacovazzo, A. Guagliardi, M. C. Burla, G. Polidori and M. Camalli, “SIR92”, *J. Appl. Crystallogr.*, 1994, 27, 435–436.
- 29 G. M. Sheldrick, *SHELXL-2014/7. Program for Crystal Structure Refinement from Diffraction Data*, University of Göttingen, Göttingen, 2014.
- 30 V. Kubiček, J. Havlíčková, J. Kotek, G. Tircsó, P. Hermann, É. Tóth and I. Lukeš, *Inorg. Chem.*, 2010, 49, 10960–10969.
- 31 C. F. Baes Jr. and R. E. Mesmer, *The Hydrolysis of Cations*, Wiley, New York, 1976.
- 32 M. Kývala and I. Lukeš, International Conference, Chemometrics '95, Pardubice, Czech Republic, 1995, p. 63. Full version of “OPIUM” is available (free of charge) on <http://www.natur.cuni.cz/~kyvala/opium.html>.
- 33 M. Meyer, V. Dahaoui-Gindrey, C. Lecomte and R. Guillard, *Coord. Chem. Rev.*, 1998, 178–180, 1313–1405.
- 34 P. Hermann, J. Kotek, V. Kubiček and I. Lukeš, *Dalton Trans.*, 2008, 3027–3047.
- 35 P. Vojtíšek, P. Cígler, J. Kotek, J. Rudovský, P. Hermann and I. Lukeš, *Inorg. Chem.*, 2005, 44, 5591–5599.
- 36 J. Kotek, J. Rudovský, P. Hermann and I. Lukeš, *Inorg. Chem.*, 2006, 45, 3097–3102.
- 37 I. Lukeš, J. Kotek, P. Vojtíšek and P. Hermann, *Coord. Chem. Rev.*, 2001, 216–217, 287–312.
- 38 M. Pniok, V. Kubiček, J. Havlíčková, J. Kotek, A. Sabatie-Gogová, J. Plutnar, S. Huclier-Markai and P. Hermann, *Chem. – Eur. J.*, 2014, 20, 7944–7955.
- 39 T. David, S. Procházková, J. Kotek, V. Kubiček, P. Hermann and I. Lukeš, *Eur. J. Inorg. Chem.*, 2014, 4357–4368.
- 40 M. Pérez-Malo, G. Szabó, E. Eppard, A. Vagner, E. Brücher, I. Tóth, A. Maiocchi, E. H. Suh, Z. Kovács, Z. Baranyai and F. Rösch, *Inorg. Chem.*, 2018, 57, 6107–6117.
- 41 J. Notni, J. Plutnar and H.-J. Wester, *EJNMMIRes.*, 2012, 2, 13.

Supplementary information

Lanthanide(III) complexes of monophosphinate/monophosphonate DOTA-analogues: effect of the substituents on formation rate and radiolabelling yield

Soňa Procházková,^a Vojtěch Kubiček,^{a*} Jan Kotek,^a Adrienn Vágner,^b Johannes Notni^b and Petr Hermann^a

^a Department of Inorganic Chemistry, Faculty of Science, Charles University, Hlavova 2030, 128 43 Prague 2, Czech Republic; email: kubicek@natur.cuni.cz; tel.: +420 221951436; fax: +420 221951253.

^b Lehrstuhl für Pharmazeutische Radiochemie, Technische Universität München, Walther-Meissner-Strasse 3, D-85748 Garching, Germany.

Table of content

Figure S1. 2D coordination polymer motive found in the solid-state structure of Na[Eu(do3aP ^H)(H ₂ O)]·2NaCl·7.125H ₂ O	2
Figure S2. Crystal packing of Na[Eu(do3aP ^H)(H ₂ O)]·2NaCl·7.125H ₂ O	3
Isolation and structure of DO3A lactame – H ₂ do3a ^{lac}	4
Figure S3. Molecular structure of (H ₄ do3a ^{lac}) ²⁺ cation found in the crystal structure of (H ₄ do3a ^{lac})Cl ₂ ·2H ₂ O	4
Table S1. Experimental data of the reported crystal structures	5
Table S2. Overall protonation constants logβ of ligands.....	6
Figure S4. Representative absorption spectra: Ce ^{III} aqua ion, <i>out-of-cage</i> and <i>in-cage</i> Ce ^{III} -do3aP ^{PIN} complex	7
Figure S5. Representative absorption spectra of Ce ^{III} -H ₄ do3aP ^H and Ce ^{III} -H ₅ do3aP ^{PIN} systems measured immediately after mixing at various	7
Figure S6. Formation of <i>out-of-cage</i> complexes: pH dependence of absorbance measured immediately after mixing of the components	8
Figure S7. Changes of absorption spectra in the course of complexation of H ₅ do3aP ^{PIN} and H ₄ do3aP ^{AM} and time dependences of absorbance of the <i>in-cage</i> complex.....	9
Figure S8. pH dependence of the formation rate constants under the Ce ^{III} excess and under the ligand excess	10

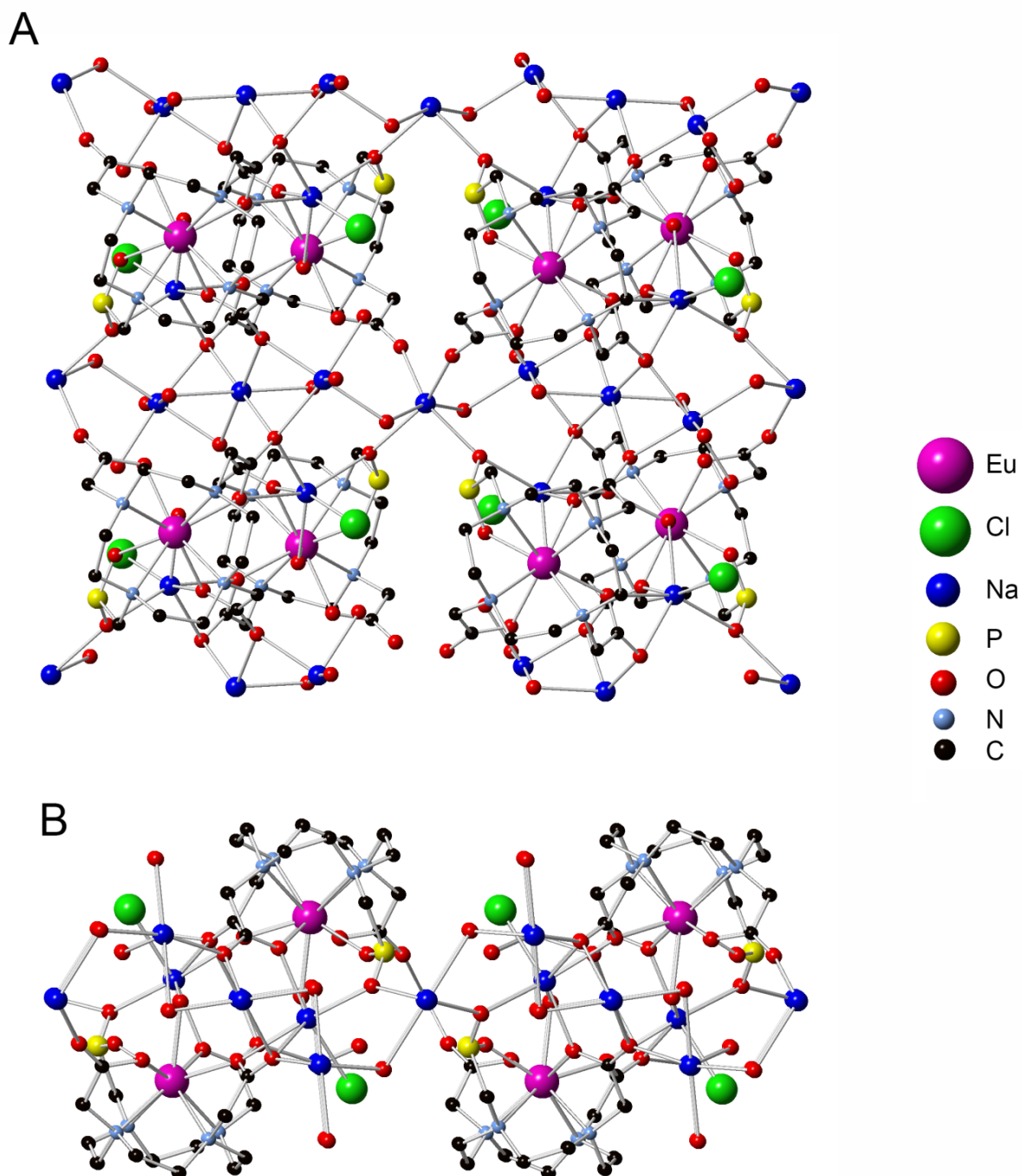


Figure S1. 2D coordination polymer motive found in the solid-state structure of $\text{Na}[\text{Eu}(\text{do3aP}^{\text{H}})(\text{H}_2\text{O})] \cdot 2\text{NaCl} \cdot 7.125\text{H}_2\text{O}$. The view perpendicular to O_4/N_4 -planes of the coordination spheres (**A**) and the view along the y -axis (**B**). Hydrogen atoms are omitted for clarity.

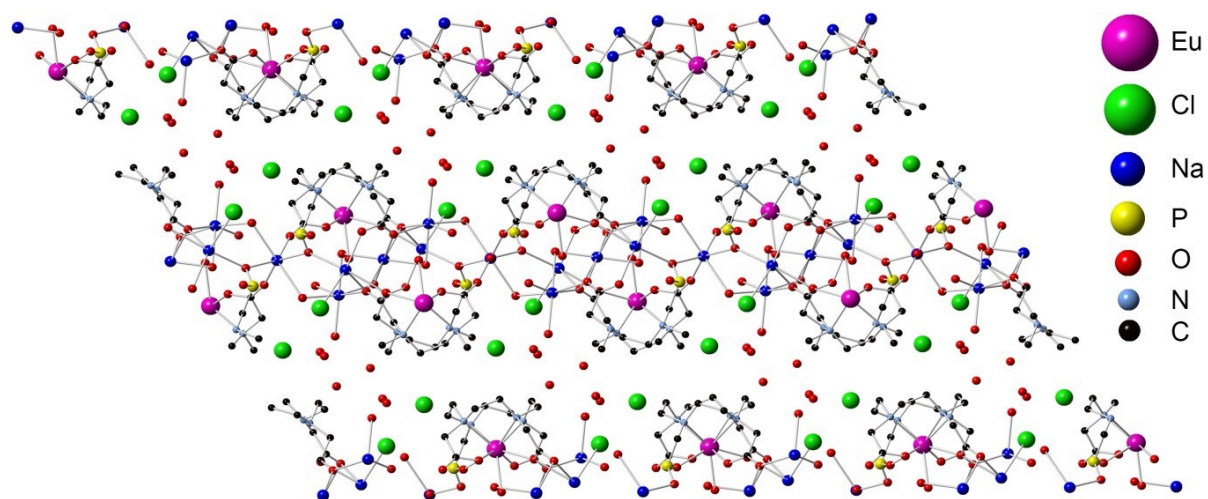
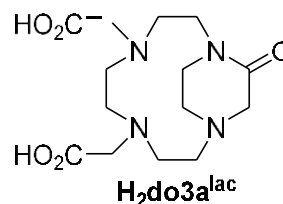


Figure S2. Crystal packing of $\text{Na}[\text{Eu}(\text{do3aP}^{\text{H}})(\text{H}_2\text{O})] \cdot 2\text{NaCl} \cdot 7.125\text{H}_2\text{O}$. The view along the y -axis. Hydrogen atoms are omitted for clarity.

Isolation and structure of DO3A lactame – $\text{H}_2\text{do3a}^{\text{lac}}$

When old batches of $\text{H}_3\text{do3a}$ were used for synthesis of $\text{H}_4\text{do3aP}^{\text{H}}$ (especially when stored in semi-solid form obtained by evaporation from acid media after deesterification), some amount of lactam $\text{H}_2\text{do3a}^{\text{lac}}$ was isolated as a late fraction of the ion exchange workup of the reaction mixture. It is probably predominantly formed on pro-longed standing of $\text{H}_3\text{do3a}$ under acid conditions (after evaporation in CF_3COOH). Its ^1H NMR spectra are rather complicated due to rigidity of the molecule and, thus, the X-ray diffraction study was performed to confirm identity of the compound (Figure S3).



Single-crystals of $(\text{H}_4\text{do3a}^{\text{lac}})\text{Cl}_2 \cdot 2\text{H}_2\text{O}$ were grown by vapour diffusion of THF into the solution of the $\text{H}_4\text{do3a}^{\text{lac}}$ in 6 M aq. HCl. In the crystal structure of $(\text{H}_4\text{do3a}^{\text{lac}})\text{Cl}_2 \cdot 2\text{H}_2\text{O}$, no disorder was found. The thermal parameter of one water-belonging hydrogen atoms was kept using $U_{\text{eq}}(\text{H}) = 1.2 U_{\text{eq}}(\text{O})$ as it became too large when freely refined.

The macrocycle of $(\text{H}_4\text{do3a}^{\text{lac}})^{2+}$ fragment is diprotonated. One of the protons is bound to the amine atom of the lactam ring, and the other is localized on the opposite nitrogen atom bearing one of the carboxylate pendants and is involved in the medium-strong intramolecular hydrogen bond ($d_{\text{N}\cdots\text{O}} = 2.88 \text{ \AA}$) to the lactam oxygen atom. Both carboxylic acid pendant arms are protonated and involved in intermolecular hydrogen bonding with water molecules of crystallization and chloride counter anions.

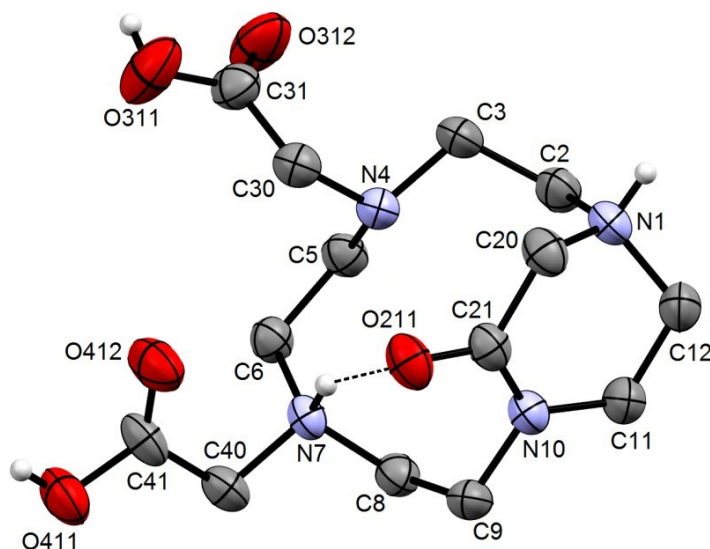


Figure S3. Molecular structure of $(\text{H}_4\text{do3a}^{\text{lac}})^{2+}$ cation found in the crystal structure of $(\text{H}_4\text{do3a}^{\text{lac}})\text{Cl}_2 \cdot 2\text{H}_2\text{O}$. The intramolecular hydrogen bond is shown as a dashed line. Carbon-bound hydrogen atoms are omitted for clarity.

Table S1. Experimental data of the reported crystal structures.

Compound	(H ₆ do3a ^H)Cl ₂ ·THF·3H ₂ O	Na[Eu(do3a ^H)(H ₂ O)]·2NaCl·7.125H ₂ O	(H ₄ do3a ^{lam})Cl ₂ ·2H ₂ O
Formula	C ₁₉ H ₄₅ N ₄ O ₁₂ P ₁ Cl ₂	C ₁₅ H _{41.25} Cl ₂ Eu ₁ N ₄ Na ₃ O _{16.125} P ₁	C ₁₄ H ₃₀ Cl ₂ N ₄ O ₇
<i>M_r</i>	623.46	858.57	437.32
Colour	colourless	colourless	colourless
Shape	prism	needle	prism
Dimensions (mm)	0.30×0.25×0.20	0.15×0.08×0.05	0.50×0.20×0.20
Crystal system	monoclinic	monoclinic	orthorhombic
Space group	C2/c	C2/c	P2 ₁ 2 ₁ 2 ₁
<i>a</i> (Å)	22.0543(3)	32.1447(5)	9.7430(4)
<i>b</i> (Å)	11.19790(10)	9.43790(10)	10.3130(5)
<i>c</i> (Å)	24.5815(4)	23.5537(4)	21.7340(10)
α (°)	90	90	90
β (°)	96.4613(8)	121.0061(8)	90
γ (°)	90	90	90
<i>V</i> (Å ³)	6032.13(14)	6124.65(16)	2183.82(17)
<i>Z</i>	8	8	4
<i>D_c</i> (g cm ⁻³)	1.373	1.862	1.330
μ (mm ⁻¹)	0.329	2.392	0.337
<i>F</i> (000)	2656	3466	928
Reflections unique; observed (<i>I</i> _o > 2σ(<i>I</i>))	6889; 5601	7035; 6005	4220; 3435
Parameters	432	451	276
G-o-f on <i>F</i> ²	1.078	1.039	1.066
<i>R</i> ; <i>R'</i> (all data)	0.0466; 0.0650	0.0299; 0.0406	0.0439; 0.0620
<i>wR</i> ; <i>wR'</i> (all data)	0.1291; 0.1449	0.0658; 0.0709	0.0987; 0.1088
Difference max; min (e Å ⁻³)	0.474; -0.523	1.941; -1.169	0.321; -0.181

Table S2. Overall protonation constants $\log\beta$ of ligands ($I = 0.1 \text{ M NMe}_4\text{Cl}$, $25 \text{ }^\circ\text{C}$).

	$\text{H}_4\text{do3aP}^{\text{H}}$	$\text{H}_5\text{do3aP}^{\text{PIN}}$	$\text{H}_4\text{do3aP}^{\text{AM}}$
HL	12.43(1)	12.46(1)	13.29(3)
H ₂ L	21.53(1)	21.86(2)	22.85(3)
H ₃ L	25.86(1)	26.41(2)	31.30(3)
H ₄ L	28.64(1)	29.83(2)	35.41(3)
H ₅ L	30.09(1)	31.89(2)	37.27(3)
H ₆ L	–	–	38.25(4)

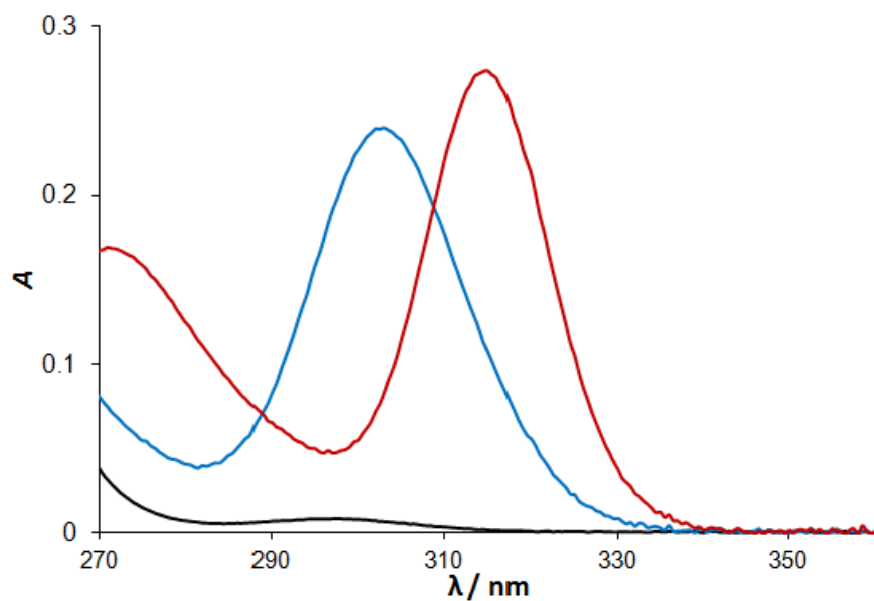


Figure S4. Representative absorption spectra: Ce^{III} aqua ion (black), *out-of-cage* (blue) and *in-cage* (red) Ce^{III} -do3aP^{PIN} complex ($c_{\text{M}} = c_{\text{L}} = 4.0 \cdot 10^{-4}$ M, 25 °C).

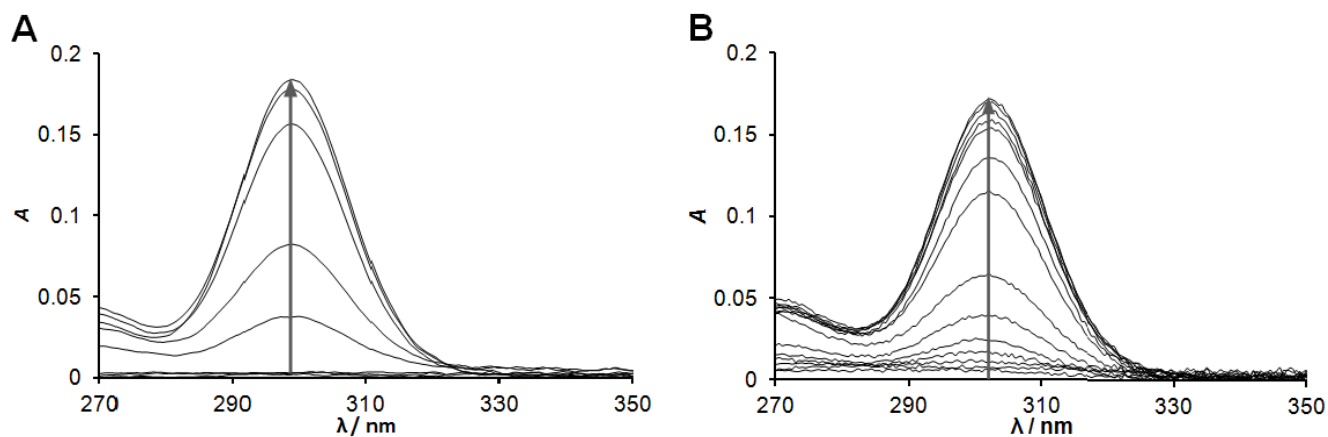


Figure S5. Representative absorption spectra of $\text{Ce}^{\text{III}}\text{-H}_4\text{do3aP}^{\text{H}}$ (**A**, pH ~ 1–3) and $\text{Ce}^{\text{III}}\text{-H}_5\text{do3aP}^{\text{PIN}}$ (**B**, pH ~ 0–3) systems measured immediately after mixing at various pH ($c_{\text{M}} = c_{\text{L}} = 4.0 \cdot 10^{-4}$ M, 25 °C). The arrow indicates increasing pH. Changes of absorbance at absorption band maximum are shown in Figure S6.

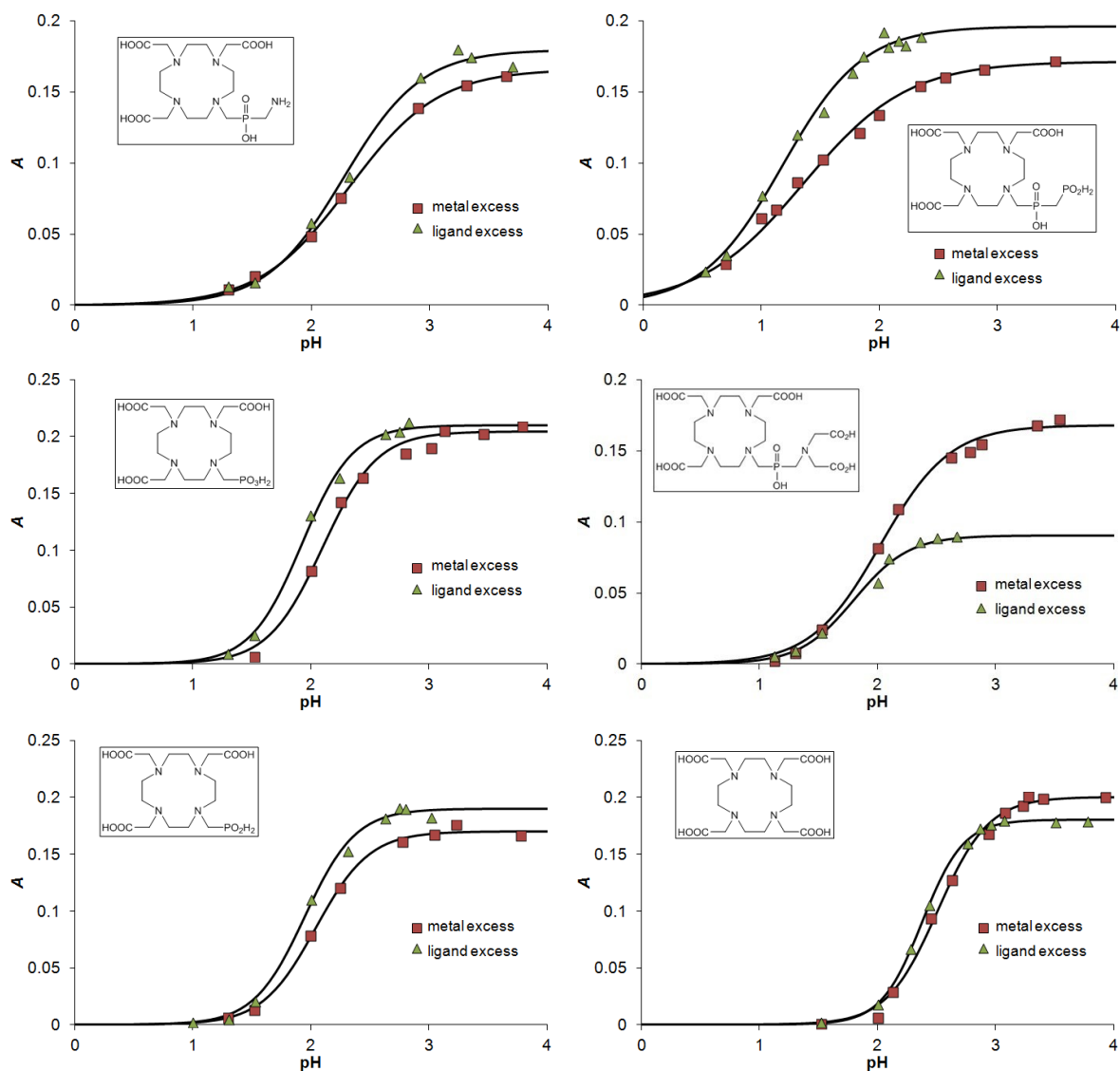


Figure S6. Formation of *out-of-cage* complexes: pH dependence of absorbance at absorption band maximum (298–305 nm) measured immediately after mixing of the components (25 °C) under the Ce^{III} excess ($4.0 \cdot 10^{-3}$ M, $c_L = 4.0 \cdot 10^{-4}$ M) and under the ligand excess ($c_{\text{Ce}} = 4.0 \cdot 10^{-4}$ M, $c_L = 4.0 \cdot 10^{-3}$ M). The lines correspond to the best fits according to Equation 2.

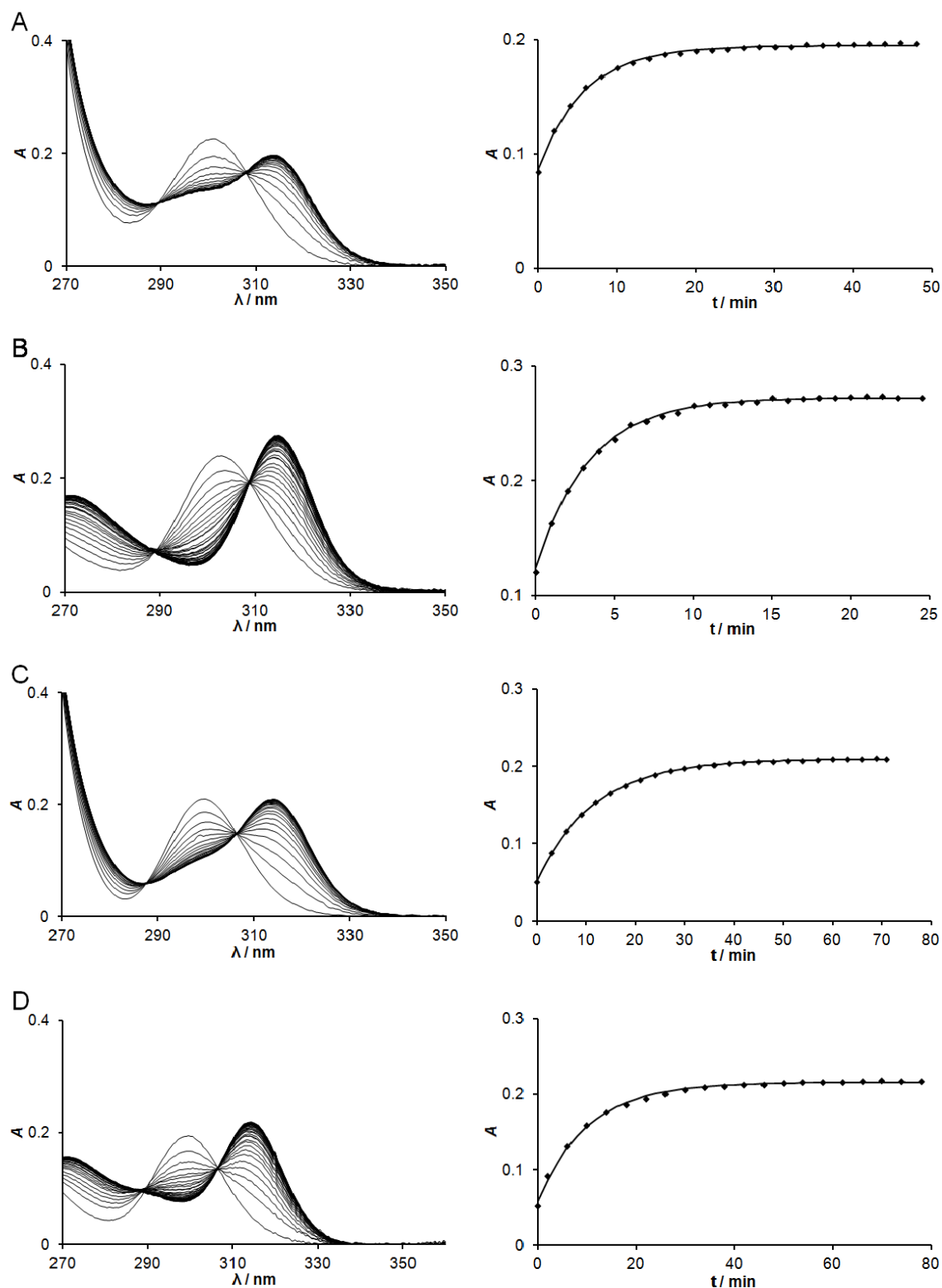


Figure S7. Changes of absorption spectra in the course of complexation of H_5do3aP^{PIN} and H_4do3aP^{AM} (left, 25 °C) and time dependences of absorbance at absorption band maximum (~ 315 nm) of the *in-cage* complex (right). The curves represent the best fit according to Equation 1. **A:** H_5do3aP^{PIN} , $c_{Ce} = 4.0 \cdot 10^{-4}$ M, $c_L = 4.0 \cdot 10^{-3}$ M, pH = 5.4; **B:** H_5do3aP^{PIN} , $c_{Ce} = 4.0 \cdot 10^{-3}$ M, $c_L = 4.0 \cdot 10^{-4}$ M, pH = 5.4; **C:** H_4do3aP^{AM} , $c_{Ce} = 4.0 \cdot 10^{-4}$ M, $c_L = 4.0 \cdot 10^{-3}$ M, pH = 5.7; **D:** H_4do3aP^{AM} , $c_{Ce} = 4.0 \cdot 10^{-3}$ M, $c_L = 4.0 \cdot 10^{-4}$ M, pH = 5.7.

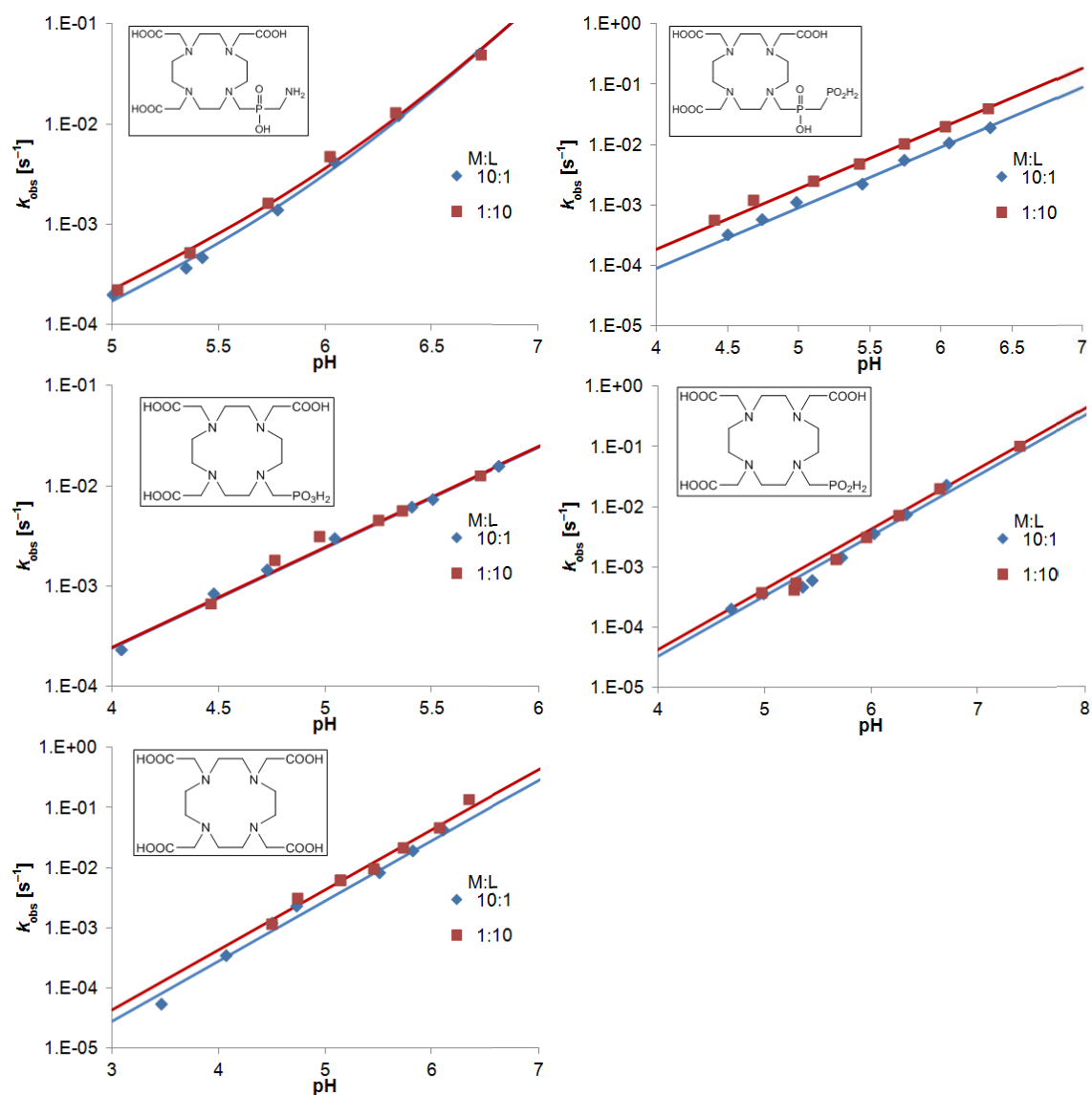


Figure S8. pH dependence of the formation rate constants (25 °C) under the Ce^{III} excess ($c_{\text{Ce}} = 4.0 \cdot 10^{-3}$ M, $c_{\text{L}} = 4.0 \cdot 10^{-4}$ M, blue diamonds) and under the ligand excess ($c_{\text{Ce}} = 4.0 \cdot 10^{-4}$ M, $c_{\text{L}} = 4.0 \cdot 10^{-3}$ M, red squares). The lines correspond to the best fits according to Equation 3.